



# manufacturing automation laboratories



**CUTPRO®**

**FUNDAMENTALS OF MACHINING**

---

*Start to Finish Guide*

*Manufacturing Automation Laboratories Inc.*

© 2013 Manufacturing Automation Laboratories Inc. All rights reserved.



## **Copyright and Trademark Information**

© 2013 Manufacturing Automation Laboratories Inc. All rights reserved.  
Unauthorized use, distribution or duplication is prohibited.

CUTPRO is a registered trademark of Manufacturing Automation Laboratories Inc.  
All other trademarks or registered trademarks are the property of their respective owners.

## **Intellectual Property Rights**

Intellectual Property Rights in the goods, any drawings supplied with them remain the property of Manufacturing Automation Laboratories Inc. “Intellectual Property Rights” means any and all registered and unregistered patents, trademarks, design rights, copyrights and other intellectual property rights of any nature of the goods, and all applications for registration of the same.

# Table of Contents



<b>1</b>	<b>Manual Overview</b> .....	<b>1</b>
<b>2</b>	<b>Modeling of Cutting Forces</b> .....	<b>1</b>
2.1	Orthogonal cutting coefficients .....	2
2.1.1	<i>Experimental setup: Determination of orthogonal cutting force coefficients</i> .....	2
2.1.2	<i>Determination of friction angle, shear angle and shear stress</i> .....	7
2.1.3	<i>Orthogonal to Oblique Transformation Method</i> .....	8
2.2	Average cutting force coefficients for milling .....	9
2.2.1	<i>Measurement Setup</i> .....	10
2.2.2	<i>Calculating the Average Cutting Force Coefficients</i> .....	11
2.2.3	<i>Simulation of cutting forces in milling using Average Cutting Force Coefficients</i> .....	12
2.2.4	<i>Fourier spectrum of cutting forces</i> .....	12
<b>3</b>	<b>Machine tool dynamics, tap testing</b> .....	<b>14</b>
3.1	Machine tool dynamics in milling .....	14
3.2	Measurement setup .....	14
3.3	Hammer selection .....	15
3.4	Displacement sensor/accelerometer selection .....	16
3.5	Evaluation of the FRF .....	17
3.6	Example of Frequency Response Function identification .....	18
3.7	Converting a FRF into modal parameters .....	24
<b>4</b>	<b>Chatter stability lobes</b> .....	<b>27</b>
4.1	Frequency Response Function (FRF) of the machine tool structure .....	27
4.2	Calculation of stability lobes .....	29
4.3	Experimental verification of stability lobes .....	32
<b>5</b>	<b>Chatter free milling of titanium and nickel alloys</b> .....	<b>34</b>
5.1	Face milling of titanium alloys .....	34
5.2	Variable pitch cutter design for difficult to machine materials at low speeds .....	37
<b>6</b>	<b>Machining Strategies for Thin Gauge Aircraft Parts</b> .....	<b>39</b>
6.1	Aluminum Machining: Fixturing strategy .....	39
6.2	Aluminum Machining: Machine tools .....	40

6.3	Aluminum Machining: Machining steps .....	40
6.3.1	<i>Roughing</i> .....	40
6.3.2	<i>Semi-finishing</i> .....	40
6.3.3	<i>Finishing</i> .....	41
6.3.3.1	<i>Thin pocket walls (ribs)</i> .....	41
6.3.3.2	<i>Thin pocket floors (webs)</i> .....	42
6.3.3.3	<i>Small pocket corner radii</i> .....	42
6.3.3.4	<i>5-axis features</i> .....	43
6.3.3.5	<i>Part vibration counter measures</i> .....	43
6.4	Demo part High Speed Machining in Aluminum .....	43
6.4.1	<i>Aluminum demo part design</i> .....	43
6.4.2	<i>Machine &amp; cutter selection</i> .....	44
6.4.3	<i>Machining strategy</i> .....	45
6.4.4	<i>CutPro: Selection of cutting conditions</i> .....	45
6.4.5	<i>Thin Wall Machining Experiments</i> .....	47
6.4.6	<i>NC Program Methods</i> .....	50
6.4.7	<i>Part Machining</i> .....	52
6.4.8	<i>MACHpro Optimization</i> .....	52
6.5	Titanium Machining: Machining steps .....	53
6.5.1	<i>Roughing</i> .....	53
6.5.2	<i>Semi finishing</i> .....	54
6.5.3	<i>Finishing</i> .....	54
6.5.3.1	<i>Thin pocket walls</i> .....	54
6.6	Demo part High Performance / High Speed Machining in Titanium .....	55
6.6.1	<i>Titanium demo part design</i> .....	55
6.6.2	<i>Machine &amp; cutter selection</i> .....	55
6.6.3	<i>Machining strategy</i> .....	56
6.6.4	<i>CutPro: Selection of cutting conditions</i> .....	57
6.6.5	<i>Thin Wall Machining Experiments</i> .....	60
6.6.6	<i>MACHpro Form Error function</i> .....	64
6.6.7	<i>NC Program Methods</i> .....	65
6.6.8	<i>Part Machining</i> .....	67

<b>Appendix A</b>	<b>– Processing cutting <i>F</i> data in Excel to determine orthogonal cutting parameters</b> ....	<b>70</b>
<b>Appendix B</b>	<b>– Average Cutting Coefficient Identification in CutPro</b> .....	<b>71</b>
<b>Appendix C</b>	<b>– Time Domain Simulation in CutPro</b> .....	<b>73</b>
<b>Appendix D</b>	<b>– Basics of Modal Analysis</b> .....	<b>76</b>
<b>Appendix E</b>	<b>– List of main Equipment used in Document</b> .....	<b>82</b>

# 1 Manual Overview

In this manual you will learn the different methods for modeling machining processes that are available in CutPro. This manual will mainly focus on milling. The modeling involves the prediction of cutting forces under various cutting conditions, based on experimental data, and the prediction of the dynamic behaviour of machine tools, also based on experimentally collected data. These experimental data are used in the CutPro software, in order to predict chatter vibration free cutting conditions. These data are represented in stability charts called “stability lobes”, which gives the chatter free depth of cut as a function of the spindle speed on the machine tool.

The manual will start off with the orthogonal cutting force model and will show you how to conduct experiments to identify orthogonal cutting coefficients for different materials with dedicated cutting tools in turning experiments. Once these coefficients are identified, they can be used to predict cutting forces for a variety of cutting tool geometries in milling, using the orthogonal to oblique transformation. This transformation will also be discussed.

The orthogonal to oblique transformation is very powerful, but it does require extensive testing, which may be too costly or time consuming. Instead, more simple mechanistic models can be used, for example the method of average cutting coefficients identification. This method allows you to predict cutting forces in milling for a cutting tool - workpiece pair, and requires only a very short test. However, the coefficients identified in such a test are only applicable to that combination of tool and workpiece. The use of a few other mechanistic models will also be demonstrated.

In order to identify the dynamic characteristics of machine tool structures, tap tests are conducted with dedicated impact hammers and sensors. This manual will show you how to conduct hammer test experiments, judge the measured data, and identify important properties of the transfer function, which is a plot of the frequency-dependent behaviour of the machine tool.

When the Frequency Response Function (FRF) of the machine tool (machine tool dynamics) and the cutting coefficients (cutting mechanics) are identified, we can use CutPro to determine chatter free cutting conditions via simulations in frequency and time domain. The manual will show you how to verify the simulated results experimentally and how stable and unstable cutting conditions can be identified using different sensors. It will also be shown how CutPro can be used to design special, variable pitch milling cutters for cutting difficult to cut, thermal resistant alloys.

## 2 Modeling of Cutting Forces

In order to conduct offline process planning by simulation, we need to be able to predict the cutting forces that will occur in the actual machining process. From cutting force measurements, cutting coefficients can be determined for different types of cutting force models, which will allow us to predict the cutting forces for a variety of cutting conditions. This section first discusses cutting force modeling by coefficients determined from orthogonal cutting experiments, and the orthogonal to oblique transformation that uses these coefficients to predict forces in oblique cutting processes. The chapter concludes with a mechanistic cutting force model, called “average cutting force coefficients”, which is a practical method, used in milling.



## 2.1 Orthogonal cutting coefficients

The big advantage of cutting coefficients determined from simple orthogonal cutting experiments is that one can predict the cutting forces for any oblique tool geometry and any cutting condition, machining the identified workpiece material. The transformation of the cutting coefficients from orthogonal cutting experiments to cutting coefficients for a specific oblique cutting geometry is called the “orthogonal to oblique transformation”. This cutting force coefficient model can be used for predicting cutting forces in milling, turning, boring, and drilling. The simple orthogonal cutting tests are conducted on a lathe for each workpiece material.

These coefficients are determined by measuring the cutting forces for different feedrates in turning tubular workpieces with a tool without inclination angle or chip breaker grooves, and with a flat rake face. The oblique cutting tools, for which the forces are to be predicted, usually contain a range of rake angles and therefore you need to conduct experiments with a few different rake angles that cover the range used. The cutting coefficients will therefore be a function of the rake angle and uncut chip thickness (i.e. feed rate). The cutting coefficients can be dependent on the cutting speed as well, and you should also measure a range of cutting speeds. The number of experiments can thus become large:

$n_h \times n \times n_v = \text{number of feedrates} \times \text{number of rake angles} \times \text{number of cutting speeds}$ , which means that if you use 6 different values for each parameter, you end up conducting 216 experiments.

### 2.1.1 Experimental setup: Determination of orthogonal cutting force coefficients

The experimental identification of orthogonal cutting coefficients is conducted as follows:

- Set up a tube on a lathe. The tube wall thickness is the width of cut in this orthogonal cutting process and may be 0.0787” ( $b = 2.00\text{mm}$ ). Use a turning tool with a zero inclination angle and a flat rake face without any chip breaker. It is best to grind tools from carbide blocks. Select the cutting speed which will be most used on your production floor. You can repeat the tests at different speeds if necessary.
- Measure the average cutting forces from the tube turning operation by using a cutting force dynamometer, and collect the chips for each test separately. Make sure that the force data and chips are collected when the tool is fully engaged in the part. Avoid considering the chips and forces when the tool is at the entry or exit state. Save the chips in separate envelopes for each test. Mark them with the corresponding test conditions (rake angle, feed rate, width of cut, cutting speed and material).
- For each cutting speed and rake angle you need to measure the cutting forces for a few different feedrates.
- After the cutting experiments you select 3-4 chips from each test, which should be as flat and as long as possible. Measure the total length of these chips in [mm], and write the total chip length on the envelope. Measure the total weight of these chips on a scale and write the total weight in [gram] also on the envelope.
- Use the Excel template file called “[Orthogonal Template](http://www.malinc.com/Documents/Orthogonal_template.xls)” ([http://www.malinc.com/Documents/Orthogonal\\_template.xls](http://www.malinc.com/Documents/Orthogonal_template.xls)). This template allows you to process measurement data for one rake angle, cutting speed and workpiece material.

Enter the feed rates, corresponding measured total chip length, total chip weight and cutting force data in tangential and feed direction. The template will calculate the average of the measured data and plot those values in the plot “Average orthogonal cutting forces”. Enter the edge force intercepts, which are automatically displayed on the line fit graph in the Excel template.



The experimental setup is shown in Figure 2.1 with the directions of the tangential and feed forces.

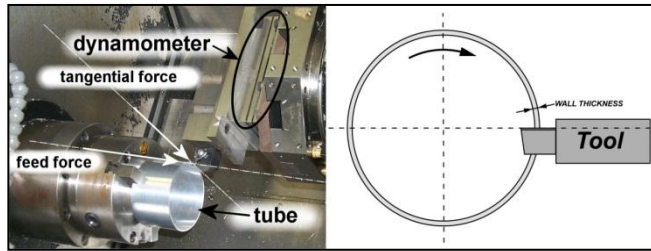


Figure 2.1: Experimental setup for determination of Orthogonal Cutting Coefficients

A typical measurement of the cutting forces for one feedrate is displayed in Figure 2.2

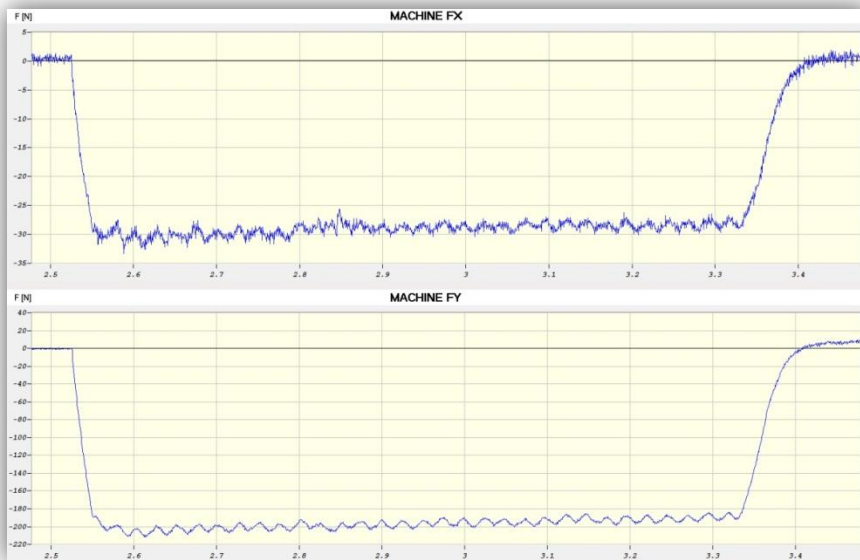


Figure 2.2: Tangential and Feed Force versus Time to determine Orthogonal Cutting Parameters

The cutting forces should be constant, but will always show small variations in time. The feed force and tangential force, schematically shown in Figure 2.3, are measured with the dynamometer and the data is collected with a PC using MALDAQ. For each cutting condition, 1000 data points for each of the two channels are collected by sampling at 1000 Hz for a period of 1 second. The cutting conditions that are used in this example are shown in table 1. The data can then be loaded into Excel (you will have two columns with each 1000 values) and Excel determines the average of the measurement values. These average values are also shown in table 2.1.

Table 2.1: Cutting conditions and resulting average forces for orthogonal cutting coefficient identification test for one cutting speed and rake angle: AL 7050-T7451

Rake 8 1500 m/min					
Test No:	Feed Rate $h$ [mm/rev]	Chip Length [mm]	Chip Weight [gr]	Measured $F_t$ [N]	Measured $F_f$ [N]
1	0.050	87.85	0.0362	101.08	32.68
2	0.075	76.34	0.0445	140.31	35.49
3	0.100	131.30	0.0997	175.45	39.06
4	0.125	157.34	0.1477	213.87	41.99
5	0.150	168.06	0.1868	250.51	41.17
6	0.175	83.04	0.1041	282.60	36.82
7	0.200	33.46	0.0470	313.40	34.24

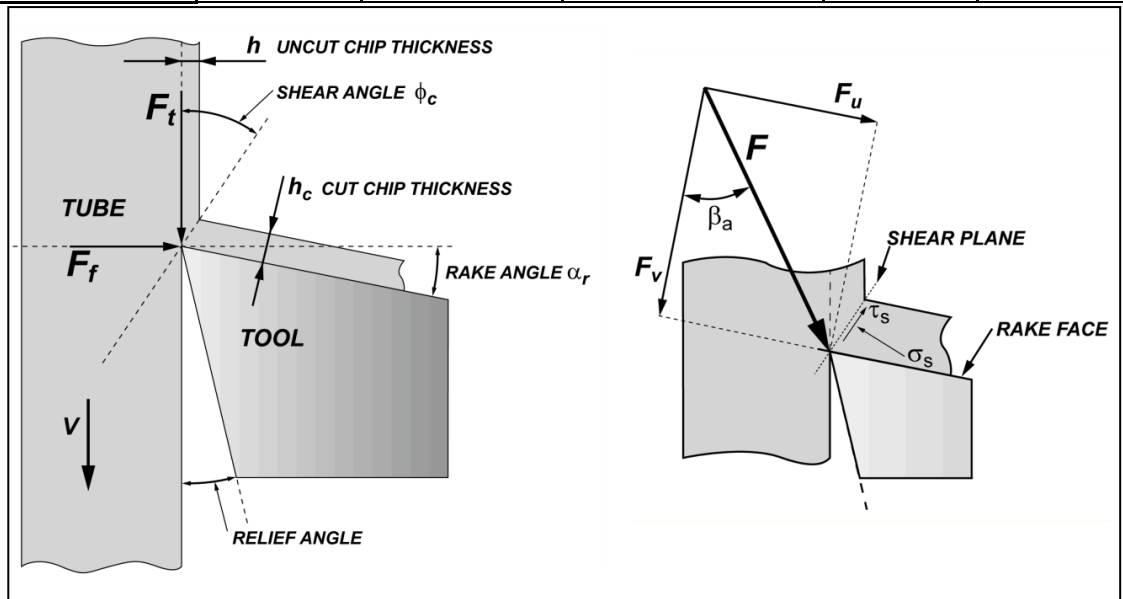


Figure 2.3: Schematic diagram of orthogonal cutting, showing feed  $F_f$  and tangential  $F_t$  forces

In the left part of Figure 2.3 the tangential force  $F_t$  and the feed force  $F_f$ , which are measured with the dynamometer, are shown.  $V$  is the cutting speed and  $h_c$  is the uncut chip thickness. The tool is characterized by its rake angle  $\alpha_r$  and the relief angle. The cut chip thickness  $h_c$  and the shear angle  $\phi_c$  will be determined from the geometry of the chips.  $F$  is the cutting force acting on the tool, which can be broken down into the force normal to the rake face  $F_v$ , which makes the friction angle (*ie.* with the cutting force  $F$ , and the friction force acting along the rake face  $F_u$ . The shearing process taking place on the shear plane is characterized by the shear stress  $\tau_s$  along the shear plane and the normal stress  $\sigma_s$  normal to the shear plane.

The associated forces are the normal force  $F_n$  and the shear force  $F_s$  and are shown in Figure 2.4.

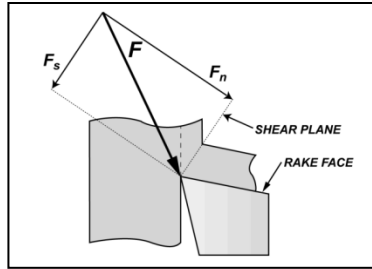


Figure 2.4: Cutting force  $F$  broken down in the components normal force  $F_n$  and shearing force  $F_s$

Figure 2.5 shows a complete set of average values, determined from seven measurements plotted in Excel.

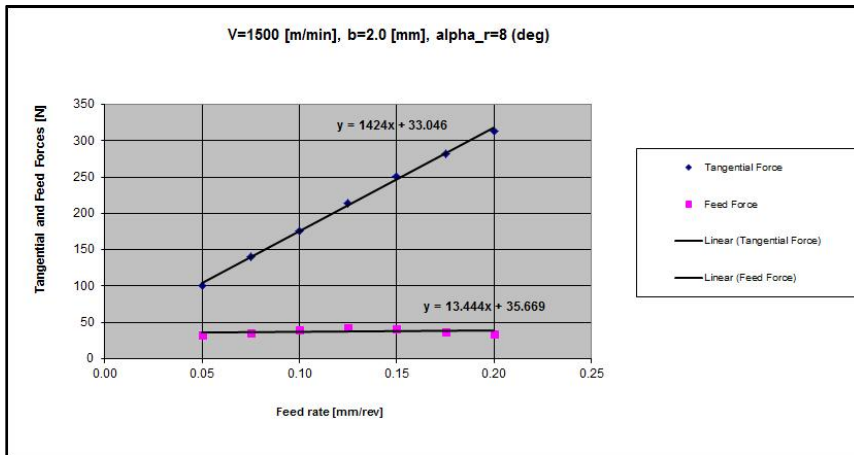


Figure 2.5: Orthogonal Test Results

In orthogonal cutting the uncut chip thickness  $h$  equals the feed per revolution  $c$ . We fit lines passing through the average value points, and these lines will give an average experimental relation between uncut chip thickness  $h$  /the feed  $c$  [mm / rev] and the Tangential and Feed Force. The lines are expressed through the following equations [1]:

Tangential Force:  $F_t = F_{tc} + F_{te} = K_{tc}bh + K_{te}b$

Feed Force:  $F_f = F_{fc} + F_{fe} = K_{fc}bh + K_{fe}b$

Where  $K_{tc}b$  and  $K_{fc}b$  are the slopes of the lines for tangential and feed forces, respectively.

$K_{te}b$  and  $K_{fe}b$  are the edge forces in tangential and feed directions, respectively, and  $b$  is the width of cut. Edge forces are created by the friction between the clearance face of the tool and the finished surface; hence they are not dependent on the feed rate. The edge forces do not contribute to the shearing of the material. The tangential and feed forces can therefore be expressed as follows:

Tangential Force:  $F_{tc} = F_t - F_{te} = K_{tc}bh$

Feed Force:  $F_{fc} = F_f - F_{fe} = K_{fc}bh$

They are expressed in this manner such that the edge forces do not contribute to the shearing. The tangential and feed forces are linearly dependent on the width of cut  $b$ . From there, the cutting coefficients are found:

$$\begin{aligned} \text{Shearing coefficients :} \quad & \frac{F_{tc}}{h} = K_{tc}b, \quad K_{tc} = \frac{F_{tc}}{bh} \quad ; \quad \frac{F_{fc}}{h} = K_{fc}b, \quad K_{fc} = \frac{F_{fc}}{bh} \\ \text{Edge force coefficients:} \quad & F_{te} = K_{te}b, \quad K_{te} = \frac{F_{te}}{b} \quad ; \quad F_{fe} = K_{fe}b, \quad K_{fe} = \frac{F_{fe}}{b} \end{aligned}$$

Figure 2.6 shows the fitted lines and the average value points, and the expressions  $F_t = 1424h + 33.046$  and  $F_f = 13.444h + 35.669$ . Appendix A describes how to fit these lines to the measurement points using Excel. The edge force for the tangential face is 33.046N and the edge force on the feed face is 35.669N.

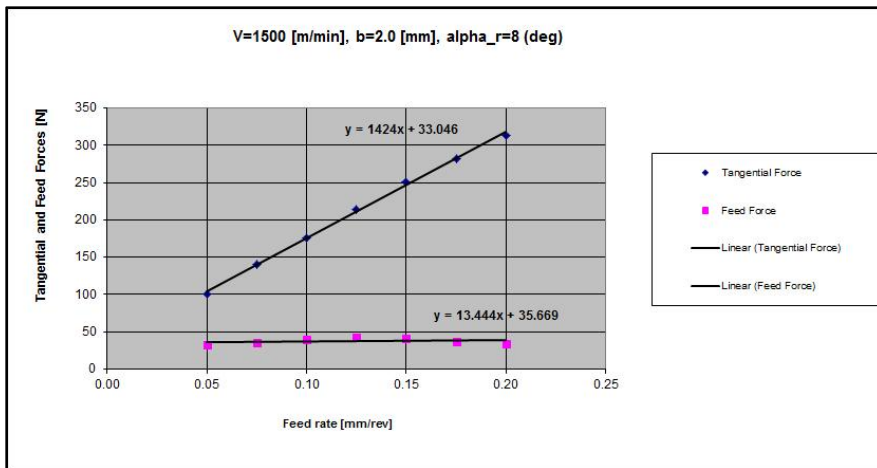


Figure 2.6: Fitted lines for Tangential and Feed Force

Excel shows the expression for the feed and tangential force in the form  $y = ax + b$ . In this case:

$$\begin{aligned} \text{Tangential Force:} \quad & F_t = 1424h + 33.046 \quad K_{tc}b = 1424 \quad K_{te}b = 33.046 \\ \text{Feed Force:} \quad & F_f = 13.444h + 35.669 \quad K_{fc}b = 13.444 \quad K_{fe}b = 35.669 \end{aligned}$$

The parameter in this dataset is the feedrate  $c$  [mm/rev], which corresponds to  $h$  here. All measurements are taken for one width of cut  $b$ , which is the wall thickness of the hollow cylinder. Thus in order to find the cutting coefficients, we have to divide the coefficients  $K_{tc}$ ,  $K_{te}$ ,  $K_{fc}$  and  $K_{fe}$  by the width of cut  $b$ , as follows:

$$\begin{aligned} F_{te} = K_{te}b & \quad K_{te} = 33.046/2 = 16.52 \text{ [N/mm}^2\text{]} \\ F_{fe} = K_{fe}b & \quad K_{fe} = 35.669/2 = 17.83 \text{ [N/mm}^2\text{]} \\ \frac{F_{tc}}{h} = K_{tc}b & \quad K_{tc} = 1424/2 = 711.98 \text{ [N/mm}^2\text{]} \\ \frac{F_{fc}}{h} = K_{fc}b & \quad K_{fc} = 13.444/2 = 6.72 \text{ [N/mm}^2\text{]} \end{aligned}$$



### 2.1.2 Determination of friction angle, shear angle and shear stress

The cut chip thickness  $h_c$  [mm] is estimated from the length and weight of a few chips, as it is difficult to measure accurately. Take a few chips that are as flat and as long as possible.

The cut chip thickness is determined from  $h_c = \frac{m}{bl_c\rho}$ , where:

- $\rho = 0.00283$  [grams/mm<sup>3</sup>] (the specific density of the material)
- $b = 2.000$  [mm] (the width of cut or wall thickness of the tube)
- $l_c$  [mm] (the total length of the chips)
- $m$  [grams] (the total weight of the chips)

Chip ratio ( $r_c$ ), friction angle ( $\beta_a$ ), shear angle ( $\phi_c$ ) and shear stress ( $\tau_s$ ) are determined from the following expressions derived from the geometry of the orthogonal cutting:

- $F_{fc} = F_f - F_{fe}$  (the feed cutting force equals the feed force minus the feed edge force)
- $F_{tc} = F_t - F_{te}$  (the tangential cutting force equals the tangential force minus the tangential edge force)
- $F_c = \sqrt{F_{tc}^2 + F_{fc}^2}$  (the cutting force equals the square root of the sum of the squared cutting components)
- $r_c = \frac{h}{h_c}$  (the chip ratio: the ratio of the uncut chip thickness  $h$  and the cut chip thickness  $h_c$ )
- $\beta_a = \alpha_r + \tan^{-1} \frac{F_{fc}}{F_{tc}}$  (the average friction angle equals the sum of the rake angle and the arctan of  $\frac{F_{fc}}{F_{tc}}$ )
- $\phi_c = \tan^{-1} \frac{r_c \cos(\alpha_r)}{1 - r_c \sin(\alpha_r)}$  (the shear angle is determined from the chip ratio  $r_c$  and the rake angle  $\alpha_r$ )
- $\tau_s = \frac{F_c \sin(\phi_c + \beta_a - \alpha_r)}{bh}$  (the shear stress is determined from  $F_c$ ,  $\phi_c$ ,  $\beta_a$  and  $\alpha_r$ )

$h_c$ ,  $\alpha_r$ ,  $b$  are the cut chip thickness, rake angle, and width of cut, respectively. Note that the edge forces are subtracted from the measured forces before orthogonal cutting parameters are evaluated, as the edge forces do not contribute to the shearing.

The Excel template automatically calculates the shear angle, friction angle and shear stress from the measured chip length, weight, average tangential force, average feed force, and chip thickness, for each cutting condition. The calculation results are shown in table 2.2. For the cutting force model, we will use the average value of the shear angle, friction angle, and shear stress.

Table 2.2: Calculated cutting forces, friction angle, cut chip thickness, chip ratio, shear angle, and shear stress

Feed Rate h [mm/rev]	Chip Length [mm]	Chip Weight [gr]	Measured Ft [N]	Measured Ff [N]	Chip Thickness hc [mm]	Chip Ratio rc	Shear Angle phi_c (deg)	Friction Angle beta_a (deg)	Shear Stress tau_s [MPa]
0.0500	87.85	0.0362	101.08	32.68	0.0728	0.6868	36.9421	25.9186	367.4687
0.0750	76.34	0.0445	140.31	35.49	0.1030	0.7282	38.7461	22.1960	363.9115
0.1000	131.30	0.0997	175.45	39.06	0.1342	0.7454	39.4740	20.5507	351.5641
0.125	157.34	0.1477	213.87	41.99	0.1659	0.7537	39.8213	19.1079	351.8951
0.150	168.06	0.1868	250.51	41.17	0.1964	0.7638	40.2434	17.3322	354.4963
0.175	83.04	0.1041	282.6	36.82	0.2215	0.7901	41.3184	15.4218	354.5795
0.200	33.46	0.0470	313.4	34.24	0.2482	0.8059	41.9510	14.2336	351.3244
					Average	0.75	39.79	19.25	356.46

Thus the orthogonal cutting parameters are found to be:

- Average shear angle,  $\phi_c$  ..... 39.79 [Degrees]
- Average friction angle,  $\beta_a$  ..... 19.25 [Degrees]
- Average shear stress,  $\tau_s$  ..... 356.46 [MPa]



### 2.1.3 Orthogonal to Oblique Transformation Method

In orthogonal cutting, the material is removed by a cutting edge that is perpendicular to the direction of relative tool-workpiece motion (see both Figures 2.3 and 2.7). The orthogonal cutting resembles a shaping process with a straight tool whose cutting edge is perpendicular to the cutting velocity  $V$ . A metal chip with a width of cut  $b$  and a depth of cut  $h$  is sheared away from the workpiece with velocity  $V_c$ . In orthogonal cutting, the cutting is assumed to be uniform along the cutting edge, and it can therefore be represented by a two-dimensional plane strain deformation process, as shown in Figure 2.3 and 2.4. The cutting forces are exerted only in the directions of the velocity  $V$  and the uncut chip thickness  $h$ , which are called tangential and feed forces. In oblique cutting, the cutting edge is oriented with an inclination angle  $i$  and the additional third force acts in the radial direction:  $F_r$ , as shown in Figure 2.7.

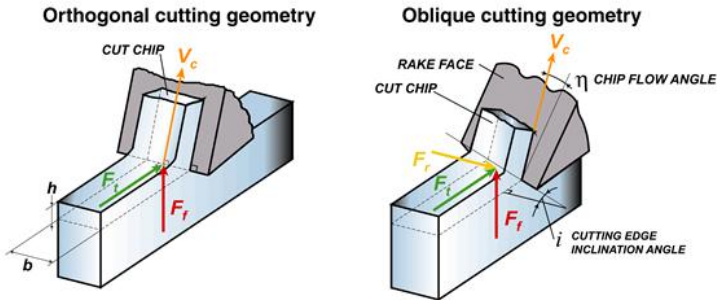


Figure 2.7: Schematic representation of orthogonal and oblique cutting geometry

When the orthogonal cutting parameters  $(\phi_s, \beta_a, \tau_s)$  are determined from orthogonal cutting experiments, as described in the above, oblique cutting forces can be predicted by the following steps [1].

First, the following assumptions are made:

- The orthogonal shear angle is equal to the normal shear angle in oblique cutting,  $\phi_c \equiv \phi_n$
- The normal rake angle is equal to the rake angle in orthogonal cutting,  $\alpha_r \equiv \alpha_n$
- The chip flow angle is equal to the oblique angle,  $\eta \equiv i$
- The friction coefficient  $\beta_a$ , and shear stress  $\tau_s$  are the same in both orthogonal and oblique cutting operations for a given cutting speed, chip load, and tool-work material pair.

Calculate the normal friction angle as follows,

$$\beta_n = \tan^{-1}(\tan\beta_a \cos \eta), \quad \text{where } \eta \text{ is the oblique angle}$$

Predict the cutting forces using the oblique cutting constants:

$$K_{tc} = \frac{\tau_s}{\sin(\phi_\eta)} \frac{\cos(\beta_n - \alpha_n) + \tan(i) \tan(\eta) \sin(\beta_n)}{\sqrt{\cos^2(\phi_n + \beta_n - \alpha_n) + \tan^2(\eta) \sin^2(\beta_n)}}$$

$$K_{fc} = \frac{\tau_s}{\sin(\phi_c) \cos(i)} \frac{\sin(\beta_n - \alpha_n)}{\sqrt{\cos^2(\phi_n + \beta_n - \alpha_n) + \tan^2(\eta) \sin^2(\beta_n)}}$$

$$K_{rc} = \frac{\tau_s}{\sin(\phi_\eta)} \frac{\cos(\beta_n - \alpha_n) \tan(i) - \tan(\eta) \sin(\beta_n)}{\sqrt{\cos^2(\phi_n + \beta_n - \alpha_n) + \tan^2(\eta) \sin^2(\beta_n)}}$$

### Example:

Consider a cutter with a 30° oblique angle, a 8° rake angle and AL 7050-T7451 workpiece material. We can perform the orthogonal to oblique transformation method for data collected, as the rake angle is the same. In this case we have determined the cutting coefficients for one rake angle. A complete model requires tests for a range of rake angles, and we can then find cutting coefficients which are a function of the rake angle. Tangential, feed and radial force coefficients can be calculated using the above formulas and they are found to be:

$$\beta_n = \tan^{-1}[\tan(\beta_a) \cos(\eta)] = \tan^{-1}[\tan(19.25)\cos(30)] = 16.83^\circ$$

$$K_{tc} = \frac{356.46}{\sin(39.79)} \frac{\cos(16.83 - 8) + \tan(30) \tan(30) \sin(16.83)}{\sqrt{\cos^2(39.79 + 16.83 - 8) + \tan^2(30)\sin^2(16.83)}} = 886.08 \text{ [MPa]} = 128.52 \text{ [ksi]}$$

$$K_{fc} = \frac{356.46}{\sin(39.79)\cos(30)} \frac{\sin(16.83 - 8)}{\sqrt{\cos^2(39.79 + 16.83 - 8) + \tan^2(30)\sin^2(16.83)}} = 144.79 \text{ [MPa]} = 21.0 \text{ [ksi]}$$

$$K_{rc} = \frac{356.46}{\sin(39.79)} \frac{\cos(16.83 - 8) \tan(30) - \tan(30) \sin(16.83)}{\sqrt{\cos^2(39.79 + 16.83 - 8) + \tan^2(30)\sin^2(16.83)}} = 329.48 \text{ [MPa]} = 47.787 \text{ [ksi]}$$

The edge cutting coefficients are considered to be the same as those found from orthogonal cutting experiments, and the radial component of the edge force is assumed to be zero (i.e.,  $K_{re} = 0$ ). Since the depth of cut is the same for all conditions, the edge cutting forces are constant, and they are obtained as the following.

$$F_{te} = 33.046 \text{ [N]} = 7.429 \text{ [lbf]} \quad F_{fe} = 35.669 \text{ [N]} = 8.019 \text{ [lbf]} \quad F_{re} = 0.0 \text{ [N]} = 0.0 \text{ [lbf]}$$

## 2.2 Average cutting force coefficients for milling

In order to create a complete set of orthogonal cutting parameters, a lot of tests have to be conducted, and this is obviously costly and time-consuming. Instead, we can conduct a small series of experiments with different feedrates, but constant depth of cut and full immersion (slotting). From these measurements, average cutting force coefficients can be calculated, which are valid for that specific combination of tool and workpiece only. The Average Cutting forces ( $\bar{F}_x$ ,  $\bar{F}_y$ ,  $\bar{F}_z$ ) in milling can be defined as a function of cutting conditions [1] ( $a$  = depth of cut,  $c$  = feed per tooth) and the cutting constants ( $K_{rc}$ ,  $K_{re}$ ,  $K_{tc}$ ,  $K_{te}$ ,  $K_{ac}$ ,  $K_{ae}$ ):

$$\bar{F}_x = -\frac{Na}{4}K_{rc}c - \frac{Na}{\pi}K_{re} \quad \bar{F}_y = \frac{Na}{4}K_{tc}c + \frac{Na}{\pi}K_{te} \quad \bar{F}_z = \frac{Na}{\pi}K_{ac}c + \frac{Na}{2}K_{ae}$$

$N$  is the number of teeth on the cutter. The subscripts  $r$ ,  $t$ , and  $a$  correspond to the radial, tangential and axial force coefficients, respectively. Please note that the radial direction in milling corresponds to the feed direction in turning and the axial direction in milling corresponds to the radial direction in turning. Thus, the average cutting force is expressed by a linear function of the feed rate  $c$ , with slope  $K_c$  and an offset contributed by the edge forces  $K_e$ .



### 2.2.1 Measurement Setup

In order to determine the average cutting force coefficients, we measure the cutting forces during slotting cuts with a dynamometer for different feedrates. Depending on the type of the workpiece material and cutting conditions, different width of cuts can also be employed. The test setup is as follows:

- Use a small workpiece and clamp it rigidly to the dynamometer
- Make sure the dynamometer is clamped rigidly to the table
- Measure the cutting forces at a stable depth of cut and at a low cutting speed
- Collect cutting forces for a full number of revolutions.

The workpiece mass and clamping determine the bandwidth of the dynamometer-workpiece combination. The tooth passing frequency should be kept low (well within the bandwidth) in order to stay within the linear region of the measurement system. The experimental setup is shown in Figure 2.8

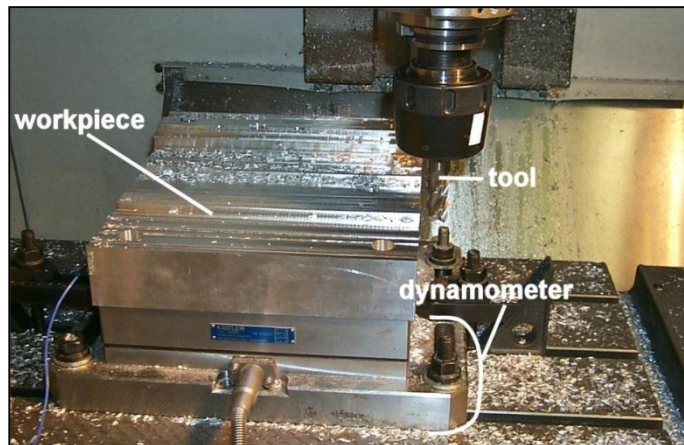


Figure 2.8: Average cutting force coefficients measurement setup

A typical measurement of a two-fluted cutter is shown in Figure 2.9. In the plot you can see a peak in the force for each flute, and the height of the peaks is not the same because of runout errors on the tool. From this plot, the tooth passing frequency can be identified: one tool revolution equals 0.09s and in this period two teeth enter the workpiece.

The number of teeth that enters the workpiece in one second equals the tooth passing frequency:

$$\frac{2 \text{ teeth}}{0.09\text{s}} = \frac{22.22 \text{ teeth}}{\text{s}} = 22.22\text{Hz} \text{ (for this case)}$$

The tooth passing frequency can also be calculated directly from the spindle speed and the number of teeth:

$$2 \frac{\text{teeth}}{\text{rev}} \times 700 \frac{\text{rev}}{\text{min}} = 23.3\text{Hz}$$

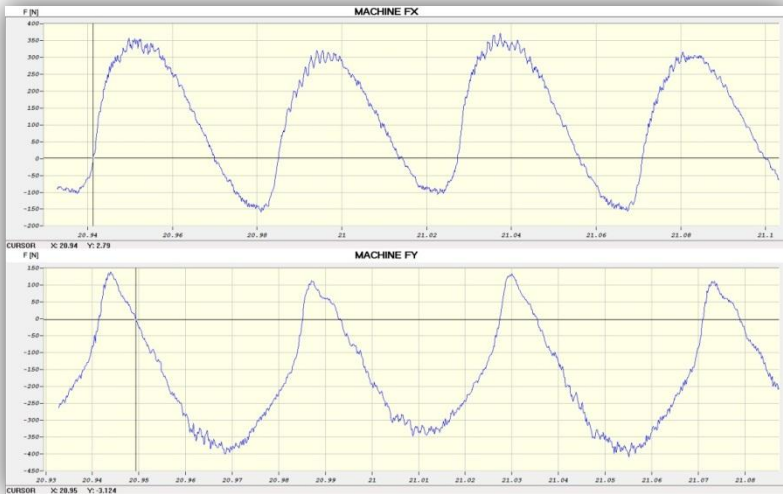


Figure 2.9: Typical Cutting Force Measurement Example (for 2 revolutions of the cutter)

### 2.2.2 Calculating the Average Cutting Force Coefficients

After collecting the cutting forces for five or more different feedrates, the data files can be used in CutPro to identify the average cutting force coefficients. CutPro will calculate the average cutting forces in X, Y and Z directions from the measurement data and from the corresponding feedrates and the depth of cut used, it will calculate the average cutting force coefficients. Appendix B covers the procedure used to identify the average cutting coefficients in CutPro. The output results for average cutting force identification are shown in Figure 2.10. The influence of the runout of the tool is eliminated by considering an exact number of spindle revolutions.

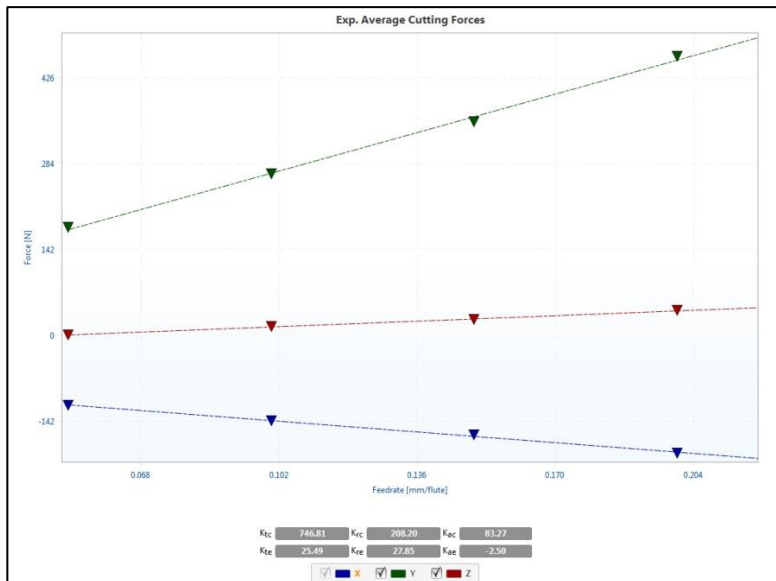


Figure 2.10: Average Cutting Force Identification in CutPro; Outputs: Graph and coefficients

### 2.2.3 Simulation of cutting forces in milling using Average Cutting Force Coefficients

From the identified parameters, the forces can be simulated. Figure 2.11 shows the simulation results for the measurement shown in Figure 2.9. For this simulation, the machine tool is assumed to be very rigid, and the tool is assumed to be perfect (no runout at all). In the simulation, the helix angle of the tool has to be entered in CutPro, as the cutting forces depend on it. This is an example of a “Single Time Domain Simulation” and Appendix C discusses how to run such a simulation in CutPro. It is also possible to take the runout of the tool into account in CutPro. The runout measured at the tip of the tool is as follows: 5, 0 microns[ $\mu m$ ]. Figure 2.12 shows the comparison between the measured forces and the simulated forces, where the runout has been taken into account. Measuring the runout and using in the simulation will increase the accuracy of cutting force prediction in CutPro (see blue curve difference).

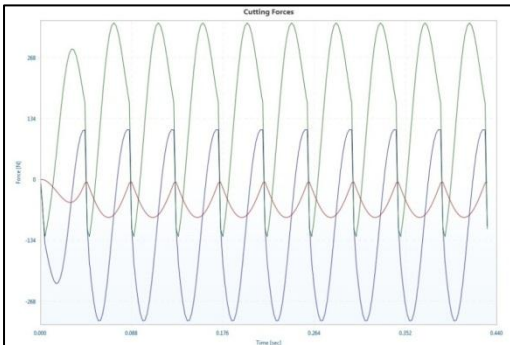


Figure 2.11: Forces Simulated in CutPro for similar measurement shown in figure 2.9

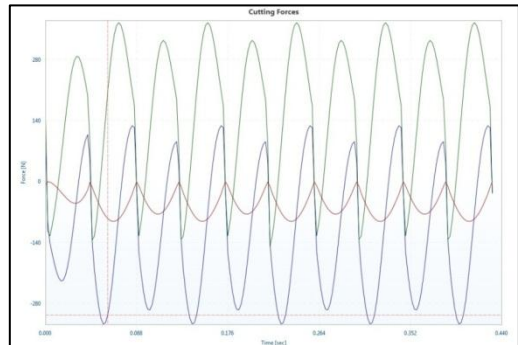


Figure 2.12: Comparison between measured and simulated cutting forces, runout taken into account

### 2.2.4 Fourier spectrum of cutting forces

After modifying the number of revolutions to a greater number (5 to 20) and looking at the Fourier spectrum, we can deduct useful information about the (in)stability of the cut, as we will discuss later. In Figure 2.13, the Fourier spectrum of the predicted cutting forces is shown. The algorithm used to calculate the Fourier spectrum is the Fast Fourier Transform, abbreviated as FFT. This simulation assumes a perfect tool, and the spectrum shows the tooth passing frequency (23.3Hz) and several harmonics (46.6Hz, 69.9Hz, and other multiples of 23.3Hz). Figure 2.14 shows the Fourier spectrum of the simulated forces with the runout taken into account. The simulation now shows a very good agreement with the Fourier spectrum of the measured cutting forces, which are shown in Figure 2.15.

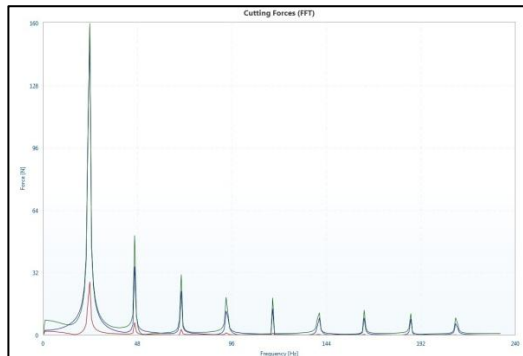


Figure 2.13: Fourier spectrum of simulated cutting forces in X, Y & Z direction (without runout)



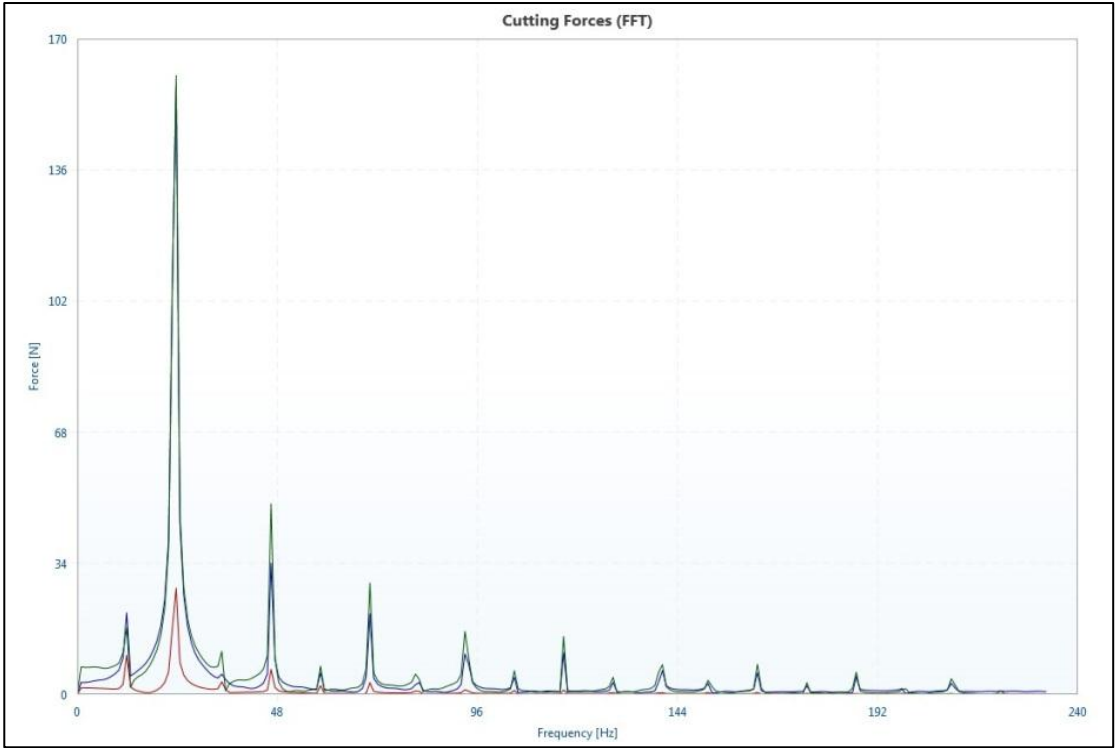


Figure 2.14: Fourier spectrum of simulated cutting forces in X, Y & Z direction (with runout)

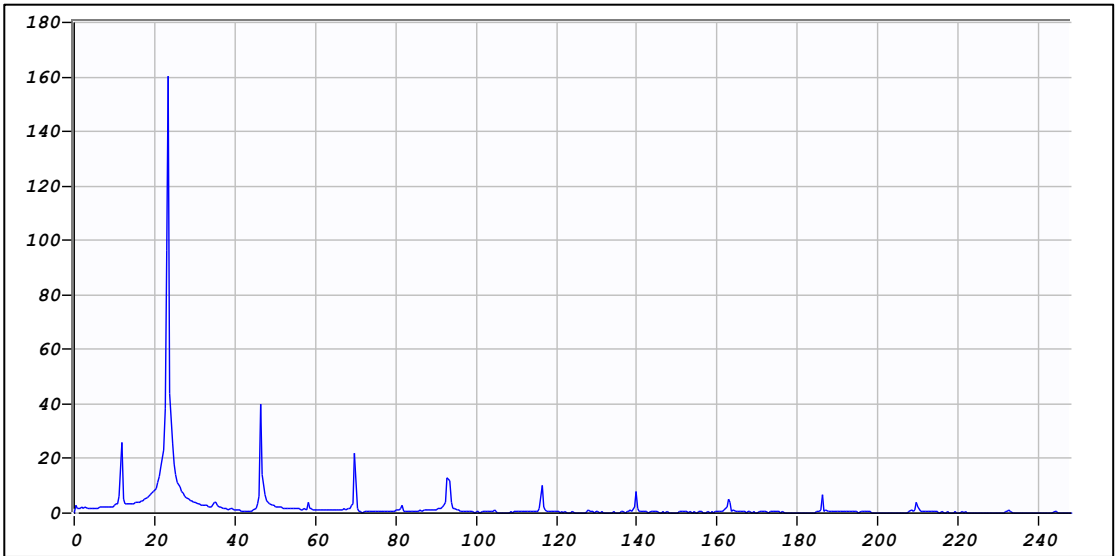


Figure 2.15: Fourier spectrum of recorded cutting forces in Y direction (spindle has runout)

### 3 Machine tool dynamics, tap testing

The dynamics of a machine tool structure needs to be measured in order to predict the maximum stable depth of cut as a function of spindle speed. The machine tool dynamics are determined from a so-called tap test (hammer test). In the tap test, the machine tool structure is excited by hitting it with an impulse force hammer. This impact will excite the structure over a certain frequency range, depending on the size of the hammer, the type of tooltip used, and the structure itself. The hammer tip, the mass of the hammer, and the velocity of the hammer will determine the energy transmitted to the structure by the impact and thus they also determine the magnitude of the exciting force. The structure will show a response after the impact, which characterizes (a part of) the dynamics of the structure. This response can then be measured using a displacement sensor, a velocity sensor, or an accelerometer. The dynamic characteristics are determined by combining the Fourier-spectrum of both the impact force measurement and the displacement/accelerometer measurement. When using an accelerometer, the signal needs to be integrated twice in frequency domain, in order to get the displacement. The signal from a velocity sensor needs to be integrated once. The combination of these two measurements results in the Frequency Response Function (FRF), also called Frequency Response Function (FRF). The FRF is a plot of the dynamic stiffness in [N/m, lbf/in] of the structure as a function of frequency [Hz].

#### 3.1 Machine tool dynamics in milling

In milling machine tools, the dynamic behaviour of the spindle-toolholder-tool system (SHT) is usually the limiting factor for the machining process. The SHT system is the most flexible component in the process. We therefore need to model the machine tool as being flexible. In some applications, such as thin wall machining, the product itself may be the limiting factor and then you should also conduct a tap test for the workpiece. The workpiece should then also be modeled as being flexible.

In milling the machine tool structure is generally flexible in all three X, Y and Z directions. However, in milling applications where endmills are used, we usually only need to consider the flexibility in the X-Y plane (two directions), because the flexibility in Z-direction is much smaller (the stiffness in Z-direction is much higher). In this case we can neglect the dynamic behaviour in Z-direction. In this case we have to measure the FRF in two directions (X and Y) for the prediction of the dynamic behaviour. However, in heavy face milling operations, the flexibility in Z-direction may be of the same order of magnitude as the flexibility in the X-Y plane and then we must take this flexibility into account as well. We then need to measure the FRF in three directions.

#### 3.2 Measurement setup

When a laser displacement sensor is used to measure the transfer function, we need to align the sensor with the axis to be measured. The relief face of the tool is usually used to identify the FRF and we need to orient the tool so that the laser beam is reflected on this relief surface. We will hit the relief face on the other side of the tool. It is important to let the hammer hit the tool with as perfect an alignment as possible with the axis measured. Of course there will always be some errors involved in this procedure. If you are using a tool with an uneven number of teeth, we will not have two teeth opposite to each other, and we will need to use a different measurement location for the sensor or a different location for the hammer to excite the structure.



The measurement setup with a laser displacement sensor is shown in Figure 3.1. The dashed line shows the direction of the hit. In this case the FRF is determined for the tip of the tool in X-direction. If we use an accelerometer to measure the transfer function, the procedure is similar, the only difference is that we need to mount the accelerometer on the tool using special wax (which comes with the accelerometer). The measurement setup is shown in Figure 3.2.

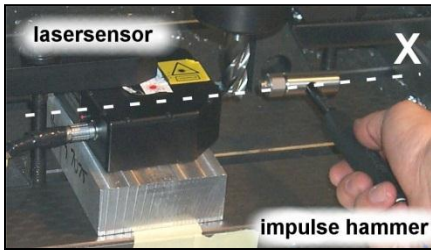


Figure 3.1: Measurement setup with laser displacement sensor

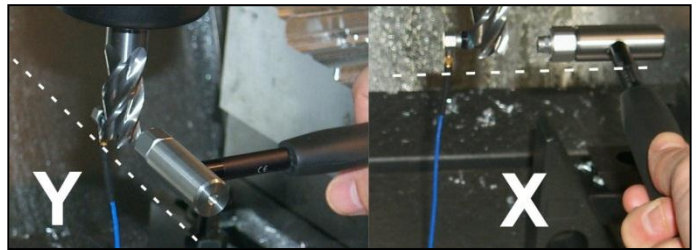


Figure 3.2: Measurement setup/or FRF measurement with accelerometer

### 3.3 Hammer selection

The frequency range that can be excited by a hammer is inversely proportional to the contact time of the impact. The frequency range which can be excited properly by the hammer is also dependent on the type of tip used. The tip influences the contact time and the contact force. In order to get a good dynamic characterization of the structure (FRF), we need to excite the structure in the frequency range of interest with an appropriate force. Thus we should know the characteristics of the forces exciting the structure in advance. Table 3.1 shows parameters and variables taken into account when exciting frequencies. Figure 3.3 shows the detailed influence of tip selection on the excitation force versus time graph for three tip types.

	HARD TIP (Short Impact)	SOFT TIP (Long Impact)	ADDED MASS	LARGE HAMMER	SMALL HAMMER
FREQUENCY RANGE	Long	Short	Shortened	Large Components of Machine: Low Frequency	Small Components of Machine: Higher Frequency
FREQUENCY EXCITATION	Good for High Frequencies	Good for Low Frequencies	Increased		
EXCITED STRUCTURE	Hard & Stiff	Flexible	Varies		

Table 3.1: Hammer Selection Parameters

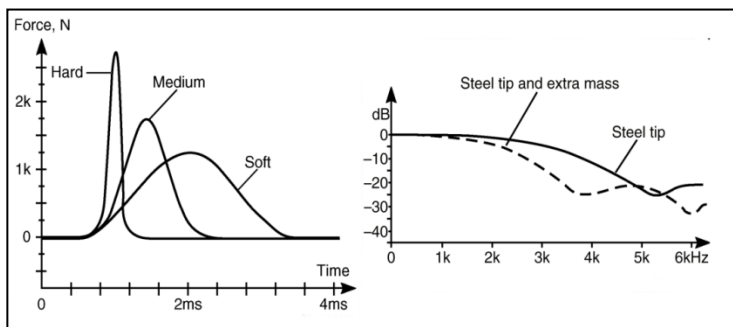


Figure 3.3: Influence of tip selection and additional mass on force change and frequency content of the excitation

Always look at the Fourier spectrum of the hammer signal during tap tests and identify which frequency range is excited.

Figure 3.4 shows the range of some of the impact hammers at the Manufacturing Automation Lab with some important specifications (maximum excitation bandwidth and force). The very big hammer can be used for tap testing of feeddrives and large structures. The smaller ones are used to conduct hammer tests in milling applications. The hammer sensitivities are given in table 3.2.

Figure 3.4: Impact hammers at the Manufacturing Automation lab

Table 3.2: Hammer sensitivities

Hammer model	Configuration	Sensitivity [mV/N]
PCB 086D80	Steel tip	22.2
	Steel tip, with extender	24.8
	Vinyl tip	19.7
	Vinyl tip, with extender	20.2
Kistler 9722A2000	Steel tip 9902A	2.13
	Nylon tip (white) 9904A	2.13
PCB 086C05	Steel tip	0.22
	Plastic/nylon, with & without extender	0.22
PCB 086C41	Any tip, without extender	0.24



The frequency spectrum for the Kistler hammer with different tip types is shown in Figure 3.5. The Kistler catalogue lists a maximum excitation bandwidth of 9300Hz, but the bandwidth is specified for a drop in excitation amplitude of 10dB, which corresponds to a signal drop of 70%, which is quite large. A more common bandwidth criterion is the -3dB crossing, which for the steel tip occurs at just over 5000Hz. The curve is flat up to 2000 Hz.

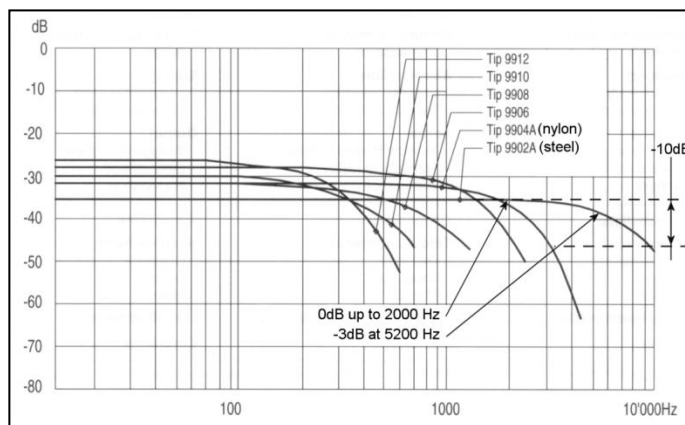


Figure 3.5: Frequency excitation chart for the Kistler 9722A2000 model impulse hammer with tips

### 3.4 Displacement sensor/accelerometer selection

Displacement sensors are desirable to obtain good static and low frequency measurements. Capacitance- or inductance-type displacement pickups can be used, but laser displacement and other optical sensors are usually easier to mount on a machine tool. Also, the face of the tool that is used to determine the FRF does not need to be flat for a laser or optical displacement sensor in order to achieve a good linearity, as the beam is very small. A displacement sensor is characterized by its measurements range, resolution, and the sample rate of its electronics.



The displacements which are measured during a tap test are very small, and thus the measurement range should be small. The resolution should be as high as possible in order to capture the vibrations accurately. The sampling rate should also be high in order to get enough measurement points during a test. In general, displacements are smaller for higher frequencies, and it is therefore difficult to accurately measure vibrations over a wide frequency range using a displacement sensor.

The use of accelerometers is more common in vibration measurement and for TF measurement it is very practical. The mass and the frequency range of the accelerometer need to be selected properly, because the accelerometer mounted on the structure acts as an extra mass and may alter the frequency characteristics of the system. If we use very small endmills (for example, 6 or 8 mm diameter) the accelerometer should weigh less than 0.5grams. The bonding and interface materials between the structure and accelerometer must also be selected carefully in order to obtain accurate measurements. These materials have to transmit the vibration of the structure properly. Common bonding materials are petro-wax and locktite. Table 3.3 lists some important characteristics of the sensors available at MAL.

Table 3.3: Characteristics of sensors at MAL (note: not all are listed)

<b>Accelerometer model</b>	<b>Frequency range [Hz]</b>	<b>Mass (gram)</b>	<b>Sensitivity [mV/g]</b>	<b>Measurement range [g]</b>
PCB 353B11 S/N 9690	1 ... 10000	2	5.48	1000
PCB 353B11 S/N 65847	1 ... 10000	2	5.23	1000
PCB 353B31 S/N 68836	1 ... 5000	20	51.2	100
Kistler 8702B500 S/N C128797	0.5 ... 10000	10	10.09	500
Kistler 8630A50 S/N C82836	0.5 ... 7000	5	100	50
Kistler 8628B5 S/N C121339	0.5 ... 2000	6.7	1010	5
<b>Displacement sensor model</b>	<b>Frequency range [Hz]</b>	<b>Mass (gram)</b>	<b>Sensitivity [mV/m]</b>	<b>Measurement range [m]</b>
Dynavision LTS 2.9	1 ... 50000Hz	n.a.	5000000	0.00145

### 3.5 Evaluation of the FRF

In order to minimize errors during the tap testing, we always recommend taking several measurements, and average them. After each hit, you should examine the signals to identify whether it was a good hit. A hit is considered bad if a multiple hit occurred (the hammer bounces, loses contact and hits the structure again), this is called “bouncing”; or when you hit the wrong spot on the tool (you have to see that yourself). A bounce can easily be detected and it is automatically rejected by MALTF or ShopPro. When enough good hits are collected, they are automatically averaged, and we examine the result. First, the power spectra of the signals will give us important information. The frequency spectrum of the hammer signal will tell us which frequency range was excited during the test. It will also give the amplitude of the excitation force. For increasing frequency, the spectrum will drop to zero. We only use the part where the signal is 50% or more of the signal at zero frequency. In calculating the transfer function, the frequency spectrum of the displacement signal (or acceleration integrated twice, velocity integrated once) is divided by the frequency spectrum of the hammer. Dividing by a very small value of hammer excitation will give erroneous Frequency Response Function results.



As mentioned above, an accelerometer signal needs to be integrated twice and a velocity signal once. Each integration involves dividing the signal by the frequency, for acceleration, the signal is divided by the frequency squared. For very low frequencies, thus dividing the signal by the frequency squared will lead to very high values, for zero frequency it will give infinity. For a displacement sensor, no integration is necessary. Accelerometers, velocity and displacement pickups have an upper frequency limit, which should also be taken into account.

For a displacement sensor, we can use the frequency range from zero up to the lowest of the bandwidths of either the hammer signal or the sensor. The bandwidth of the displacement sensor is specified in the technical data. If we use an accelerometer, the upper frequency bandwidth is determined in the same manner. The lower bandwidth is determined from the frequency where it crosses the x-axis in the FRF-plot.

### 3.6 Example of Frequency Response Function identification

In this example, we will show the use of the different hammers and sensors to clarify how to conduct a tap test, and how to judge the results from the measurement data and spectra. Throughout the examples, keep in mind that tap tests need to be done in both the Feed (x, blue) direction and the Normal (y, red) direction. All explanations below will only concentrate on values in the feed direction (x, blue). For these examples we will measure the FRF of a four-fluted solid carbide end mill, and an HSK63A shrinkfit toolholder which can be found in Figure 3.6.

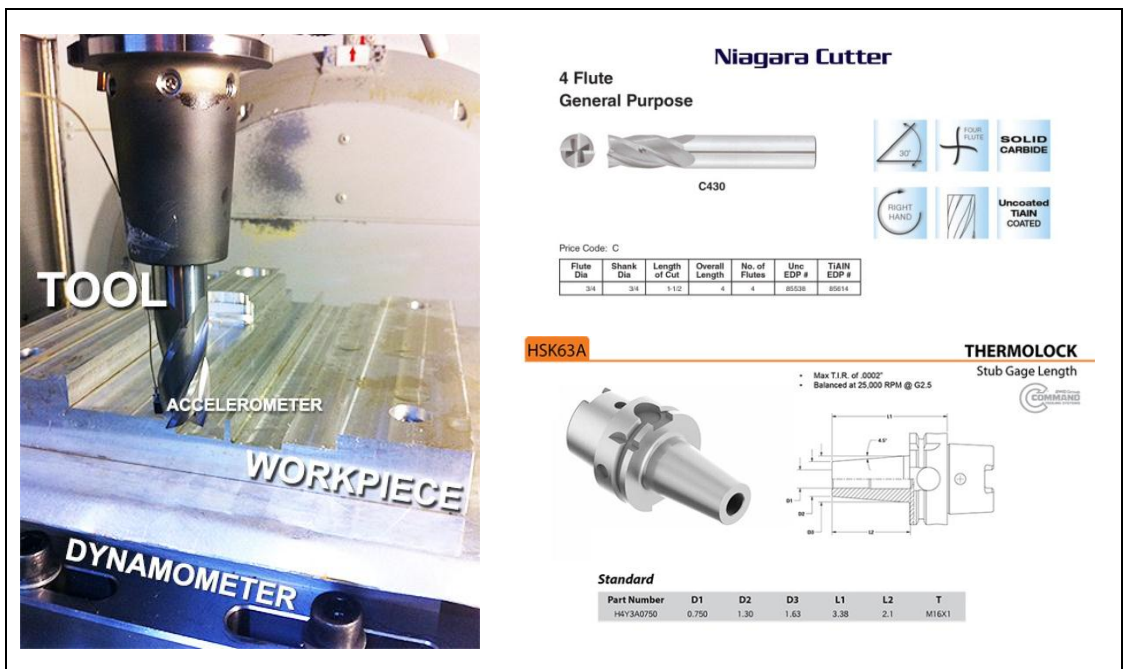


Figure 3.6: Test Setup Geometry, and Tooling Properties (dynamometer not required for tap test)

The machine used for these tap tests was performed on a Mori Seiki NMV5000 DCG milling center. The first test is conducted with the Endevco 2302-10 hammer (2.38 mV/N sensitivity) using an Aluminum tip, and an Endevco 25B accelerometer (4.801 mV/g sensitivity). After the tap test is performed, we must analyse the measured frequency response function.

Figure 3.7 shows the signals in time domain. Since we are looking at the X direction (blue), we note that the impulse lasts for about 0.0006s, the vibration at the tool tip is almost zero after 0.018s on the graph. The signal of the hammer shows no second hit, and therefore no bouncing has occurred. In this Figure, blue lines show the tap test in X direction of the machine and red line shows the measurement in Y direction.

Figure 3.8 shows the coherence of the measurement. Ideally it is best to have a straight line along a value of “1” to ensure a good measurement, but this is not always possible. More information on this issue will be discussed further in the section.

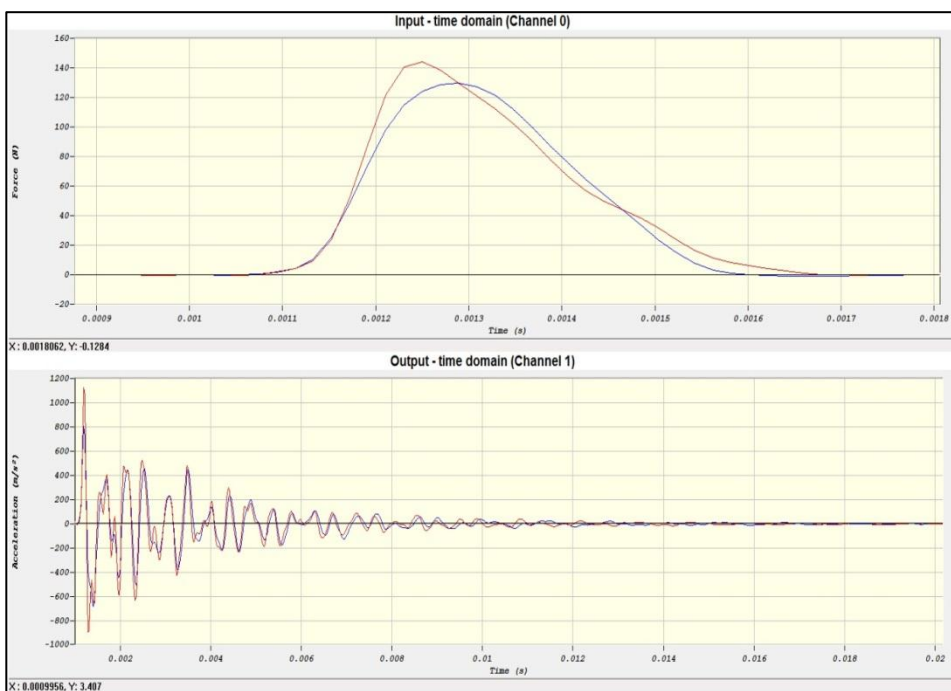


Figure 3.7: Time responses of tap test with Endevco Hammer (metal tip) and Endevco Accelerometer

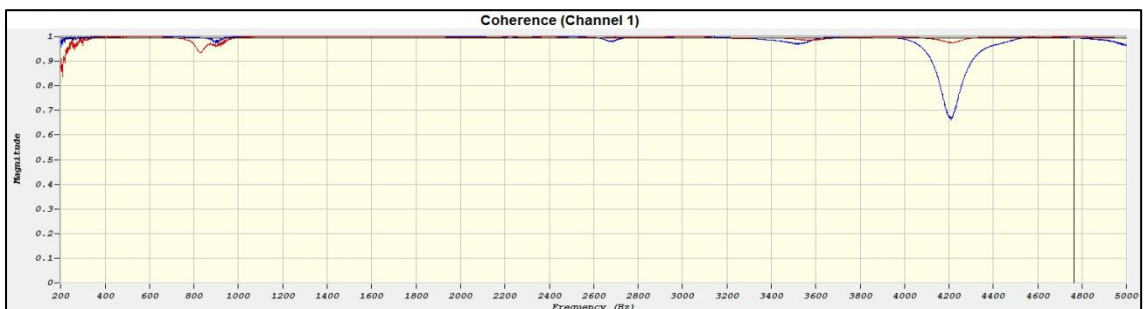


Figure 3.8: Coherence of tap test with Endevco Hammer (metal tip) and Endevco Accelerometer



Once we have assured a proper measurement, we must identify the range of frequencies to which our measurements are accurate. This is done by looking at the input power spectrum, and identifying the frequency at which the power falls to 20% of the original value. In Figure 3.9, we notice this drop occurs at around 2600 Hz. We then look at the output spectrum, the magnitude, and the phase, which are found in Figures 3.9 & 3.10 to identify weak points in the structure.

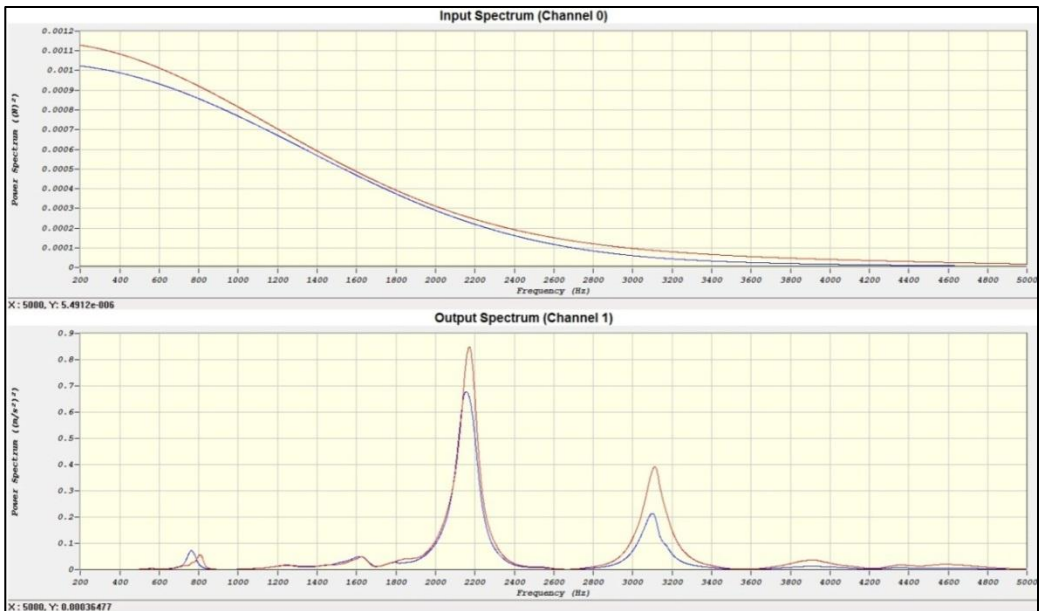


Figure 3.9: Power spectra of tap test with Endevco Hammer (metal tip) and Endevco Accelerometer

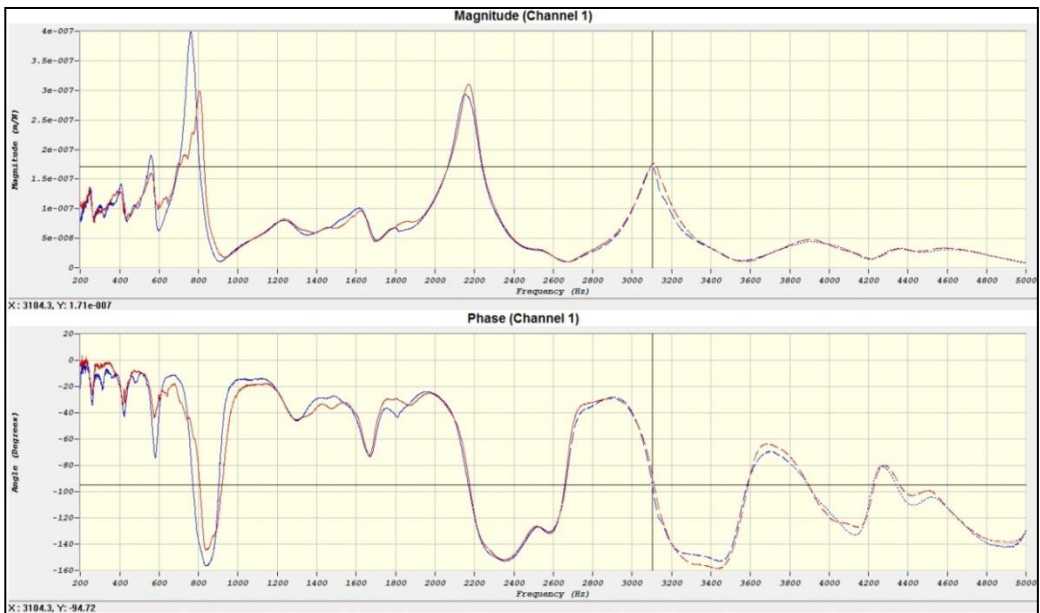


Figure 3.10: Transfer function; Magnitude-Phase; Tap test with Endevco Hammer (metal tip) and Endevco Accelerometer

Notice the dashed/dotted lines which occur past 2600 Hz: this warns the user that the input power has dropped significantly; hence we cannot fully excite these denoted structural modes past 2600 Hz. In the “Magnitude” graph, we notice three large peaks (770, 2150, and 3100 Hz), which represent the weakest points of our structure. Lower frequencies represent high masses, and on the contrary, higher frequencies represent low masses. The dashed lines occur at the 3100 Hz (which could be considered a higher frequency dependant on the situation), so we should keep this frequency in mind as a critical location in our analysis. The best measurement (although physically impossible) would be to taptest directly across the tool, with an excellent ( $I$ ) coherence, and an input spectrum of infinity ( $\infty$ ). Lastly we can observe the real & imaginary parts of the FRF shown in Figure 3.11, which is simply used to calculate the magnitude.

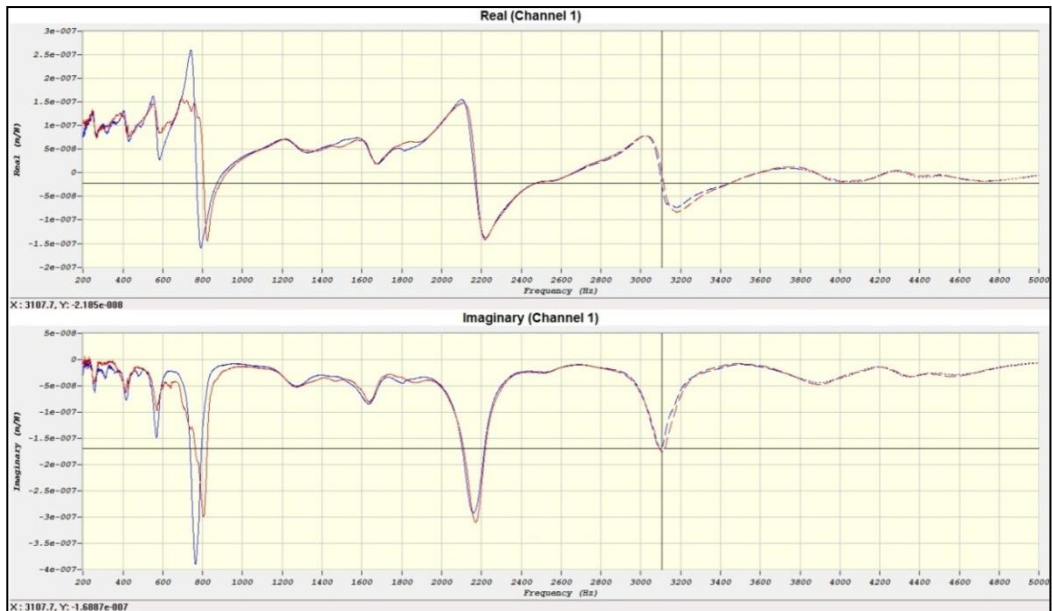


Figure 3.11: Transfer function; Real-Imaginary parts; Tap test with Endevco Hammer (metal tip) and Endevco Accelerometer

Next, we will use the very same tool & machine setup, but replace the metal tip of the hammer with a nylon tip. The time responses are shown in Figure 3.13 and the coherence are displayed in Figure 3.12.

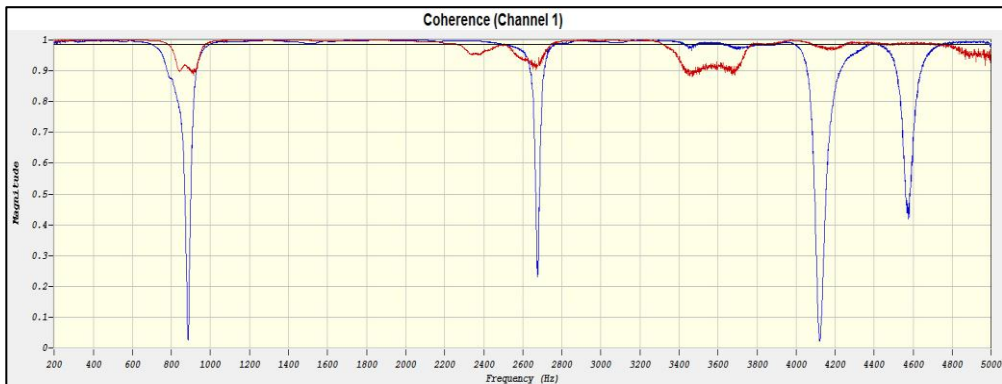


Figure 3.12: Coherence of tap test with Endevco Hammer (nylon tip) and Endevco Accelerometer

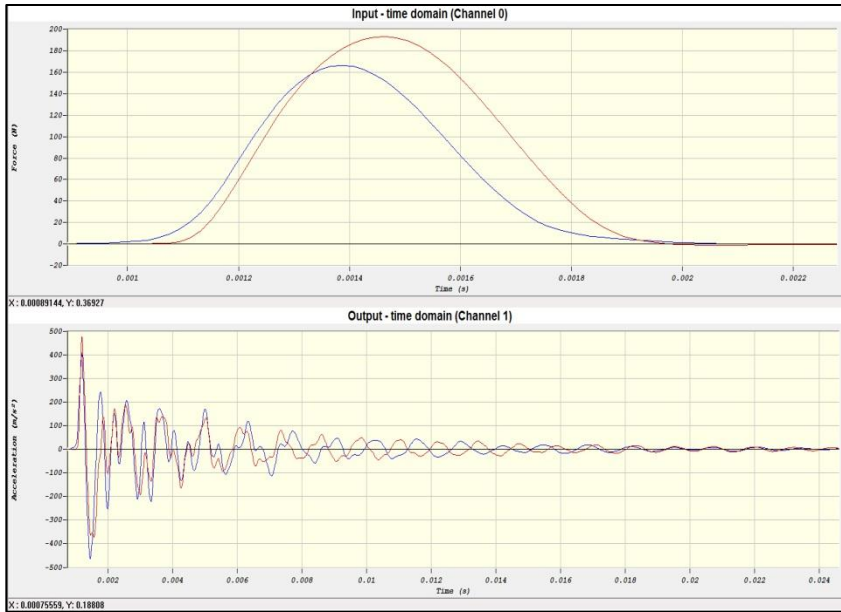


Figure 3.13: Time responses of tap test with Endevco Hammer (nylon tip) and Endevco Accelerometer

Similarly to the metal tip, the nylon tip could easily provide a single hit as shown in the force input graph in Figure 3.13. However, notice the problems in our coherence; some frequencies (900, 2700, 4150 and 4600 Hz) drastically show poor measurements (0). Keep these frequency values in mind when analyzing any farther in the frequency response function.

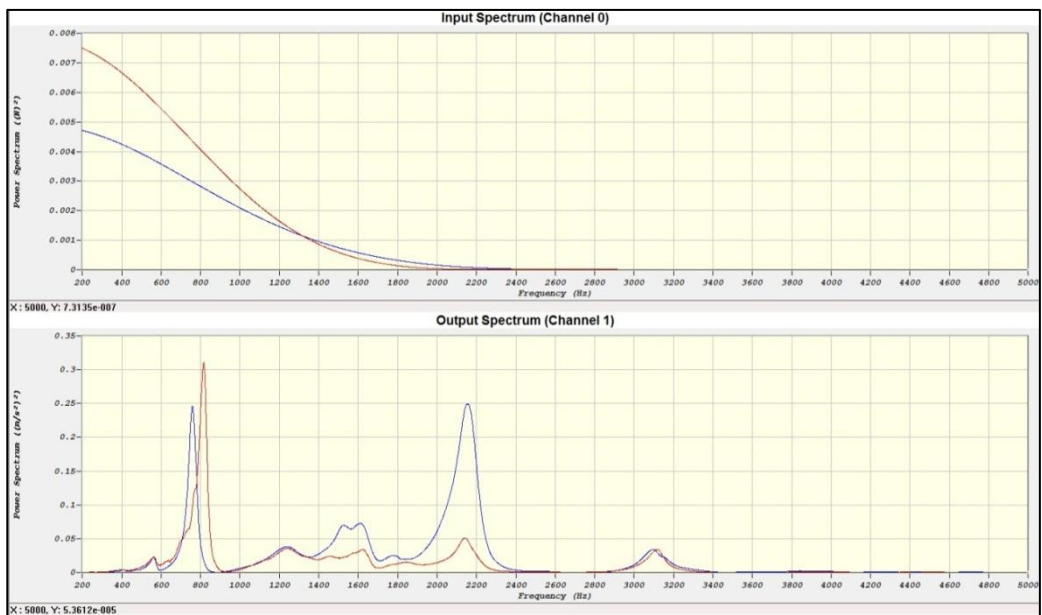


Figure 3.14: Power spectra of tap test with Endevco Hammer (nylon tip) and Endevco Accelerometer

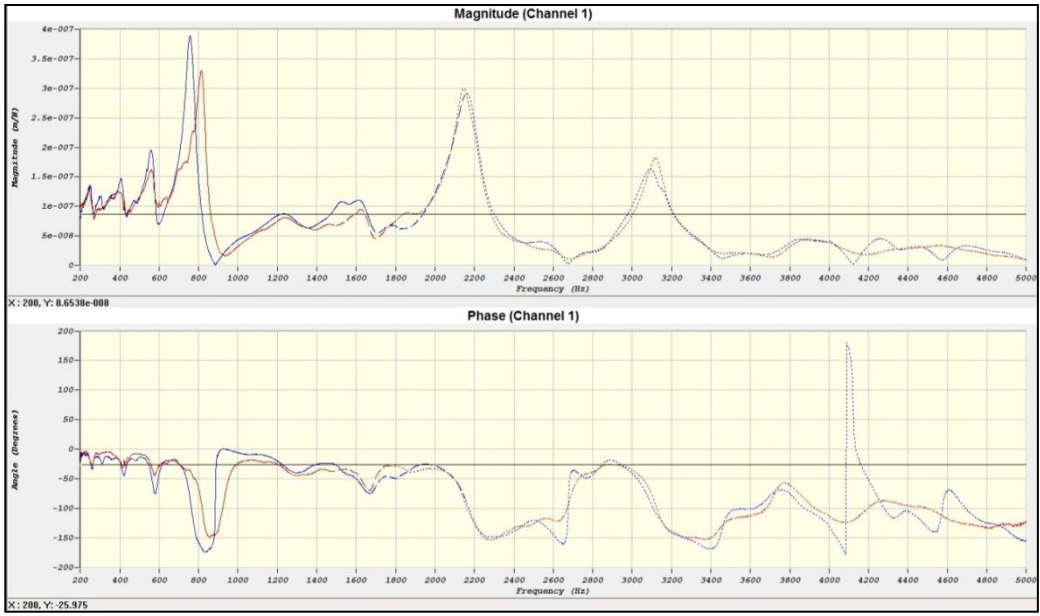


Figure 3.15: Transfer function; Magnitude-Phase; Tap test with Endevco Hammer (nylon tip) and Endevco Accelerometer

Once again, notice the dashed/dotted lines which occur past the 20% input power location (1400Hz). Unlike the metal tip, we were not able to excite higher frequencies. For this specific tool setup, we can now see that using a metal tip on the Endevco hammer is more suitable. The locations of our peaks are somewhat similar, however are not as accurate as those shown in our FRF when using a metal tip for impact.

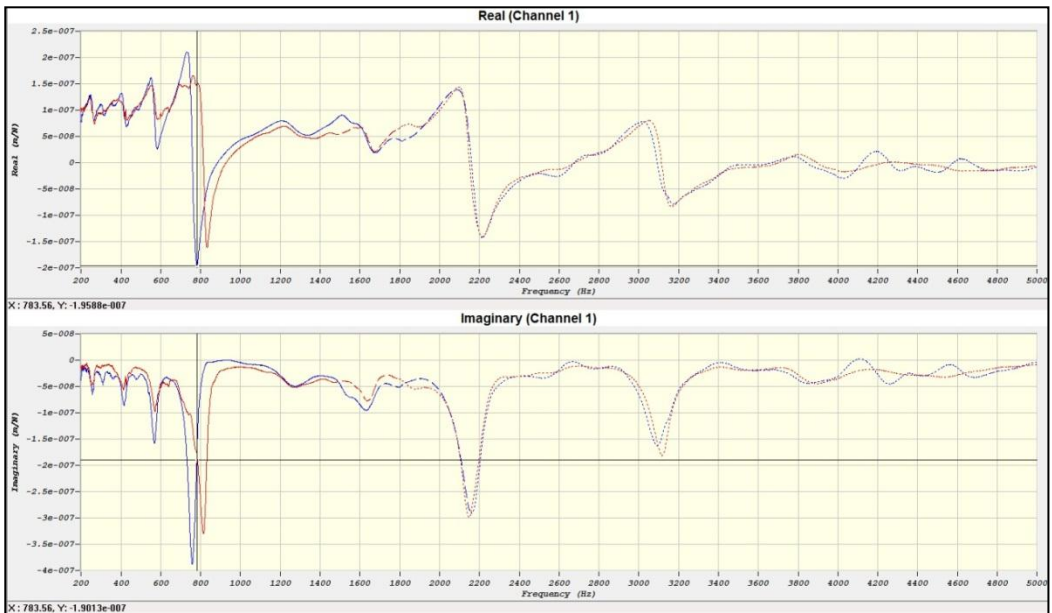


Figure 3.16: Transfer function; Real-Imaginary parts; Tap test with Endevco Hammer (nylon tip) and Endevco Accelerometer

## This brings us to some important points when conducting hammer tests:

- Always ensure a single impact when using an impulse hammer (different tips / hammer size)
- A harder tip is preferred due to its frequency excitation range, however may cause a double hit.
- Figure out the accuracy and range of results
- Understand how measurement accuracies affect the magnitude plot; which directly affects stability lobes.

### Scenario 1 – Metal Tip:

- Good hits (single impact)
- Good coherence
- High frequencies excited in power spectra
- Magnitudes are accurate for highest peaks

### Scenario 2 – Nylon Tip:

- Good hits (single impact)
- Decent coherence
- Low frequencies excited in power spectra
- Magnitudes are not accurate for peaks, except for the first peak.

## 3.7 Converting a FRF into modal parameters

If we want to use the FRF in CutPro Time Domain simulation or Discrete Stability Lobe calculations, we first have to model the FRF mathematically by identifying its modal parameters. In this conversion, we take out the unreliable parts of the FRF by considering only the part between a lower frequency bound and an upper frequency bound. Start the modal analysis module by clicking the “Modal” button in the CutPro toolbar. First, we load the measurement in the modal analysis module by choosing “Select FRF-file” from the file-menu in the modal analysis module. The interface that shows up is shown in Figure 3.17. Location  $z = 0mm$  is chosen as we measured at the tip of the tool. The FRF-type is displacement, as we use the measurement which was taken with an accelerometer which allows displacement measurability. For the Modal Model we choose Real Modes, which is suitable for this application. The frequency range is set to 10-5000Hz, which is ok, as it should always start with a nonzero value. The gain constant is 1, as the sensitivities of the hammer and accelerometer are already taken into account in the measurement. The raw measurement (real part of the transfer function) is shown in Figure 3.18.

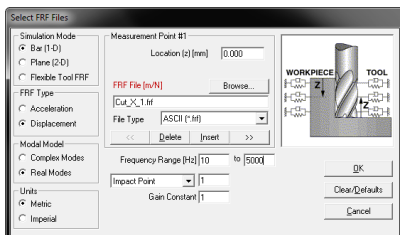


Figure 3.17: Dialogue box in Modal Analysis module

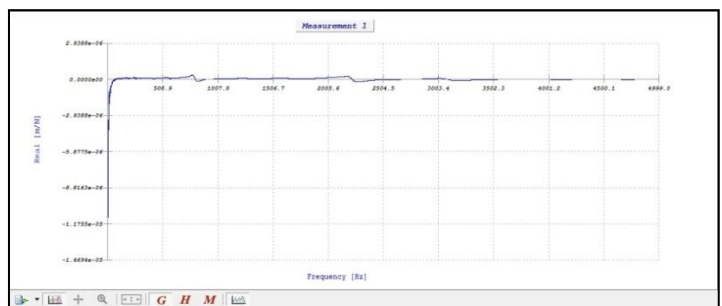


Figure 3.18: Raw data from tap test in modal analysis module

For very low frequency, the value of the TF goes to infinity. This is a phenomenon typical for FRF measurement with an accelerometer, and is generated from noise. We should not include that, as it is physically impossible.

We can use 200Hz as lower boundary here, because the graph should be flat up to this value, reflecting the static stiffness of the system. We can use 5000Hz as the upper boundary; because there are no significant negative peaks in the plot after this frequency and the quality of the data decreases after that (the force gets smaller, and thus the signal to noise ratio). If we adjust the boundaries, the plot will look like Figure 3.19.

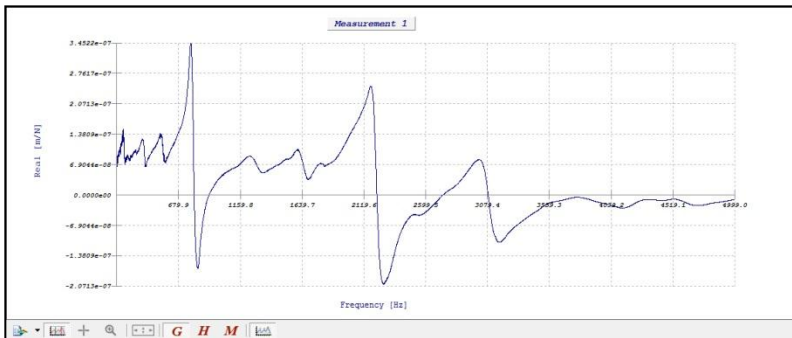


Figure 3.19: Real part of the transfer function, after adjusting upper and lower frequency bound

We then need to select the modes from the Magnitude menu, which are highlighted in gray triangles. This may be done by either clicking the gray triangle modes, or by applying filters and selecting remaining modes. See toolbar in Figure 3.20.

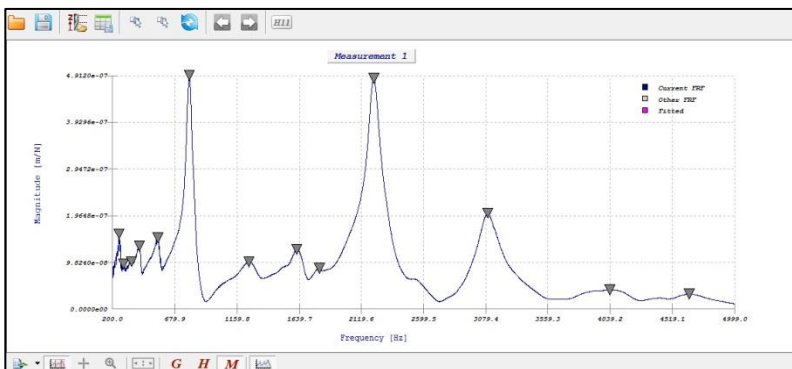


Figure 3.20: Toolbar modal analysis module CutPro

The procedure is illustrated in Figure 3.19 for the real part of the FRF and in Figure 3.20 for its magnitude. For this FRF, we will apply range filters, then select modes, and finally apply a curvefit. There are both vertical and horizontal range filters which may be found as shown. The horizontal filter is applied by clicking on the dark black line on the left of the graph, followed by a drag and release.

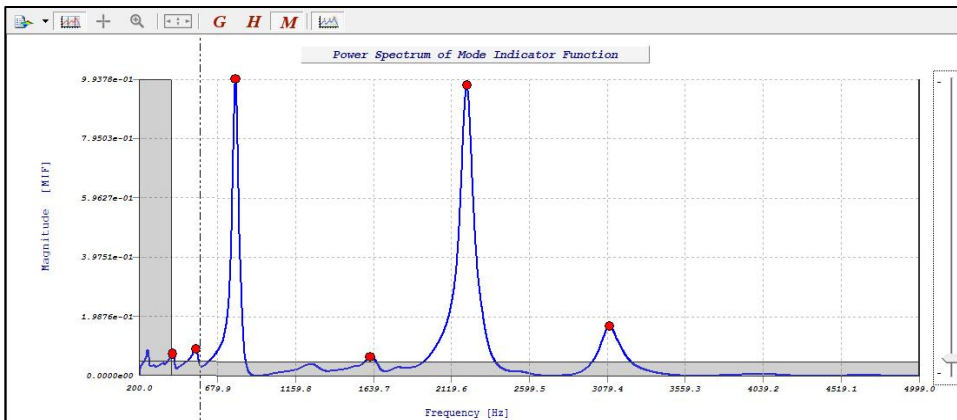


Figure 3.21: Selecting the modes in the modal analysis module, filtering the power spectrum



Figure 3.22: Selecting the modes(1) in the modal analysis module, and applying a curvefit(2) (in magnitude of transfer function) Saving Modal Parameters in modal analysis module (right)

After the selection and curvefit, we let the software optimize the curvefit: the following graph and tables are automatically generated

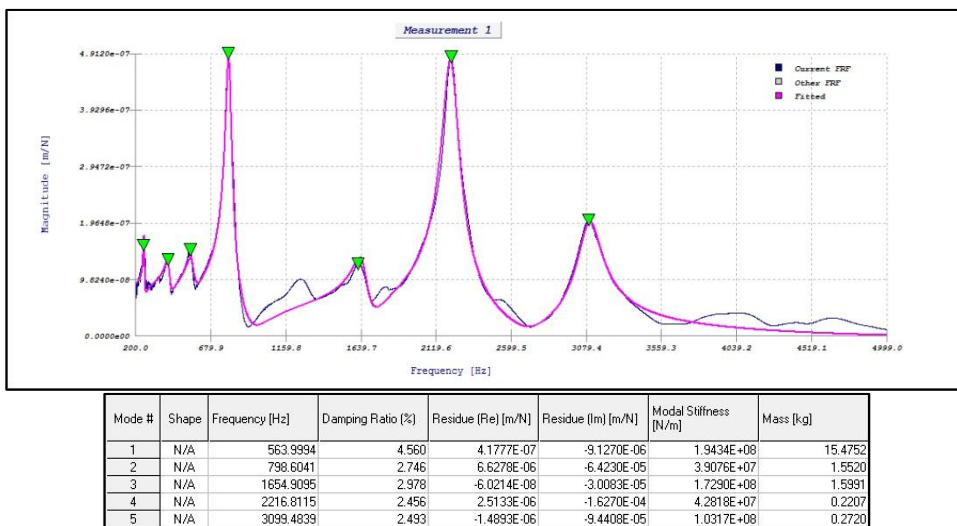


Figure 3.23: Curve fit after optimizing (magnitude of the transfer function)

Once again, this procedure may be done by simply clicking desired modes and then applying the curvefit. Afterwards we select “Save Modal Parameters” from the file menu and store the prepared data in a parameter file, which can be used in CutPro now, as shown in Figure 3.22.

## 4 Chatter stability lobes

Once the cutting coefficients are determined and the FRF has been measured on the machine tool, this data can be used in CutPro software to determine the stability lobes. The chatter stability lobes make up a spindle speed (frequency) dependent dividing line between stable and unstable depth of cut for a certain width of cut. The stability lobes can then be used to determine what the optimal cutting conditions are for the measured configuration. Thus stability lobes allow for an efficient way of selecting optimal conditions instead of trial and error based extensive testing to find good cutting conditions.

### 4.1 Frequency Response Function (FRF) of the machine tool structure

The FRFs measured at the tip of the tool are measured in X and Y directions are shown in Figures 4.1 and 4.2 with fitted curves.

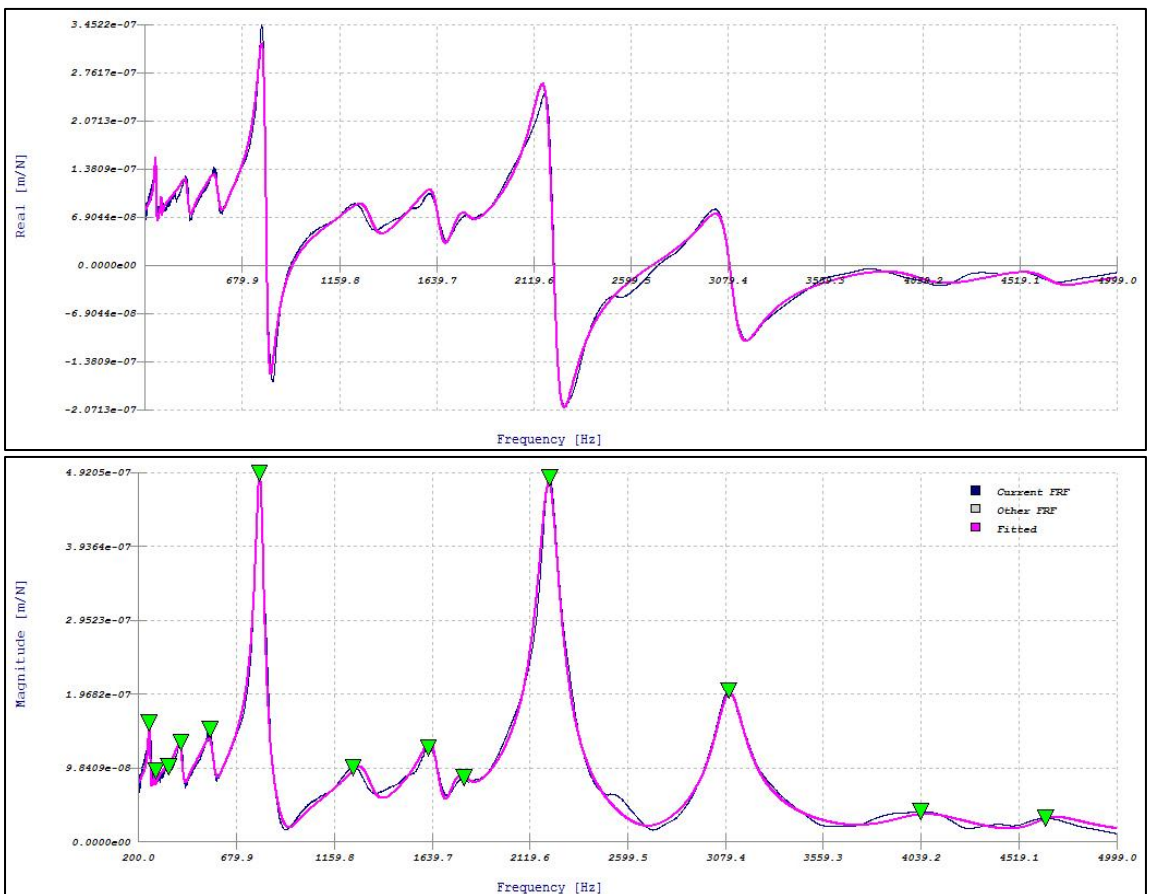


Figure 4.1: Frequency Response Function in X Direction; Endevco 2302-10 hammer (metal tip) & 25B accelerometer

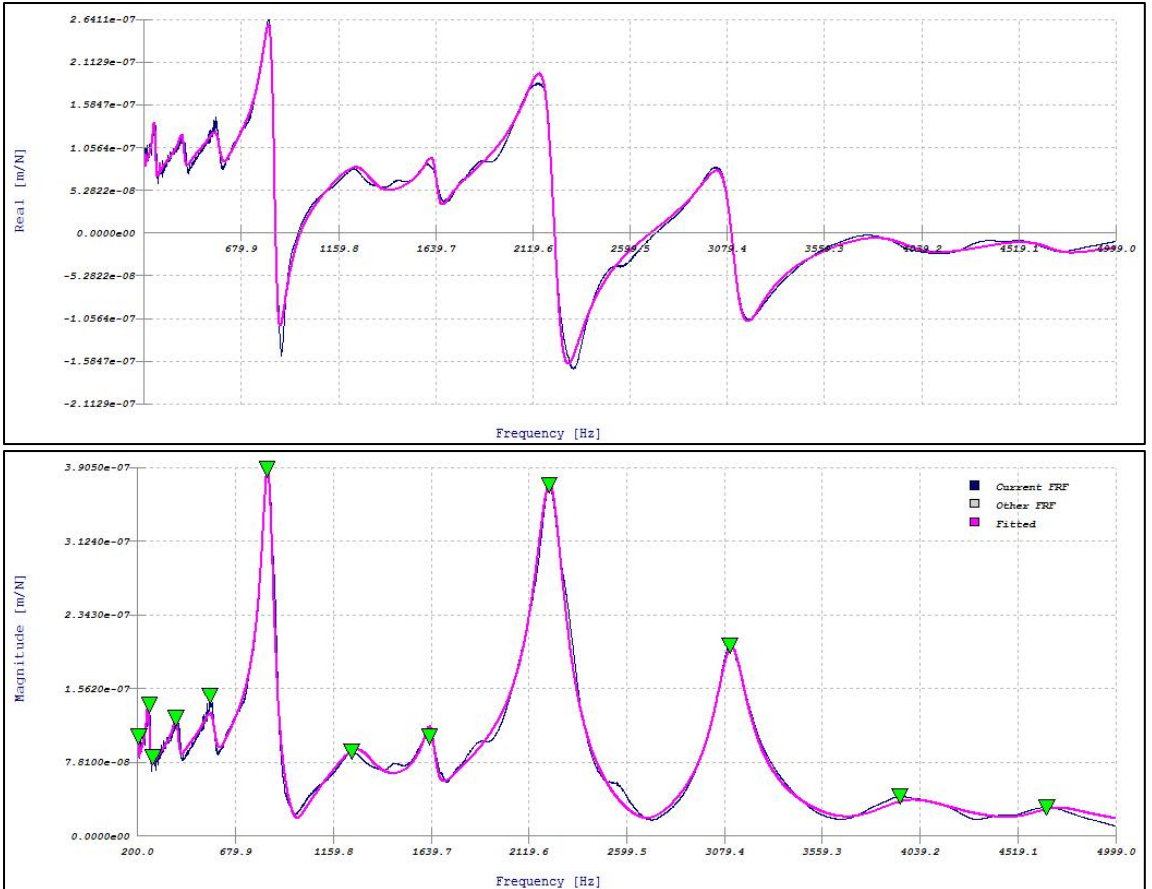


Figure 4.2: Frequency Response Function in Y Direction; Endevo 2302-10 hammer (metal tip) & 25B accelerometer

Notice how both transfer functions in X and Y are similar; this denotes a symmetrical machine.

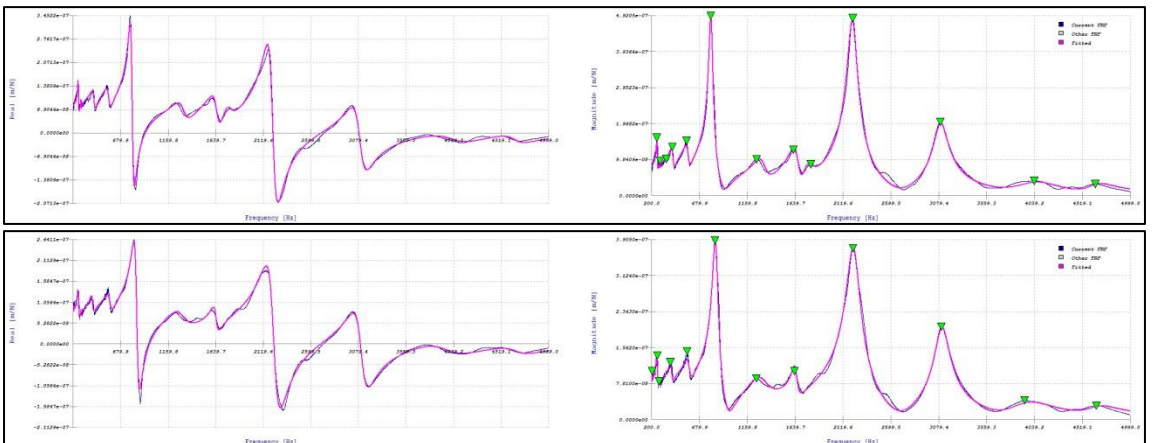


Figure 4.3: Comparison of transfer functions in X and Y

The modal parameters are shown in tables 4.1 and 4.2.

Mode #	Shape	Frequency [Hz]	Damping Ratio (%)	Residue (Re) [m/N]	Residue (Im) [m/N]	Modal Stiffness [N/m]	Mass [kg]
1	N/A	206.9134	0.147	3.4426E-08	-3.5944E-08	1.8085E+10	10699.9445
2	N/A	256.3804	3.060	1.6053E-06	-3.0554E-06	2.6374E+08	101.6346
3	N/A	277.2371	0.164	3.9361E-08	-1.2664E-08	6.8776E+10	22665.9474
4	N/A	397.1745	3.505	1.0203E-06	-3.5707E-06	3.4966E+08	56.1464
5	N/A	575.2875	5.065	-5.0216E-07	-8.4907E-06	2.1313E+08	16.3125
6	N/A	845.2456	3.474	-4.1140E-07	-6.9344E-05	3.8317E+07	1.3585
7	N/A	1299.1810	9.469	1.8448E-05	-3.4336E-05	1.1941E+08	1.7920
8	N/A	1645.0584	1.899	7.1884E-07	-1.2690E-05	4.0732E+08	3.8125
9	N/A	2229.6352	3.280	-1.2607E-05	-1.6672E-04	4.2038E+07	0.2142
10	N/A	3113.7713	2.548	-9.9187E-06	-9.6074E-05	1.0185E+08	0.2661
11	N/A	3965.1949	6.044	-5.6757E-07	-4.7608E-05	2.6214E+08	0.4223
12	N/A	4679.5886	3.661	-4.8031E-06	-2.0438E-05	7.1980E+08	0.8326

Table 4.1: Generated curve-fit modal parameters for the X-direction

Mode #	Shape	Frequency [Hz]	Damping Ratio (%)	Residue (Re) [m/N]	Residue (Im) [m/N]	Modal Stiffness [N/m]	Mass [kg]
1	N/A	255.9703	1.730	1.1333E-06	-2.3534E-06	3.4175E+08	132.1192
2	N/A	282.7465	0.496	8.1217E-08	-2.4435E-07	3.6352E+09	1151.8058
3	N/A	325.9501	0.016	-4.5615E-10	-8.7596E-10	1.1690E+12	278712.2644
4	N/A	413.9502	3.988	-9.4956E-07	-5.7880E-06	2.2486E+08	33.2400
5	N/A	563.9994	4.560	-1.4861E-06	-1.0158E-05	1.7460E+08	13.9039
6	N/A	798.6041	2.746	3.2501E-06	-6.5667E-05	3.8221E+07	1.5180
7	N/A	1318.4952	5.273	-6.1016E-07	-2.5059E-05	1.6553E+08	2.4119
8	N/A	1654.9095	2.978	-7.5480E-06	-3.0317E-05	1.7156E+08	1.5868
9	N/A	1775.0438	3.574	1.3143E-05	-1.2324E-05	4.5278E+08	3.6401
10	N/A	2216.8115	2.456	3.2759E-06	-1.6026E-04	4.3469E+07	0.2241
11	N/A	3099.4839	2.493	-8.1141E-06	-9.1414E-05	1.0655E+08	0.2809
12	N/A	4056.3059	5.688	-1.6309E-05	-3.9385E-05	3.2408E+08	0.4989
13	N/A	4669.2641	2.971	-5.9495E-06	-2.0801E-05	7.0551E+08	0.8197

Table 4.2: Generated curve-fit modal parameters for the Y-direction

## 4.2 Calculation of stability lobes

In Chapter 2 we determined the cutting coefficients for the concerned tool, and the AL7050 workpiece mounted on the table. We will now calculate the stability lobes for slot-milling (width of cut=100% of the diameter). We start CutPro and select a Milling process, see Figure 4.4.

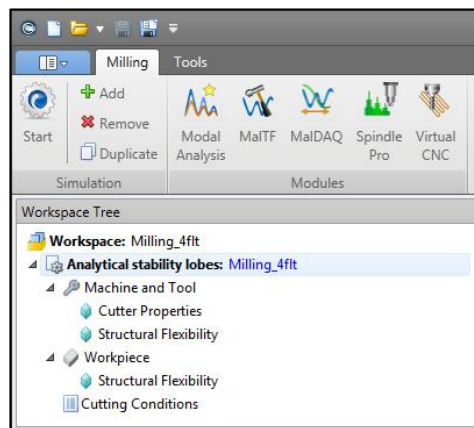


Figure 4.4: CutPro Milling toolbar

The “Workspace Tree” uses a top-to-bottom workflow process, and there are four main tabs which require attention in milling: *Simulation mode* , *Machine & Tool* , *Workpiece*  and *Cutting Conditions* .

We select the machining process “Milling” and simulation mode “Analytical Stability Lobes” (default), see Figure 4.5. Afterwards, we may move on to Machine & Tool parameters. Under the general cutter base properties we then select a cylindrical end, 4 fluted cutter, see Figure 4.6.

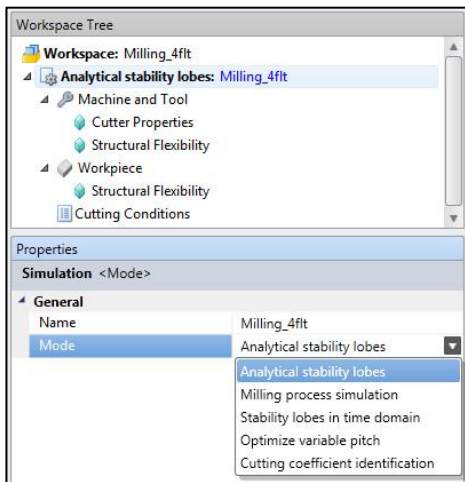


Figure 4.5: Machining process and simulation mode selection in CutPro

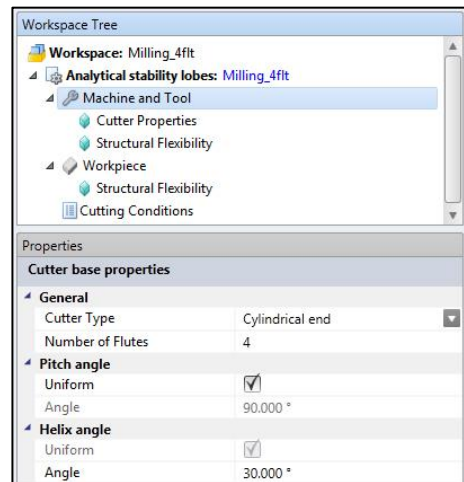


Figure 4.6: Machining & Tool parameter selection in CutPro

In “Machine & Tool” we will enter the Cutter Type, Cutter Properties and Structural Flexibility. We choose Cylindrical end Cutter Type (we assume the tipradius on the tool is negligible), with 4 teeth and uniform pitch (equal spacing between teeth).

The Cutter Material needs to be specified for the simulation of the cutting temperatures on the tool, and is of no importance for the stability lobe calculation. In Cutter Properties we specify the geometric properties of the cutter. We need to specify the tool radius, helix and rake angles. For the stability lobe calculation the tool length is not important, but it is useful for documentation. In the Structural Flexibility tab we select Structural Vibrations for the Machine & Tool model, as we model the spindle-toolholder-tool structure to be flexible. We use the modal parameter files created in the modal analysis module by selecting the option Modal/residue data files. It is also possible to enter the modal parameters by hand using the option “Dynamic parameters”. If the FRF does not need any processing in the modal analysis module (this is sometimes the case for displacement measurement files), we can select the option “Measured t.f. file” and use the measurement directly. If you want to evaluate the influence of the dynamic properties in one direction only, you can make the X or direction rigid by checking the “Rigid” box.

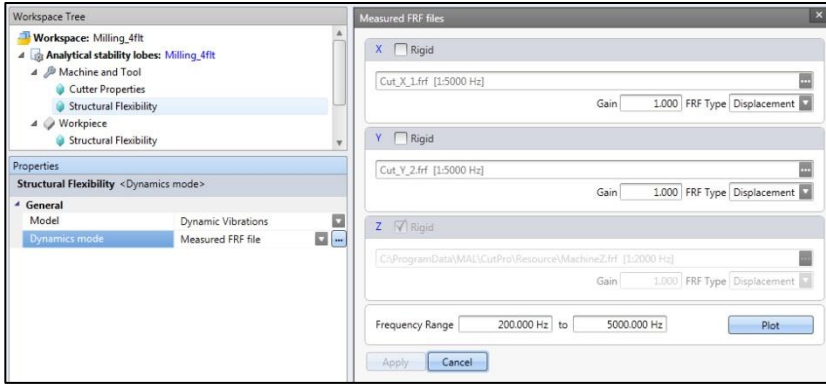


Figure 4.7: Machine tool dynamics with corresponding FRF files and Frequency Range

Next we specify in the Workpiece tab the workpiece material, which was added to CutPro’s database earlier by using the average cutting coefficient identification. The workpiece structural flexibility can be specified in the same manner as the structural flexibility of the spindle-toolholder-tool structure. Also remember that CutPro can seamlessly change between metric and imperial units.

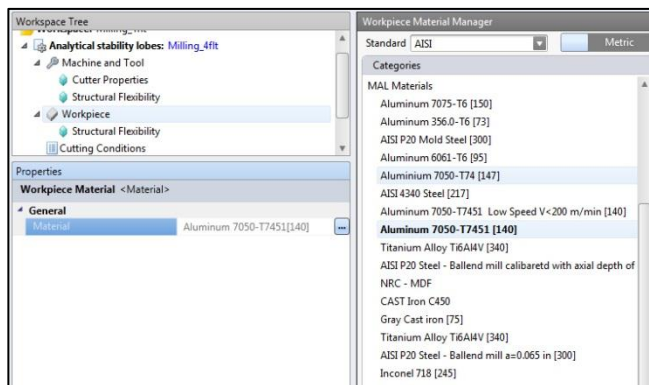


Figure 4.8: Specification of workpiece material- AL 7050-T7451

Next we specify the Cutting Conditions. The feedrate does not influence the calculation of the stability lobes, but it is practical to enter a value for documentation.

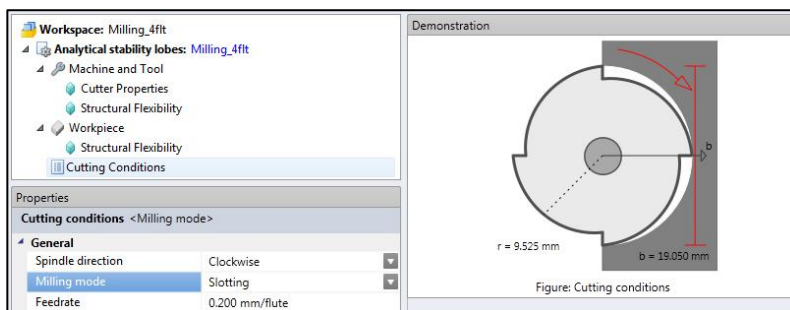


Figure 4.9: Specification of Cutting Conditions

Save the simulation file. We will now start the simulation by selecting “Start” from the CutPro toolbar. When the simulation is finished, we can plot the results by clicking the “Plot All” button (just beside the results tab). The Analytical Stability Lobes are currently calculated for spindle speeds of up to 30000rpm. Using the simulation mode “Stability Lobes in Time Domain”, stability lobes up to 100000rpm can be calculated, but this method requires a lot more CPU-time. The resulting stability lobes are shown in Figure 4.10. The stability lobes are shown for a flexible tool and rigid workpiece model.

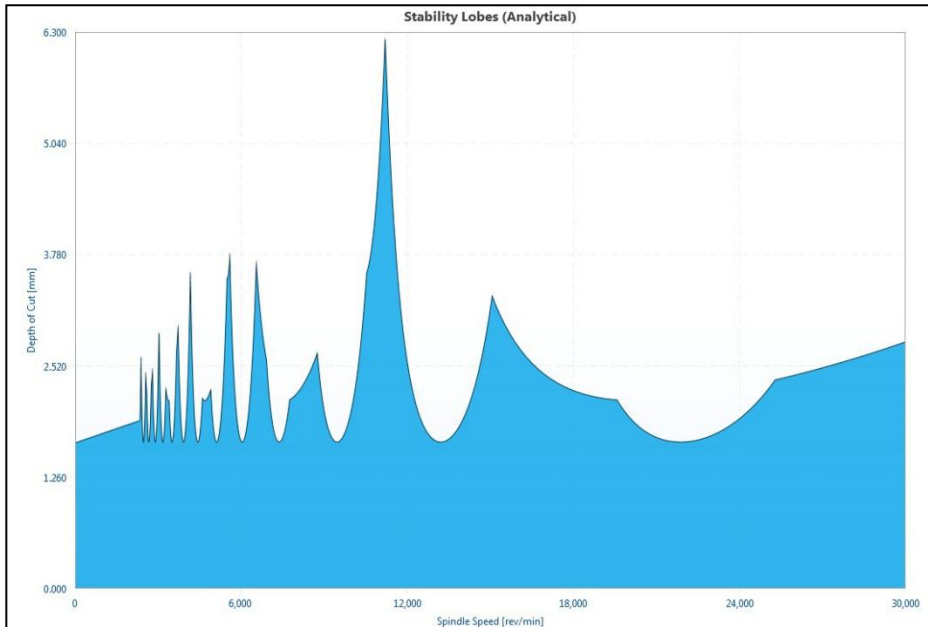


Figure 4.10: Stability lobes determined for regular four fluted 19.05mm cutter in AL7050-T7shrinkfit holder, Mori Seiki NMV5000 DCG milling machine; Flexible machine & tool structure and rigid workpiece

Including the workpiece dynamics does change the effect of stability lobes. However, if we include the workpiece dynamics in this specific calculation, the result difference between a rigid assumption and dynamic assumption will be close to zero.

Using our judgment, we choose whether or not to assume a rigid workpiece. My workpiece was simply a solid block of aluminum, bolted down into a dynamometer, and various slot cut tests were performed. A more complex fixture, along with a more flexible workpiece could impact stability lobes significantly.

### 4.3 Experimental verification of stability lobes

When the stability lobes have been determined, it is important to investigate how well the simulated lobes match the stability in practice. In order to verify the stability lobes experimentally, we will take a series of test cuts during which we will record the sound pressure. From the sound pressure we can deduce some useful information on what is happening in the cutting process. It is also possible to use a dynamometer or acceleration sensors on the machine to get similar information on the cutting process. Figure 4.11 shows the stability lobes with a rigid workpiece, and the measured cuts, which will be discussed.

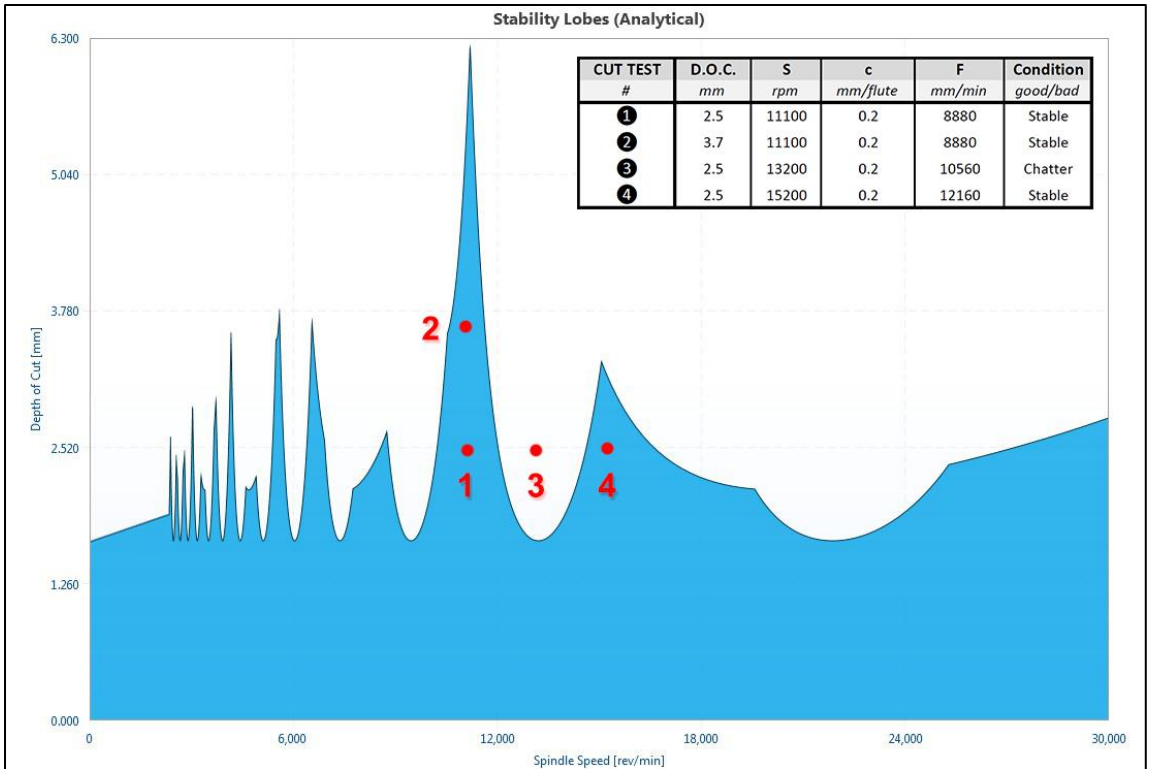


Figure 4.11: Full slot cutting tests to be performed on AL 7050-T7451

The following results shown in Figure 4.12 were obtained from the four cutting tests performed. Pictures of the floor surface finish are shown:

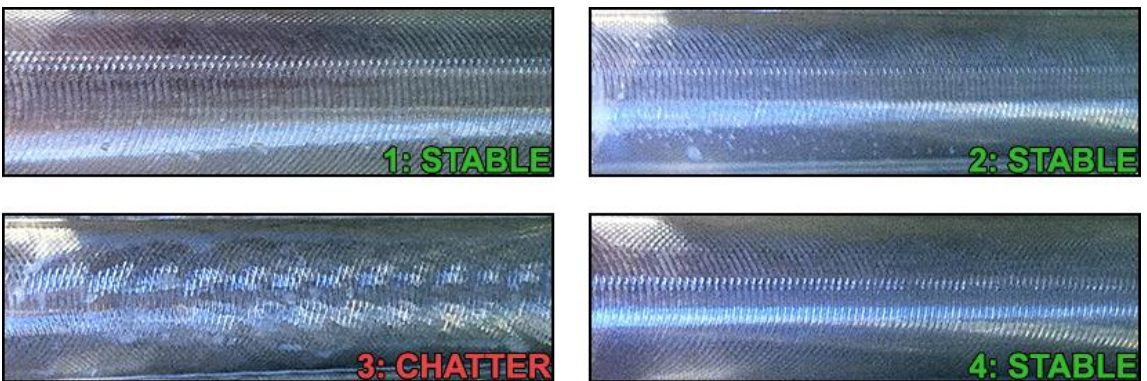


Figure 4.12: Results of full slot cutting tests performed on AL 7050-T7451

It is now clear that the simulation results of stability lobes shown in Figure 4.11 do indeed correctly predict with the expected results which are shown in Figure 4.12.

During cutting, MALDAQ was used to record the frequencies during cutting. The following four Figures represent these recordings along with hand calculations:

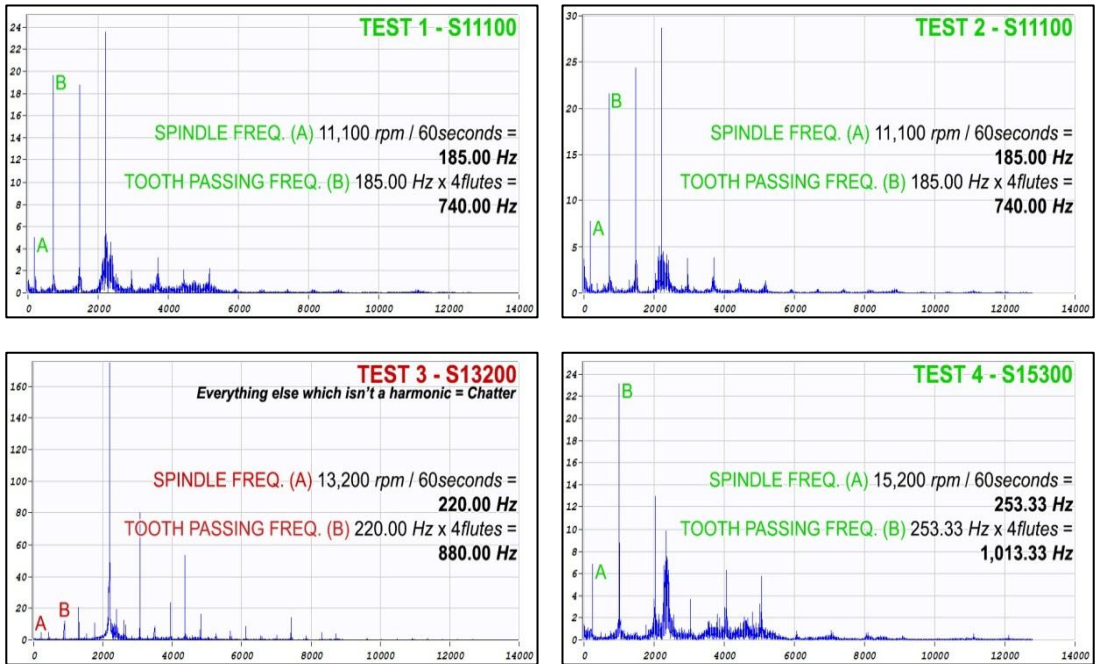


Figure 4.13: MALDAQ recordings along with hand calculations

The third cutting test which had chatter shows a large peak at 2,183 Hz with a magnitude reaching up to 703; around 25 times the amplitude experienced by the other tests.

## 5 Chatter free milling of titanium and nickel alloys

Titanium and nickel alloys are materials that are very hard to machine, because of high thermal and mechanical loading. These materials can only be machined at low cutting speeds, and thus we are not free to choose any spindle speed, that is, to use the stable pockets in the stability lobe charts. This chapter first discusses face milling of titanium alloys, then impeller machining is discussed, where variable pitch cutters are used to create stable pockets at desired cutting speeds. Machining of nickel alloys is similar to titanium machining.

### 5.1 Face milling of titanium alloys

There are four important choices that need to be made in the process planning of face milling operations of titanium alloys such as Ti6Al4V material:

- Choice of a cutter and insert geometry for optimal shearing and reduced force
- Choice of chipload (feed per tooth) without overloading the end mill shank mechanically
- Choice of an optimal surface speed without overloading the tool edge thermally
- Choice of chatter free axial and radial depth of cuts



Titanium is always machined with tools having high positive rake angles, which lead to higher shear angle, creating thinner chips. The cutting forces are also reduced, and high tensile stresses close to the cutting edge are avoided with these positive tools, which have longer chip-rake face contact length. However, the higher the positive rake is; the weaker the cutting edge becomes. Under the thermal and mechanical stresses, the weakness of the cutting edge may easily lead to chipping and caution is necessary in using these tools. The thermal loading on the tool is dependent on the combination of cutting speed, width of cut, chip load, and depth of cut. It is recommended that you select a cutting speed range of 50-70m/min for slot milling/roughing first, and increase the chip load until chipping or breakage is observed. A chip load just under the chipping limit should then be selected. CutPro can then predict the temperature on the tool for the given rake angle, speed, width (radial depth) of cut, and feed per tooth.

The cutting speed must be selected primarily based on the thermal loading of the tool when milling titanium. High cutting speeds are possible only when the radial depth of cut is very small, so that the tool does not remain in the cut long enough to soften the tool thermally. If we consider slotting, the cutter remains in cut significantly, and chips soften easily at high speeds. Hence, it is more practical to increase the material removal rate by increasing the axial depth of cut and feed per tooth. With Cimco lubricant for example, the recommended cutting speed for slot milling of titanium is about 60m/min (180ft/min). The cutting speed may be reduced or increased by 10% depending on the chatter stability of the machine/fixture assembly.

The chatter stability is dependent on the dynamic stiffness of the machine and workpiece reflected at the cutting zone (the part of the tool in cut). If the inserts have zero helix/nose radius/inclination angle, chatter vibrations may be dominated only by modes in the plane of cut (plane perpendicular to the spindle axis, X and Y direction). However, if the inserts have a high helix, inclination or circular/bull nose shape, then the structural rigidity in the third (spindle axis, the Z-axis) is also important.

Although CUTPRO uses highly sophisticated and very accurate mathematical model of chatter stability, the following approximate, manual calculation of  $T_{lusty}$  can be used to predict the approximate absolute depth of cut in milling:

$$a_{lim} = \frac{l}{2K_s \frac{N}{2} \frac{b}{d} u \times Re(G_{min})}, \text{ where}$$

$$Re(G_{min}) = \frac{1}{4k\zeta} [mm/N] : \text{Minimum real part of the transfer function}$$

$K_s = 2000 [N/mm^2]$  for Ti6Al4V alloys

$b$  = radial width of cut ;  $d$  = cutter diameter;  $N$  = number of teeth on the cutter

$u = 0.34$  for slotting;  $a_{lim}$  = limit depth of cut without chatter vibrations

The stiffness  $k$  and damping ratio  $\zeta$  are measured at the structural mode which has the minimum value for  $Re(G_{min})$ . A sample measurement is shown in Figure 5.1.



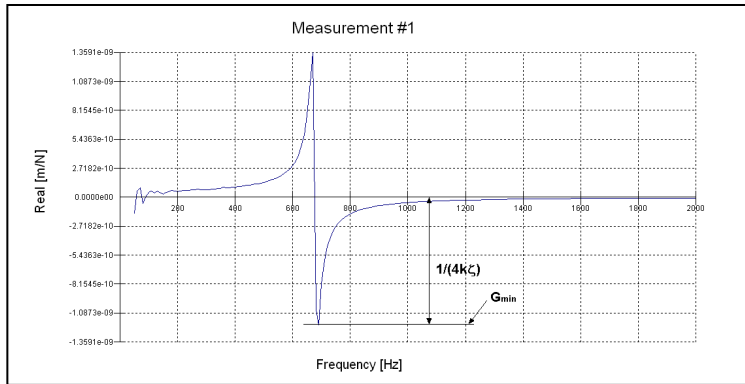


Figure 5.1: Real part of transfer function

It is recommended that the measurements be done on both the cutter and fixture. It can be seen that the maximum depth of cut depends on the stiffness  $k$  and the damping  $\zeta$  of the machine. The higher they are, the higher the material removal rate is that can be used without chatter vibrations for the machine. In addition, the machine tool must be able to deliver sufficient torque and power for heavy cuts at low speeds.

*Example:*

Titanium material has to be slot milled at 0.5inch (12.5mm) depth of cut using a 4 inch (101.6mm) diameter face milling cutter with 4 inserts. The recommended cutting speed is 60 m/min, and the chip load is  $c=0.1$  mm/rev/tooth. The dynamic stiffness, torque, and power required from the machine tool are then calculated as follows:

$$Re(G_{min}) = \frac{1}{4k\zeta} [mm/N] \text{ (Minimum real part of the transfer function)}$$

$$K_s = 2000 [N/mm^2] \text{ (Specific cutting stiffness for Ti6Al4V alloys)}$$

$$b=101.6mm, \quad d=101.6mm, \quad N=4, \quad u = 0.34 \text{ for slotting}$$

$$a_{lim} = 12.54 \text{ mm (The desired depth of cut without chatter vibrations)}$$

The minimum value of  $k\zeta$  can be determined as follows:

$$a_{lim} = \frac{12k\zeta}{m \frac{b}{d} K_s} = 0.0015k\zeta = 12.54mm \quad k\zeta = 8360 [N/mm]$$



In spindles, the damping ratio ( $\zeta$ ) is usually about 5% ( $\zeta=0.05$ ). Thus, the spindle must have at least 167,000N/mm to slot mill titanium at these cutting conditions without chatter.

$T = \frac{m}{3} K_s \times a \times c \times \frac{d}{2} = \frac{4}{3} \times 2000 \times 12.54 \times 0.1 \times 50.8 = 170.000 Nmm = 170 Nm$  is the torque required from the spindle for this type of cut, which is high for this spindle speed (190rpm).

$$V=60 \text{ m/min} = 1 \text{ m/s} \Rightarrow n = \frac{V}{\pi \times D} = \frac{60}{3.14 \times 0.101} = 191 \text{ [rev/min]}$$

$Power = Torque \times \frac{V[m/s]}{R[m]} = 170 \text{ [Nm]} \times \frac{1 \text{ [m/s]}}{0.0508 \text{ [m]}} = 3.4 \text{ kW}$  is the power required from the spindle.

However, these formulas are very approximate to give feeling about the procedures to the reader, and CUTPRO should be used for more accurate evaluations.. If we use accurate chatter theory for milling [1] instead, which is 3D and more complex to explain, the above values for the spindle characteristics give only 4.1mm (~0.16inch) chatter free axial depth of cut. This is verified experimentally and with time domain simulations.

Thus, if we keep the damping at 5%, and use the same cutting conditions (except that the static stiffness is increased from 167N/μm (specified as a minimum above) to 500N/μm, or the stiffness is increased by a factor 0.50/0.16=3.1), the chatter free axial depth of cut limit increases to 12.4mm (~0.50inch). Hence the dynamic stiffness required would be about  $k\xi=25\text{N}/\mu\text{m}$ . These calculations are made using straight edge inserts with zero helix and inclination angles. If you use circular inserts, you need less dynamic stiffness in XY-plane (about 20% less), which is perpendicular to the spindle axis. However, you need to consider the axial dynamic stiffness in the direction of spindle axis in this case. The approximate torque and power calculations can be accepted as shown in the example.

## 5.2 Variable pitch cutter design for difficult to machine materials at low speeds

In titanium machining of impellers, long, tapered ballend mills are used to reach between the blades. The slenderness of these tools makes the milling operations susceptible to chatter. If we want to increase the productivity, we cannot freely choose a spindle speed, as the cutting speed is limited by the thermal durability of the tool. Fortunately, there is another method to increase the productivity in milling operations. The teeth of a regular cutter are always equally spaced (constant pitch), and this configuration makes the milling process periodic. If we change the spacing so that the pitches between the teeth vary, we get a variable pitch cutter. This variable pitch distorts the periodicity, but at the same time it distorts the development of chatter.



Therefore, if our spindle speed is limited because we are machining titanium or another material that limits the cutting speed, we can use a variable pitch cutter instead of a regular one and influence the stability at that specific spindle speed. Figure 5.2 and 5.3 show a typical machining condition for impeller machining, and details will be discussed on the following pages.

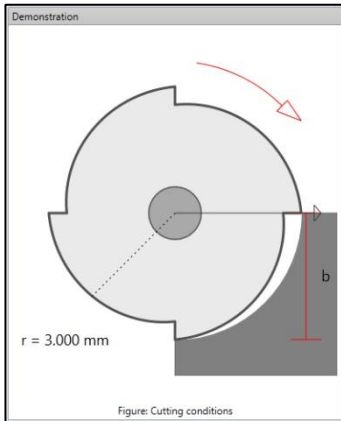


Figure 5.2: Downmilling scenario used

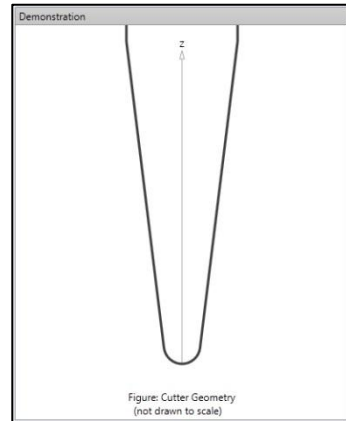


Figure 5.3: Ballend mill geometry

CutPro offers a simulation mode which allows you to design variable pitch cutters.

In order to design a variable pitch cutter, you have to measure the transfer functions of a regular cutter mounted in the spindle in the applicable toolholder. These measurements will then be used in CutPro to design the variable pitch cutter which will have the same basic geometry. The only differences between the regular and the variable pitch cutter, will be the # of teeth (can stay the same), and the pitch angles. Variable pitch cutters will only perform well at the specific spindle speed they are designed for. Due to the variable pitch angles, the performance at other spindle speeds deteriorates. In the simulation, it is assumed that the transfer functions do not change because of the change in pitch angles, as only the tool is slightly modified. A simulation determines the optimal variable pitch for a cutter by selecting the simulation mode “Optimize Variable Pitch”. Under the “Cutter Properties” tab, the tool geometry is then defined.

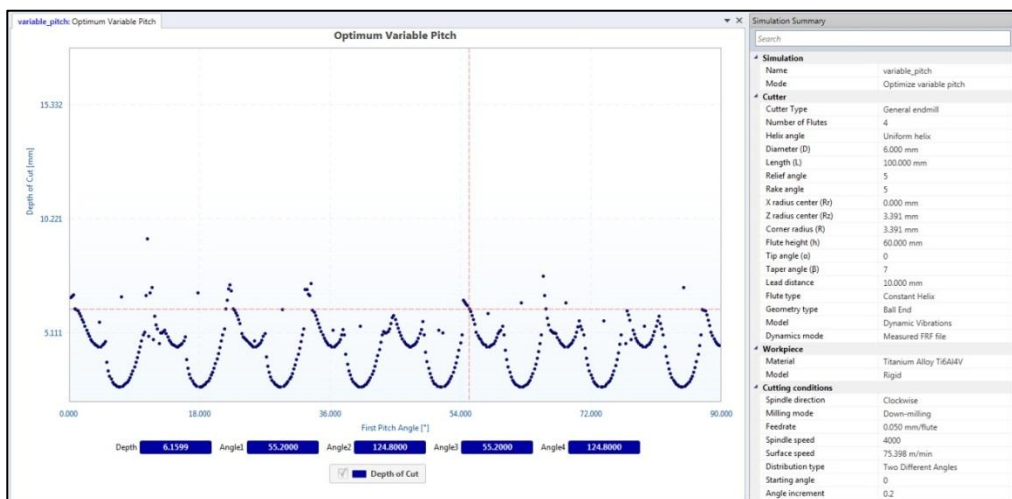


Figure 5.4: Cutting conditions and results for a variable pitch cutter used in impeller milling

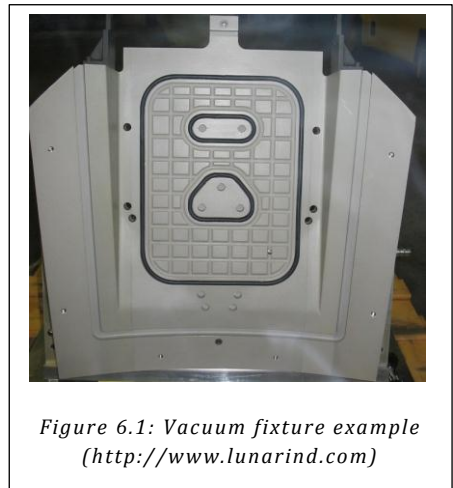
The only different settings in the simulation are the fixed spindle speed, settings for the desired pitch distribution, and pitch angle increments for the simulation. These increments determine the resolution of the simulation result (pitch angle increment, determines the specifications of the angles to be grinded on the cutter) and the speed/accuracy of the simulation. The result of the simulation is a graph with the maximum stable depth of cut as a function of the pitch angle, for the specified tool, machine tool dynamics, workpiece material and dynamics, spindle speed and width of cut. An example is shown in Figure 5.4, we can see that the highest depths of cut can be achieved if the first pitch angle is about 55 degrees (the information is shown by clicking in the graph). If 55 degrees is selected for the first pitch angle, the second pitch angle will be 125 degrees and the third and fourth will be 55 and 125 respectively, as the pitch distribution type selected is “Two different angles”. Other possible pitch distribution types are “Linear angles” and “Sinusoidal angles”.

Similar to the selection of cutting speed, it is not possible to freely choose a pitch angle distribution. In this example, a four fluted cutter is used and the regular pitch distribution has 90 degrees between the teeth. Choosing 55 and 125 degrees means there will be either very little space for the cutting teeth resulting in weak teeth, or very little space to evacuate the chips which will result in clogging of the tool. The new pitch angles in the variable pitch design should therefore not deviate too much from the regular distribution; to provide good cutting tool strength and chip evacuation. One should take into account that the higher depth of cut possible with an optimized variable pitch design, will make the chip evacuation more critical.

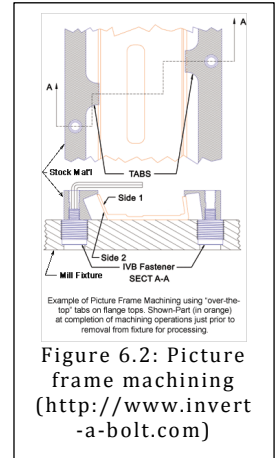
## 6 Machining Strategies for Thin Gauge Aircraft Parts

### 6.1 Aluminum Machining: Fixturing strategy

- Conventional fixturing: When using conventional mechanical fixturing, the part is held down with top and/or side or toe clamps in the first (several) setup(s) and as much excess as possible is machined away. When the part nears completion it becomes very flexible, and then the best way to hold is by resting the part with flat finished faces on vacuum tooling and sucking it down (example shown in Figure ). Mechanical and vacuum fixtures are part specific and costly, as they need to be stored and maintained. Vacuum fixtures can be used at any stage of machining, provided the part has flat areas to apply vacuum to, and with addition of mechanical clamps the part is secured to withstand cutting forces.



- Picture frame fixturing (Example in Figure 6.2) When parts are machined from plate, the plate can be bolted or toe clamped directly to the machine bed (excess is used as tooling). Tabs are machined along the external and/or internal edges of the part to hold the part in the material; the tabs are removed when machining is complete. When the second side of the part is machined, suitable programming strategies need to be used, as the part is only going to be supported at the tabs.



## 6.2 Aluminum Machining: Machine tools

Today's aluminum machining technology utilizes fast machine tools (50-100m/min rapid traverse) with high acceleration (up to 3.0G depending on machine size) and high speed spindles with significant power (33,000 rpm and 120kW, or higher speed with lower power). These machines are designed for High Speed Machining of light alloys such as aluminum. Although these machines have high power, it can normally only be used for a limited number of tools, and often chatter vibrations and poor surface finish caused by dynamic flexibility of spindle, tool holder and tool, limit the machine's productivity.

## 6.3 Aluminum Machining: Machining steps

Some aircraft parts can be machined in a single setup, but the majority requires multiple setups to control distortion of the part and/or to access all sides of the part to remove the excess material. The number of steps also depends on the machine kinematics (3, 4 or 5-axis) and the fixturing method.

### 6.3.1 Roughing

- Use large enough tools to use maximum spindle power where possible (utilizing stability lobes to optimize productivity)
- Use solid carbide endmills for small diameters (up to ¾" or 1"), indexable tools for 1" and larger (maximum 3-4" with reduced spindle speeds for insert security)
- The tool sizes used in roughing determine the amount of material that needs to be removed in semi-finishing to create a consistent stock for the finishing step
- Tools/inserts should be very sharp and can be coated for prolonged tool life
- Solid carbide tools should be necked to avoid rubbing and have 2 or 3 flutes, flute length 1.0-1.2x diameter; the flutes need to be feather-blended into the neck to avoid steps in wall finishing; small diameter (16mm and less) as well as longer tools ( $L/D > 5$ ) should have 2 flutes, unless there is very little material to remove
- Tip radius: Small tip radii (1.0mm) can be used, but larger radii provide a stronger tooth with is good for roughing and larger chip loads, and you can also rough closer to the net shape of the part. Large radii tools can also be used to finish walls and floor fillets in one operation
- Feed rates: A good starting chip load is 1% of cutter diameter, this can be increased until surface finish degrades or power limits are reached

### 6.3.2 Semi-finishing

- Remove excess material left by large diameter roughing tools to create even amount of stock for finishing



### 6.3.3 Finishing

#### 6.3.3.1 Thin pocket walls (ribs)

In order to machine thin pocket walls without vibration problems, the four-to-one rule (4:1) can be used to devise your machining plan. This approach, specific to aluminum parts, ensures the part is always stiff enough to machine, avoiding part vibrations. Aircraft structural parts have complex shapes, hence work piece chatter is difficult to eliminate as natural frequencies change constantly during machining. Using the 4:1 rule makes the part “rigid”, allowing you to focus on only optimizing your cutters to be able to achieve the cuts resulting from the method (smaller cuts can be taken but will slow down machining).

The application of the rule is done in reverse order:

- The result of roughing and semi finishing needs to result in a ratio of wall height and wall thickness of 4:1 (no more); Example: for a 36.0mm wall, the thickness after roughing and semi-finishing should be 9.0mm or more.
- When taking the final finishing pass, the **axial depth of cut** cannot be larger than 4 times the finished wall thickness; Example: for a 1.50mm thick wall, the maximum cutting depth is 6.0mm
- Finishing is typically done in two radial passes (depending on wall height), the last one removing 80% of final wall thickness, hence the **radial depth of cut** is 1.20mm in this case; The wall will be  $1.50+2 \times 1.20=3.9\text{mm}$  thick before final finishing.
- As the wall measures 9.0mm thick after rough/semi-finish, there is 5.1mm to remove before final finishing to obtain a thickness of 3.9mm, which is done by a pre-finish cut. Repeated application of the 4:1 rule allows to take us  $4 \times 3.9=15.6\text{mm}$  axial depth of cut. In this case it's practical to take a 12.0mm depth, which will then be followed by finishing in two axial passes.
- Hence, the application of the 4:1 rule on this wall results in 18 passes to complete finish machining, see Figure ; The first level has pre-finish cuts 1 & 2, and finish cuts 3, 4, 5 & 6.

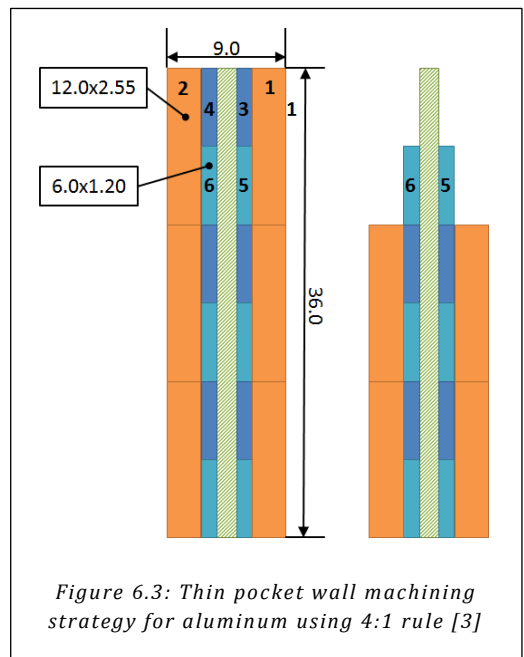


Figure 6.3: Thin pocket wall machining strategy for aluminum using 4:1 rule [3]

This method is called waterfall technique due to the shapes formed while machining (right in Figure ). One of the great benefits of this method is that the part thickness will be constant and within an acceptable tolerance, as both work piece and tool deflection are kept in check with the limited pass depths.

### 6.3.3.2 Thin pocket floors (webs)

If a thin pocket floor is fully supported by fixturing (one sided web, see Figure ), radial step-over and feed are adjusted to obtain the required surface finish, by pocketing from the center to the walls. If you have a two-sided web that is not supported (Figure) when the second side is being finished, you have to leave a thicker floor on the last side to finish. The first side can be finished as if it was supported. The last side is stepped down in small axial passes until the finished floor before you step out radially (“down and over” technique). This method will take longer to machine but has the advantage of simple and cheap fixturing. For very large production runs, vacuum tooling maybe more cost-effective.

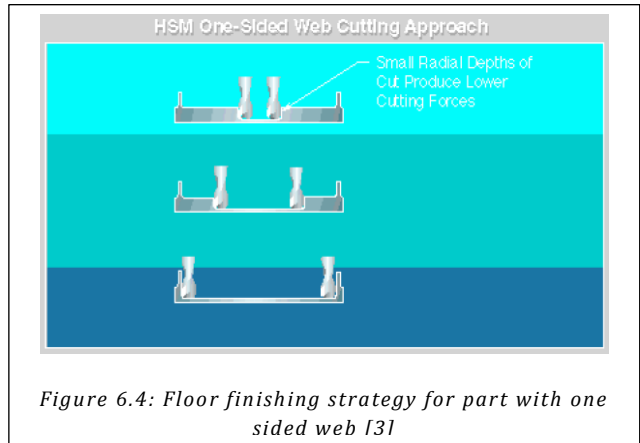


Figure 6.4: Floor finishing strategy for part with one sided web [3]



Figure 6.5: Floor finishing strategy for two sided web without fixturing support [3]

### 6.3.3.3 Small pocket corner radii

When small pocket corner radii and large flange heights require the use of high L/D ratio tools, there are two approaches to take:

- Use a larger diameter cutter to machine the part (smaller L/D); Come back in with the smaller diameter cutter to clean out the corners
- First finish the corners with the smaller diameter cutter, then finish the flanges

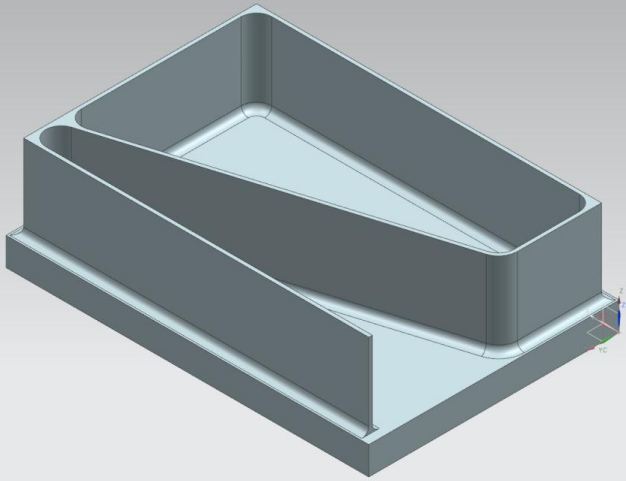
### 6.3.3.4 5-axis features

Minimize axis movement during finishing of 5-axis features, as rotary axes are typically much slower than linear axes, leading to longer cycle time and worse surface finish. The best method to use is fixed axis kellering/scanning (3+2 axis control). The preferred machining mode is down milling, but in some cases down milling can be alternated with up milling to reduce cycle time if the surface finish is acceptable.

### 6.3.3.5 Part vibration counter measures

Some parts have extremely flexible features. Normally you can successfully machine these by leaving sufficient excess, if that is not possible due to part geometry, you can partially complete machining, then add silly putty, wax, rubber or fast patch paste to strengthen and/or dampen the part again and complete machining.

## 6.4 Demo part High Speed Machining in Aluminum



**Material: AL7075-T7451**

Stock: 155 x 107 x 50 mm

Wall height = 36.0 mm

Wall thickness = 1.50 mm

Corner radius = 6.5 mm

Raw material = 2.340 kg

Finished part = 0.772 kg

Cycle time = 210 seconds

Effective MRR = 26.9 kg/hr

*Figure 6.6: Demo part aluminum machining; Part modeled in Unigraphics NX7.5*

### 6.4.1 Aluminum demo part design

The aluminum demo part includes the typical aerospace component characteristics:

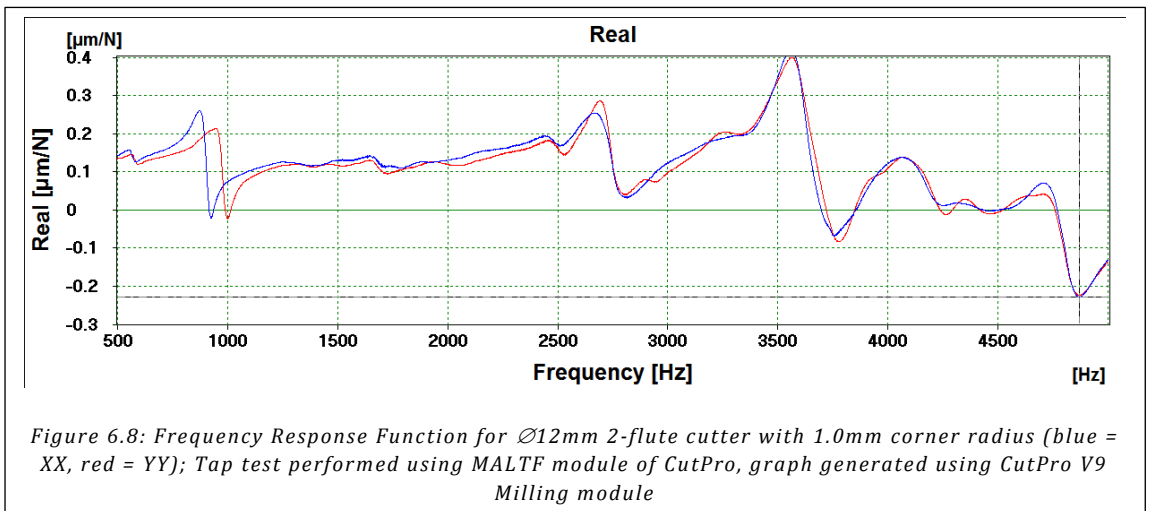
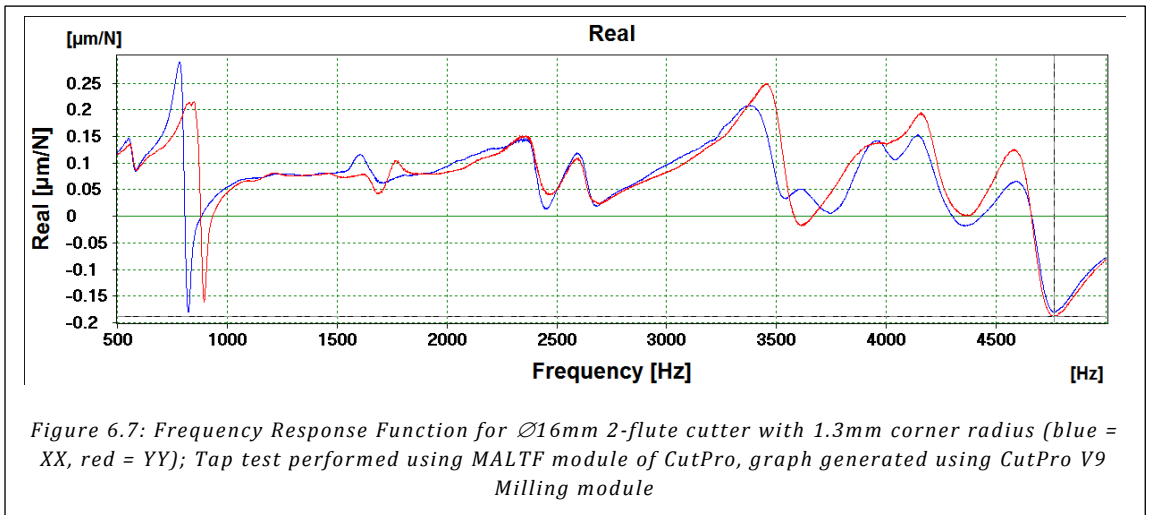
- thin wall 36.0mm high, 1.5mm thick (ratio of height to thickness = 24)
- one wall end is free-standing
- smallest closed angle is 17°
- the fillet radius between wall and base depends on the cutter used – a typical value for aerospace is 5.0mm or 4.0mm; for the project we tested 1.0, 3.2 and 5.0mm radii

### 6.4.2 Machine & cutter selection

The machine tool used is a five-axis Mori Seiki NMV5000-DCG vertical machine with trunnion table, with 20,000RPM/18,5kW HSK63A spindle, and external flood coolant. Two tools are used for machining this part from block material:

- 2-flute Seco-Jabro JH420  $\varnothing$ 16mm cutter with 1.3mm corner radius mounted in 20mm Sandvik Corogrip holder with  $\varnothing$ 20 to  $\varnothing$ 16mm sleeve;
- 2-flute Dataflute HVMag  $\varnothing$ 12mm cutter with 1.0/3.2/5.0mm corner radius mounted in 12mm Seco-EPB 5800 shrink fit holder;
- Both tool assemblies have been fine balanced to G2.5 @ 20,000RPM

The frequency response functions (FRFs) are provided in Figure 6.7 and Figure 6.8. The FRFs are later used to calculate the stability charts for each tool, and to establish the most productive cutting conditions.



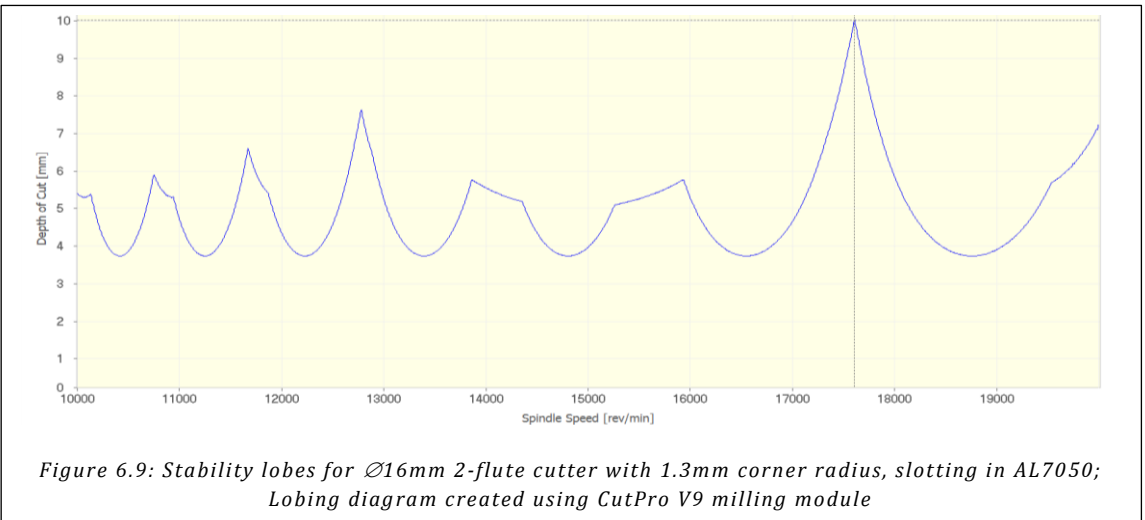
### 6.4.3 Machining strategy

We use the Ø12mm cutter to semi-finish and finish the walls using the strategy shown in Figure , hence we need to rough the part down to 9.0mm wall thickness first (+3.75mm stock on each side). Roughing is done with the Ø16mm cutter in full slotting/pocketing operation, followed by the Ø12mm cutter removing excess from the corners, also in full slot, and locally leaving only 0.10mm in the corners (due to the sharp angles).

### 6.4.4 CutPro: Selection of cutting conditions

CutPro is used to establish the chatter stability lobes for each cutter and select the best spindle speed/depth of cut combination to achieve the highest productivity. Details on the stability lobe calculation can be found in [4]. The Ø16mm cutter machines away the bulk of the raw material, up to 36.0mm deep. The stability lobes established in Figure indicate that at 20,000RPM we can achieve 7.0mm depth of cut but at 17,500RPM the maximum achievable depth is close to 10.0mm.

Cutting tests were performed with 0.10mm feed per tooth, and are shown in Figure . Slotting at 20,000RPM was stable up to 8.0mm depth of cut and became unstable at 9.0mm depth of cut. At



17,500RPM we could cut stable up to 9.0mm depth, and chatter was severe at 10mm depth of cut. These results yield the following productivity per cut:

$$20,000 \times 2 \text{ flutes} \times 0.10\text{mm chip load} \times 7.2\text{mm depth of cut} \times 16.0\text{mm width} = 461 \text{ cm}^3/\text{min}$$

$$17,500 \times 2 \text{ flutes} \times 0.10\text{mm chip load} \times 9.0\text{mm depth of cut} \times 16.0\text{mm width} = 504 \text{ cm}^3/\text{min}$$

At 20,000RPM we require 5 axial depths to rough 36.0mm deep (hence 7.2mm), but at 17,500RPM we need only 4 passes. So at 17,500RPM we have the best productivity, which is  $(504/461-1) \times (5/4) = 37\%$  higher than at 20,000RPM.

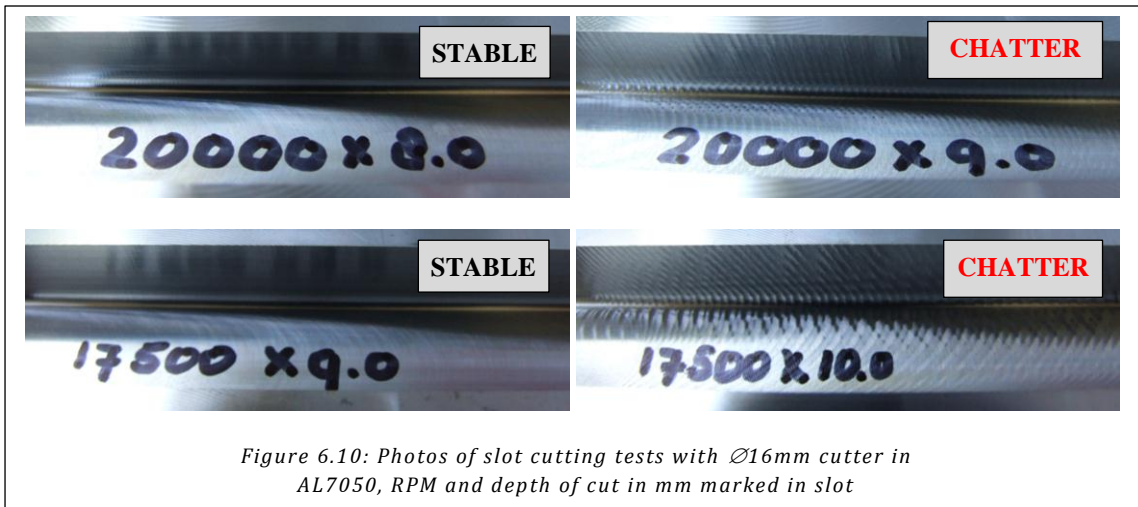


Figure 6.10: Photos of slot cutting tests with  $\varnothing 16\text{mm}$  cutter in AL7050, RPM and depth of cut in mm marked in slot

Finally, we need to establish the feed rate to be used, which depends on the available spindle power. We took four additional tests cuts at 17,500RPM slotting 9.0mm deep, as shown in Figure , steadily increasing chip load. We decided to use a chip load of 0.33mm per tooth, which results in 93% power consumption reading on the machine control – this is with a used cutter.

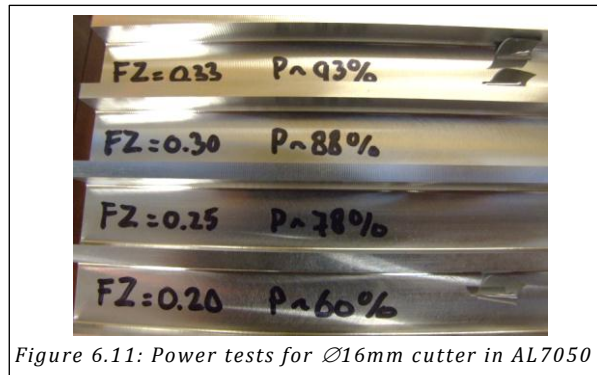


Figure 6.11: Power tests for  $\varnothing 16\text{mm}$  cutter in AL7050

The  $\varnothing 12\text{mm}$  cutter is used to rough machine the corners removing the excess left by the  $\varnothing 16\text{mm}$  cutter. After that, the  $\varnothing 12\text{mm}$  cutter is used for semi-finish and finish using the thin wall strategy. The stability lobes shown in Figure indicate that at 20,000RPM we can achieve 3.5mm depth of cut but at

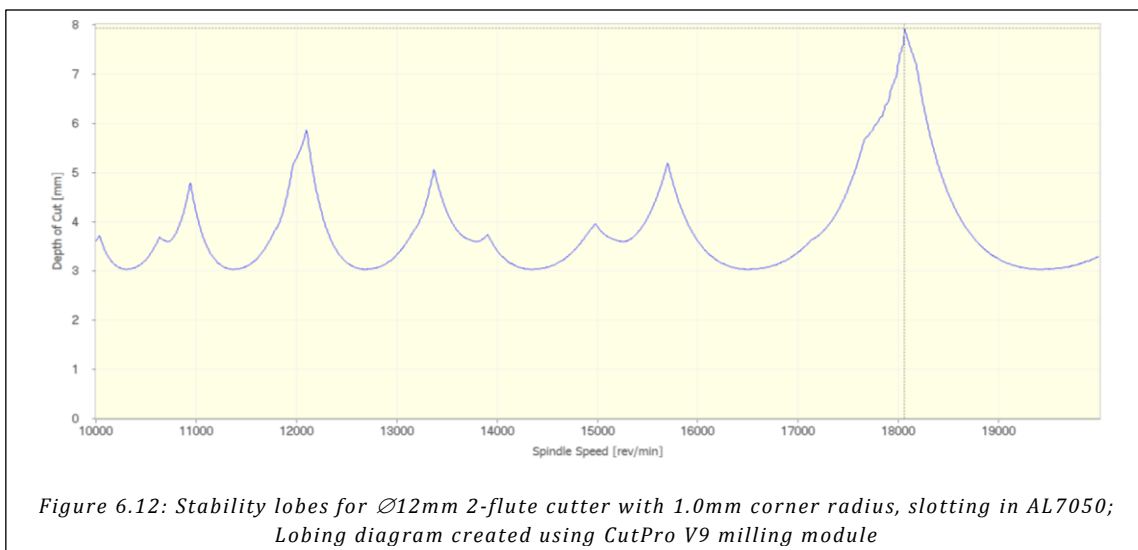


Figure 6.12: Stability lobes for  $\varnothing 12\text{mm}$  2-flute cutter with 1.0mm corner radius, slotting in AL7050; Lobing diagram created using CutPro V9 milling module

18,000RPM the maximum achievable depth is close to 8.0mm.

Cutting tests were performed with 0.10mm feed per tooth, and are shown in Figure . Slotting at 20,000RPM was actually stable up to 16.0mm depth (full flute length of the cutter), much higher than the stability lobe prediction indicates. The tool has a special geometry that creates additional damping in the cutting process to make it suitable for finishing thin walls.

Based on these results, we rough machine the corners slotting 12.0mm deep, as we need 3 passes to get 36.0mm deep.



Figure 6.13: Photos of slot cutting tests with  $\varnothing 12\text{mm}$  cutter in AL7050, RPM and depth of cut in mm marked in slot

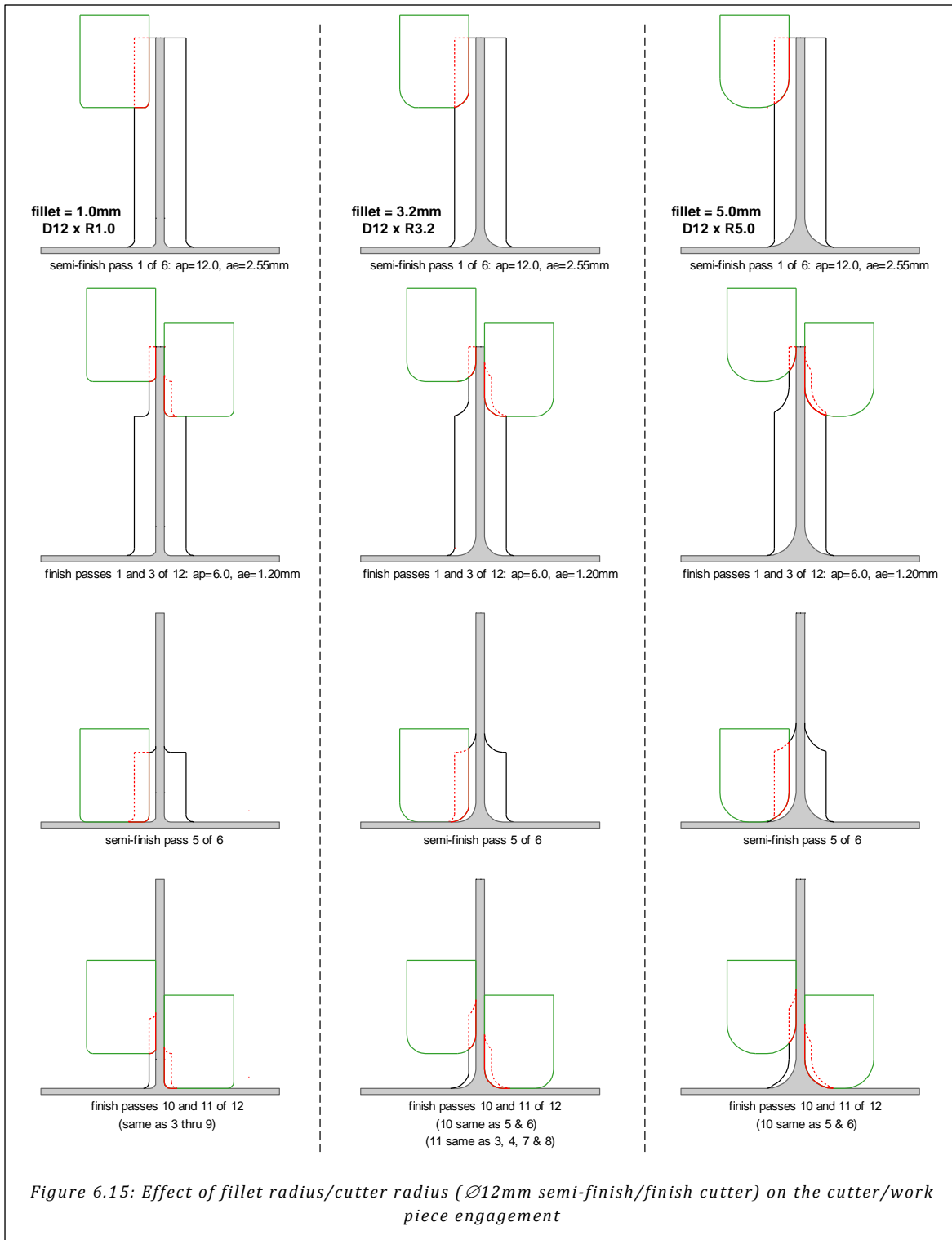
#### 6.4.5 Thin Wall Machining Experiments

The same  $\varnothing 12\text{mm}$  cutter is used for semi-finish and finish using the thin wall strategy explained in Figure . The method has been tested on AL6061-T6 plate specimens, 101.6x76.2x12.7mm (LxHxW) which were clamped in a vise. Up to 36.0mm depth, the wall is first machined to 9.0mm thickness, resulting in the step at the right side just above the vise jaw, see Figure . The top part of the specimen shows the first two 12.0mm deep semi-finish passes completed (step 1 & 2) - this portion of the wall measures 3.9mm thick, the 24.0mm wall portion below that is 9.0mm thick. The top portion will be finished with axial passes of 6.0mm deep to 1.5mm thickness alternatingly between left and right (steps 3-6).

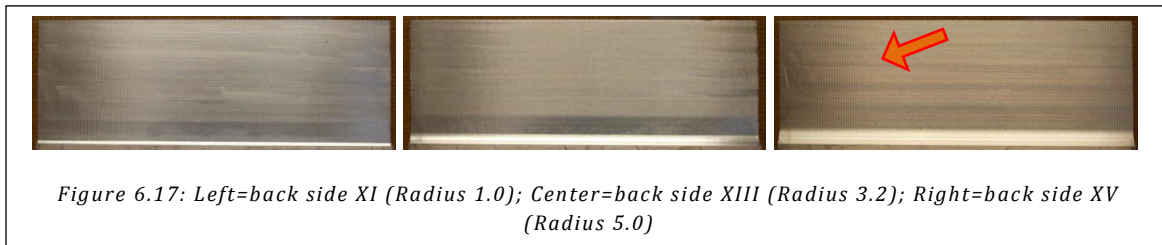
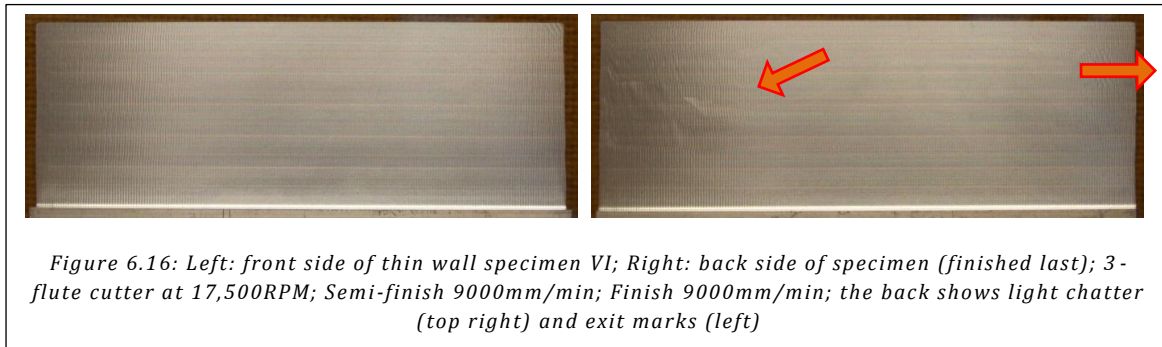
We have machined specimens with three fillet radii (between wall and floor; 1.0, 3.2 and 5.0mm), by using  $\varnothing 12\text{mm}$  cutters with that corner radius. Figure shows the cutter/work piece engagement at the various stages of semi-finishing and finishing the thin wall for each work piece fillet/cutter corner radius. The 1.0mm cutter radius results in the most flexible work piece while performing the final finishing operation. When using a large corner radius, the difference in material removal between the first level finishing and second level finishing is largest (for R5.0, see finish passes 1 and 3, as well as finish passes 10 and 11).



Figure 6.14: Thin wall specimen in vise



An example finished specimen with R1.0 is shown in Figure , which was machined with a 3-flute cutter. At each level, the front side of the plate is finished first, followed by the back side. Figure shows the backside of three specimens with fillets 1.0, 3.2 and 5.0mm, all finished with 2-flute Dataflute tools. Specimen XI (R1.0) was machined with a special semi-finish strategy, leaving 0.6mm stock on the left of the back side over a 10mm length, this is to avoid exit marks as the work piece is most flexible. Specimen XIII (R3.2) has the best surface finish. Specimen XV (R5.0) shows some exit marks, as shown in Figure , the material removal between finishing levels varies significantly, this variation could be reduced by using 6.5mm depth for the first pass, then 5.5mm for the second pass, but that would complicate NC-programming. It should be noted that a completely free standing flange - the test specimen – rarely occurs, typically only one side is free-standing, and the marks do not occur on the right for any of the cases in Figure .



Especially the specimens with a fillet radius of 1.0mm are sensitive to vibration/exit marks, and we did several experiments varying the stock removed in the finishing operation:

- 0.60mm: surface finish is even, but feed marks become very apparent as the wall is more flexible during finishing as a result of the smaller excess
- 0.90mm: slightly smaller exit marks than with 1.20mm excess
- 1.50mm: exit marks increase due to exit from a larger cut
- 3.75mm (no semi-finish at all): exit marks become worse due to exit from the larger radial depth of cut. Due to the increased radial depth of cut, the finishing chip load is smaller to obtain the same maximum chip load, and the resulting surface finish on the rest of the wall is very good

Conclusion: the thin wall machining method illustrated in Figure works well with a 2-flute cutter for radii 3.2mm and 5.0mm. For radius 1.0mm, some tool path modification is need at the end of a free-standing wall (such as the plate specimen).

### 6.4.6 NC Program Methods

The NC program for the demo part has been created in Unigraphics NX. The tool path settings as well as speed and feed, simulated tool path and Vericut simulation result are shown in Figure (roughing), Figure (corner roughing) and Figure (semi-finish & finish of the thin wall).

In rough milling, the pocket is entered by ramping a triangle due to the space limitation, and then roughed inside-out, level by level. A radius is added on the corners to smooth the tool path. The excess left of the part is 3.75mm. The excess left in the corners by the Ø16mm cutter is roughed with the Ø12mm cutter, leaving only 0.05mm-0.10mm for the finish milling. This has been done to avoid cutter chatter when it arrives in the closed angle.

Using the 4:1 rule for thin wall machining, there are three levels of semi-finish 12.0mm deep leaving 1.2mm excess on the wall. Once a semi-finish level is completed, it is directly following by 2 finishing levels 6.0mm deep. The machining steps and cutting conditions are summarized in Table 6.1. The part utilizes the high spindles speeds, feeds and power available on the machine.

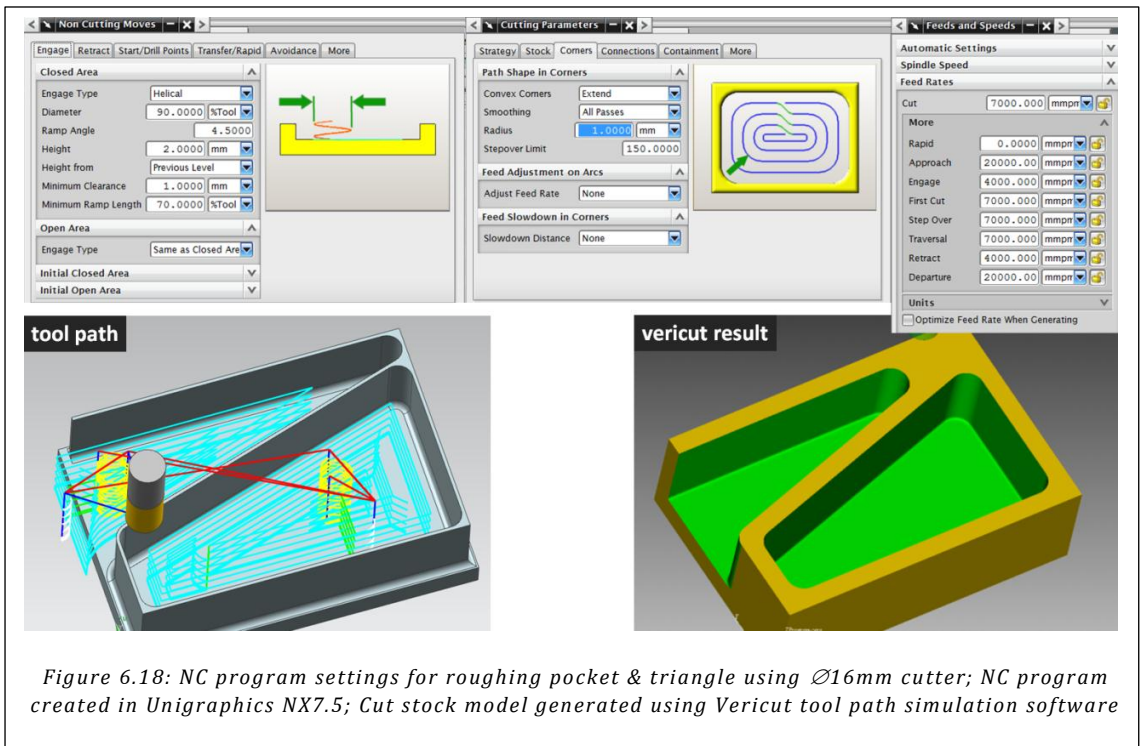


Figure 6.18: NC program settings for roughing pocket & triangle using Ø16mm cutter; NC program created in Unigraphics NX7.5; Cut stock model generated using Vericut tool path simulation software

Table 6.1: Cycle Time Summary Aluminum Demo Part

Machining Step	Cutting Tool			Machine		Stock		Cutting Conditions					Performance			
	Diameter [mm]	Teeth [-]	Radius [mm]	Speed [RPM]	F [mm/min]	Axial [mm]	Radial [mm]	ADOC [mm]	RDOC [mm]	fz [mm]	hmax [mm]	Vc [m/min]	MRR [cm3/min]	Machine [mm:ss]	Vericut [mm:ss]	
Roughing pockets	S10	16.000	2	1.30	17500	11550	0.00	3.75	9.00	16.00	0.330	0.330	879	1663	0:01:05	0:00:44
Roughing corners	S20	12.000	2	3.20	20000	8000	0.00	0.10	12.00	12.00	0.200	0.200	754	1152	0:00:21	0:00:16
Semi-finish wall	S30A	12.000	2	3.20	20000	14000	0.00	1.20	12.00	2.55	0.350	0.286	754	428	0:02:04	0:01:21
Finish wall	S30B	12.000	2	3.20	20000	10000	0.00	0.00	6.00	1.20	0.250	0.150	754	72.0		
<b>Total</b>													<b>0:03:30</b>	<b>0:02:21</b>		



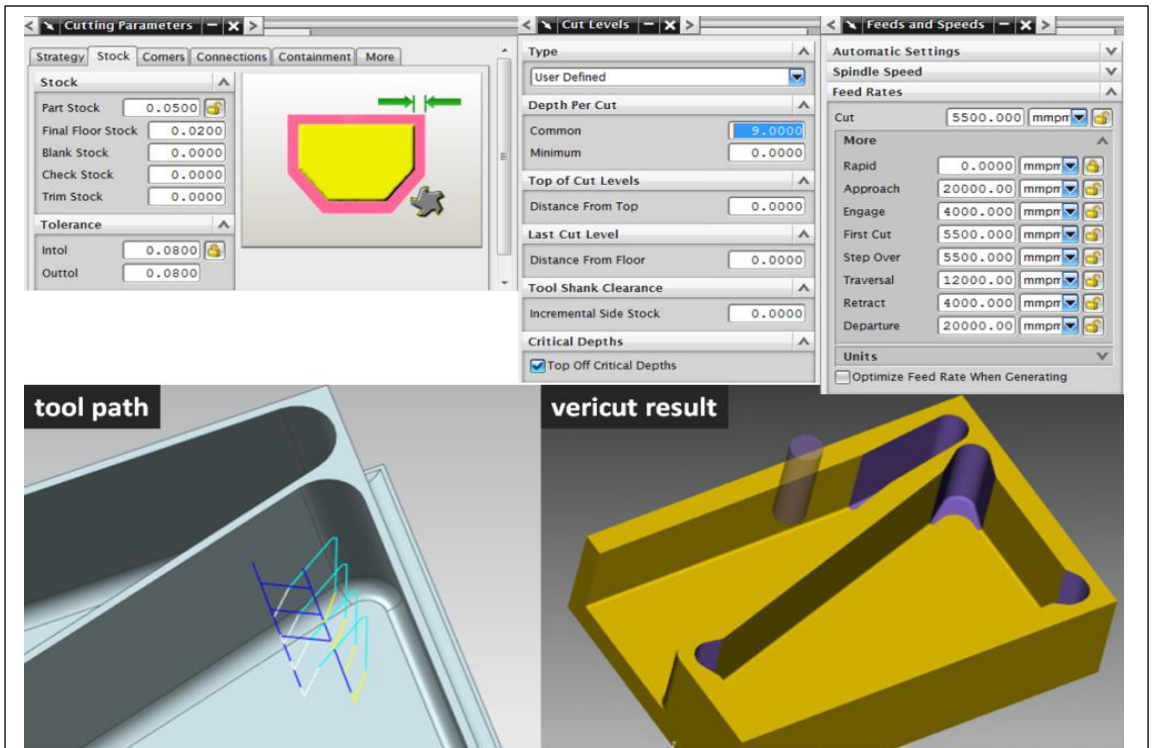


Figure 6.19: NC program settings for corner roughing using  $\varnothing 12\text{mm}$  cutter; NC program created in Unigraphics NX7.5; Cut stock model generated using Vericut software

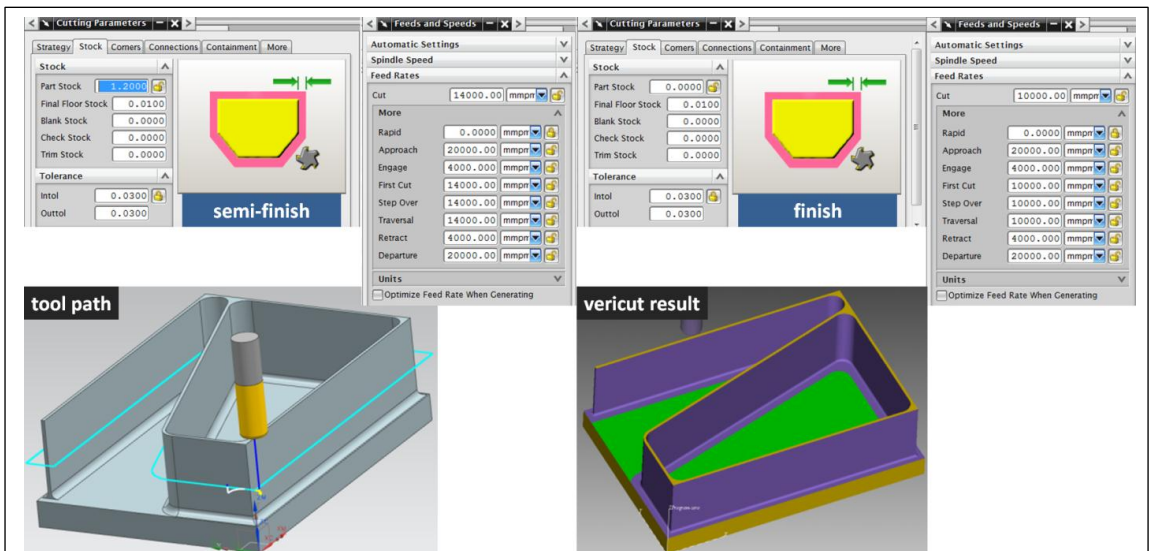


Figure 6.20: NC program settings for semi-finish and finish using  $\varnothing 12\text{mm}$  cutter (thin wall strategy, see Figure ); NC program created in Unigraphics NX7.5; Cut stock model generated using Vericut tool path simulation software

### 6.4.7 Part Machining

The left of Figure shows the part after roughing with the  $\varnothing 16\text{mm}$  cutter has been completed. The roughed walls are then 9.0mm thick. The right of Figure shows the part after all corners have been roughed using the  $\varnothing 12\text{mm}$  cutter. In the corners, we leave only 0.10mm material to remove. The final machining step semi-finishes and finishes the wall using the same  $\varnothing 12\text{mm}$  cutter.

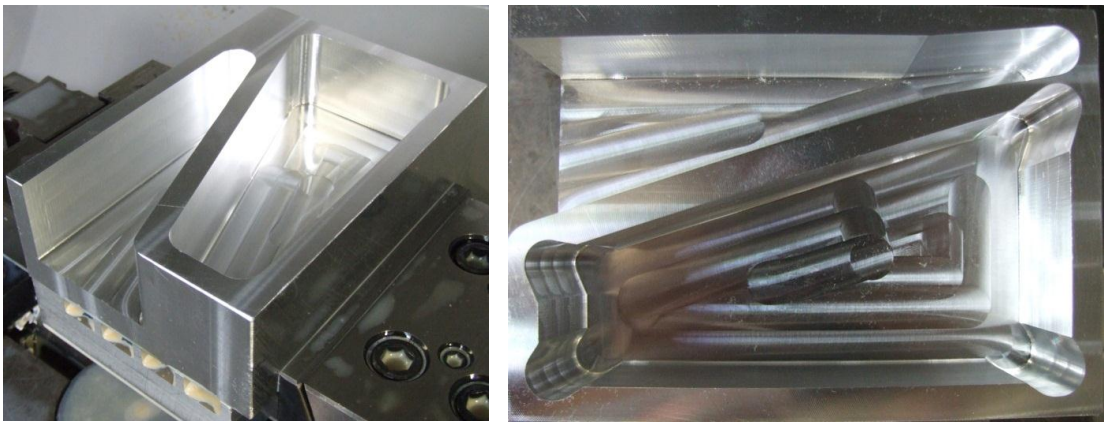


Figure 6.21: Left=rough machining with  $\varnothing 16\text{mm}$  cutter completed; Right= rough machining with  $\varnothing 12\text{mm}$  cutter completed

### 6.4.8 MACHpro Optimization

Figure shows the chip load history of the roughing operation, which has been programmed with 0.330mm chip load. In 4 places in the program, the tool ramps down into the pocket, and a reduced chip load of 0.150mm is used. The graph shows that along the tool path, the chip load is almost constant at 0.330mm, and when we apply feed optimization as explained in [6] and [7] with 0.330mm chip load as sole constraint, the productivity improvement is only 0.88%. When roughing in aluminum, radial engagement is often larger than  $0.50xD$ , which is the case for the NC program under consideration.

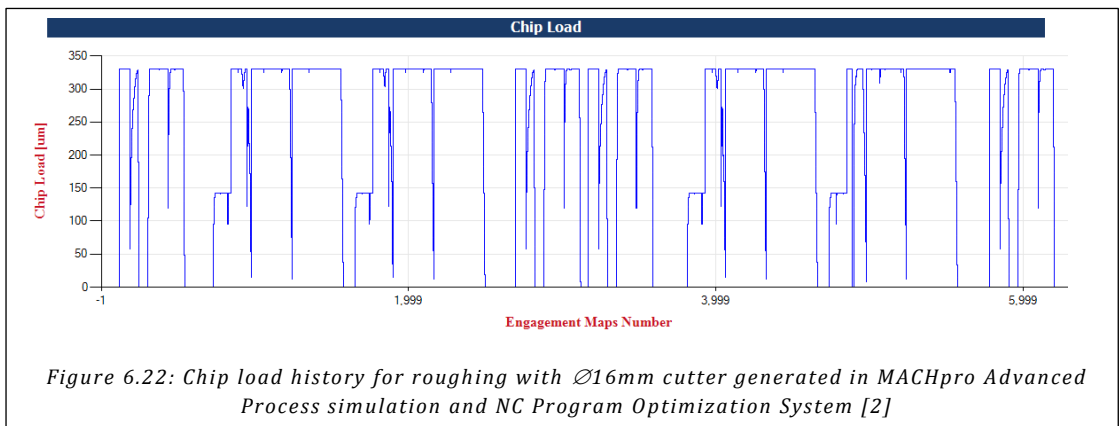


Figure 6.22: Chip load history for roughing with  $\varnothing 16\text{mm}$  cutter generated in MACHpro Advanced Process simulation and NC Program Optimization System [2]

Titanium is a strong light alloy increasingly used in aerospace due to its compatibility with Carbon Fiber Reinforced Plastic (CFRP). Titanium has poor thermal conductivity, is sensitive to work hardening and has a Young's modulus of 114GPa, which is about half that of steel (205GPa). These properties have the following implications for machining:

- Cutting speed is limited as heat generated in the cut needs to be absorbed by the cutting tool and cutting fluid; depending on radial engagement, typical cutting speed is 40-120m/min
- Sharp cutting tools and sufficient chip load have to be used to avoid ploughing/rubbing that results in work hardening
- Fixturing and/or stock left on the part have to be chosen in a way that keeps the part from deflecting away during machining

## 6.5 Titanium Machining: Machining steps

As in aluminum, aircraft parts in titanium can sometimes be machined in a single setup, but the majority requires multiple setups to control distortion of the part and/or to access all sides of the part to remove the excess material. The number of steps required depends on the machine kinematics (3, 4 or 5-axis) and the fixturing method. Titanium parts are often roughed on rigid gantry machines with multiple spindles (3 or 5-axis) and then finished on single spindle palletized machining centers.

### 6.5.1 Roughing

As cutting speed in titanium is limited, the only way to obtain good productivity is large cuts or fast cuts or combinations of these. Typically the largest cuts can be taken while machining the sides of the part with helical solid or indexable cutters, which can be run at relatively high cutting speed due to partial radial engagement. Large cuts are also made with face mills, which require significant torque at low spindle speeds. Both applications require strong and stable fixturing to avoid vibration of part and clamps. Fast cuts can be made with solid carbide tools and high feed mills. Solid carbide tools are expensive but can be very suitable for shallow pockets where small diameters are needed. High feed mills maybe productive there too, as the use of helical cutters maybe inefficient due to limited axial engagement. For long tool stick outs, high feed milling is very suitable. Face milling can also be done with high feed mills, which is an example of a large and fast cut, which could use up available torque.

- Large diameter helical cutters (cobalt, M42, high speed steel) are usually reground several times; serrated cutter geometries are more difficult to regrind. Brazed helical cutters, which can be reground and rebrazed, are used less often.
- Large, thick inserts provide the best security on indexable cutters but yield lower flute counts; small inserts can be used with care and sufficient chip evacuation and have better cutting angles and higher flute counts to their advantage.
- High feed mills come in indexable form for large diameters and solid carbide tools for small diameters. Medium size cutters ( $\varnothing$ 10-25mm) are available as solid screw-in carbide heads.

Recutting titanium chips should be avoided to prolong tool life by employing plentiful coolant and periodic removal of chips from the work piece. High speed steel/cobalt cutters are most forgiving in recutting, but carbide tools chip easily.



## 6.5.2 Semi finishing

Semi finishing in titanium is typically done with smaller diameter indexable and solid tools to remove the steps left by the large roughing cuts. Larger ball nose cutters (also solid and indexable) are used to keller curved surfaces closer to their final shape.

## 6.5.3 Finishing

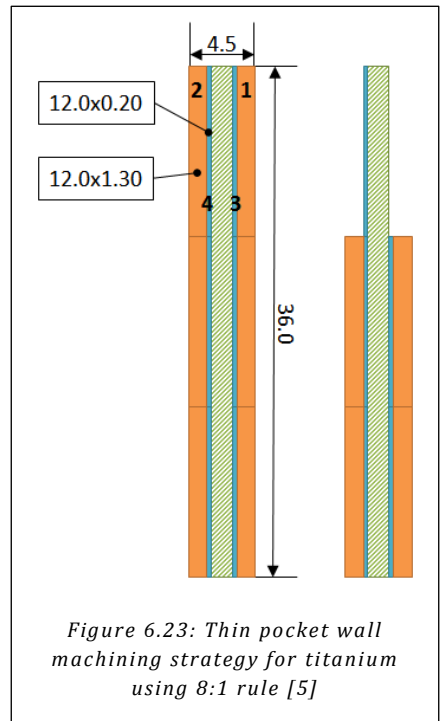
Finishing in titanium is typically done with solid tools for walls and fillets, and with indexable round insert tools for pocket floors.

### 6.5.3.1 Thin pocket walls

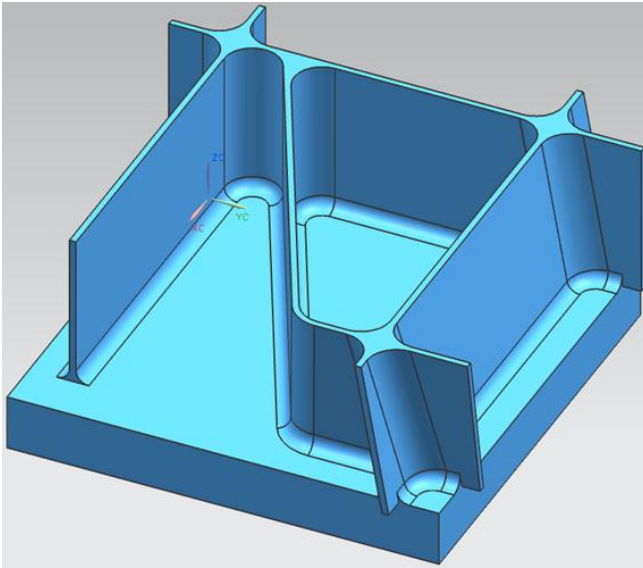
In order to machine thin pocket walls in titanium without vibration problems, the eight-to-one rule (8:1) can be used to devise the machining plan. This approach, ensures the part is always stiff enough to machine, avoiding part vibrations. Aircraft structural parts have complex shapes, hence work piece chatter is difficult to eliminate as natural frequencies change constantly during machining. Using the 8:1 rule makes the titanium part “rigid”, allowing you to focus on only optimizing your cutters to be able to achieve the cuts resulting from the method (smaller cuts can be taken but will slow down machining). Hence, titanium behaves as a stiffer material than aluminum where the ratio is 4:1.

The application of the rule is done in reverse order (Figure ):

- The result of roughing and semi finishing needs to result in a ratio of wall height and wall thickness of 8:1 (no more); Example: for a 36.0mm wall, the thickness after roughing and semi-finishing should be 4.5mm or more.
- When taking the final finishing pass, the axial depth of cut cannot be larger than 8 times the finished wall thickness; Example: for a 1.50mm thick wall, the maximum cutting depth is 12.0mm
- Finishing is typically done in two radial passes (depending on wall height), the last one removing 0.20mm; this wall will measure  $1.50+2 \times 0.20=1.9\text{mm}$  thick before final finishing.
- As the wall measures 4.5mm thick after rough/semi-finish, there is 1.30mm to remove before final finishing to obtain a 1.9mm thick wall, which is done by a pre-finish cut. Repeated application of the 8:1 rule allows to take us  $8 \times 1.9=15.2\text{mm}$  axial depth of cut. In this case it's practical to use 12.0mm depth, which will then be followed by finishing at the same depth.



## 6.6 Demo part High Performance / High Speed Machining in Titanium



**Material:** TI-6Al-4V

Stock: 100 x 100 x 50 mm

Wall height = 36.0 mm

Wall thickness = 1.50 mm

Fillet radius = 3.0 mm

Corner radius = 6.5 mm

Raw material = 2.170 kg

Finished part = 0.756 kg

Material removal = 1.414 kg

Cycle time = 56 minutes

Effective MRR = 1.52 kg/h

Figure 6.24: Demo part titanium machining; 100x100mm, 36mm high walls; Part modeled in Unigraphics NX7.5

### 6.6.1 Titanium demo part design

The titanium demo part includes the typical aerospace component characteristics:

- thin wall 36.0mm high, 1.5mm thick (ratio of height to thickness = 24)
- smallest pocket corner angle is 26°
- one wall has a 10° tilt, creating three closed angle areas
- one wall end is free-standing
- the fillet radius between wall and base depends on the cutter used – a typical value for aerospace is 3.0mm to 5.0mm; for this project we used 3.0mm

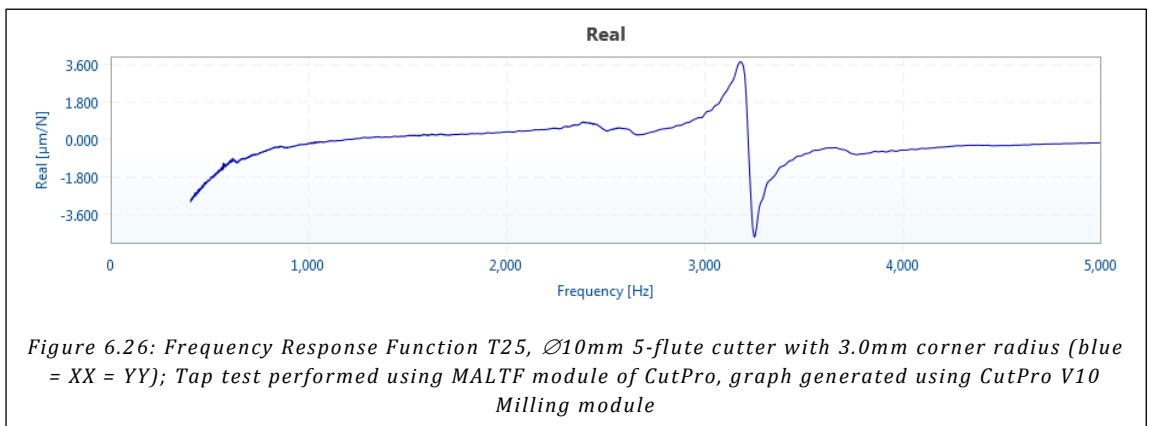
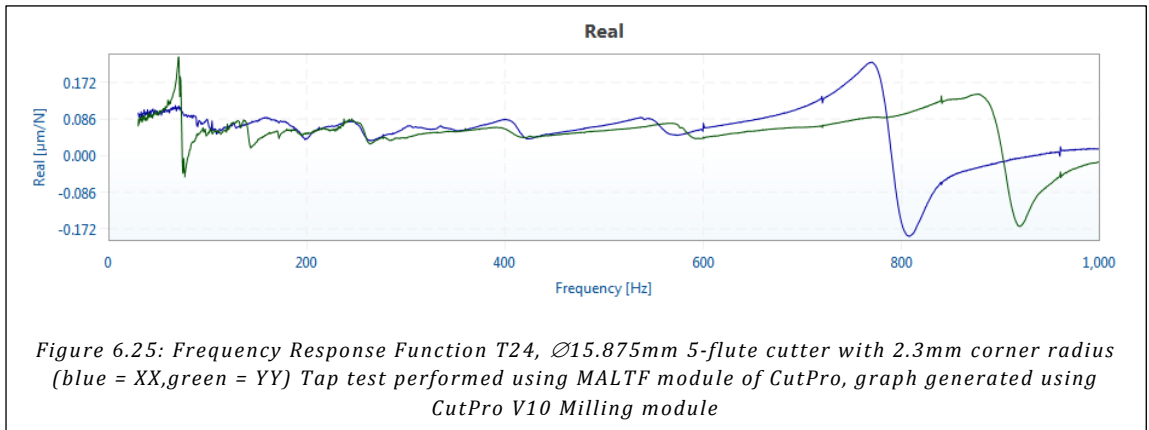
### 6.6.2 Machine & cutter selection

The machine tool used is a five-axis Mori Seiki NMV5000-DCG vertical machine with trunnion table, with 20,000RPM/18.5kW HSK63A spindle. The following tools are used for machining the part from forged block material:

- T24)** 2-flute Ø21mm U-drill in Weldon holder (Sandvik);
- T25)** 5-flute Ø5/8" endmill with 2.3mm corner radius Dataflute SSI type), held in a Corogrip holder with Ø20 to Ø5/8" sleeve;
- T26)** 4-flute Ø1/2" end mill with 0.8mm corner radius (Sandvik RA216.24 type)
- T27)** 5-flute Ø10mm endmill with 3.0mm corner radius and 35° helix (Dataflute TiW type) mounted in Hydrogrip holder with Ø20 to Ø10mm sleeve
- T28)** 4-flute Sandvik Ø6mm tapered ballnose endmill mounted in Hydrogrip holder with Ø20 to Ø10mm sleeve



The FRF of T25 and T26 have been measured and are shown in Figure and Figure .



### 6.6.3 Machining strategy

We use the  $\varnothing 10\text{mm}$  cutter to semi-finish and finish the walls using the strategy shown in Figure , hence we need to rough the part down to 4.5mm wall thickness first (+1.5mm stock on each side). The complete machining strategy can be summarized as follows:

- S10) Closed pocket: Drill a starter hole for the  $\varnothing 5/8''$  end mill
- S20) Part periphery: Rough using the  $\varnothing 5/8''$  end mill
- S30) Open pocket: Throchoidal mill using the  $\varnothing 5/8''$  end mill in small peripheral engagement
- S40) Closed pocket: Mill out the pocket using the  $\varnothing 5/8''$  end mill in small peripheral engagement – a combination of pocketing and throchoidal milling;
- S50) Finish the floor using the  $\varnothing 5/8''$  end mill
- S60) Closed-angle areas (under  $10^\circ$  slanted walls): Rough 5-axis with the  $\varnothing 5/8''$  endmill
- S70) Plunge all pocket corners with the  $\varnothing 1/2''$  end mill
- S80) Semi-finish and finish all walls using step-method (Figure ) up to 32.4mm deep
- S90) Rough closed-angle areas (under  $10^\circ$  slanted walls) using the  $\varnothing 10\text{mm}$  endmill, and finish the root of the wall in a single pass.
- S100) Scan closed-angle areas (under  $10^\circ$  slanted walls)

### 6.6.4 CutPro: Selection of cutting conditions

CutPro is used to establish the chatter stability lobes for cutter T24 to select the best spindle speed/depth of cut combination to achieve the highest productivity. T24, the Ø5/8” cutter machines away the bulk of the raw material, up to 36.0mm deep. The stability lobes established in Figure take the variable pitch geometry of the cutter into account, and are valid for 2.0mm radial depth of cut. The lobe points originate from the 900Hz Y-mode, which is the spindle and indicate that depths of cut up to 18mm are stable). Stability lobes have also been calculated while ignoring the variable pitch geometry, shown in Figure , and the narrow lobes originate from the 900Hz Y-mode. They are “trimmed” by the 70Hz structural Y-mode in the 1000-1800RPM speed range (illustrated by the dashed red line). The minimum stable depth of cut is 11.4mm. As expected, variable pitch geometry increases the stability border. Sample cutting test results are provided in Table 6.2, which were all stable. In the tests, the axial depth of cut was kept constant at 36.0mm while the radial depth of cut was increased. At three speeds (1200/1550/1800RPM) cutting is stable in both X and Y direction up to 2.50mm wide and 36.0mm deep, which is deeper than the lobes predict. The result can be attributed to process damping which occurs at relatively low cutting speeds. For the NC-program, we have selected to cut with maximum 35.5mm axial depth of cut and 1.50mm radial depth of cut.

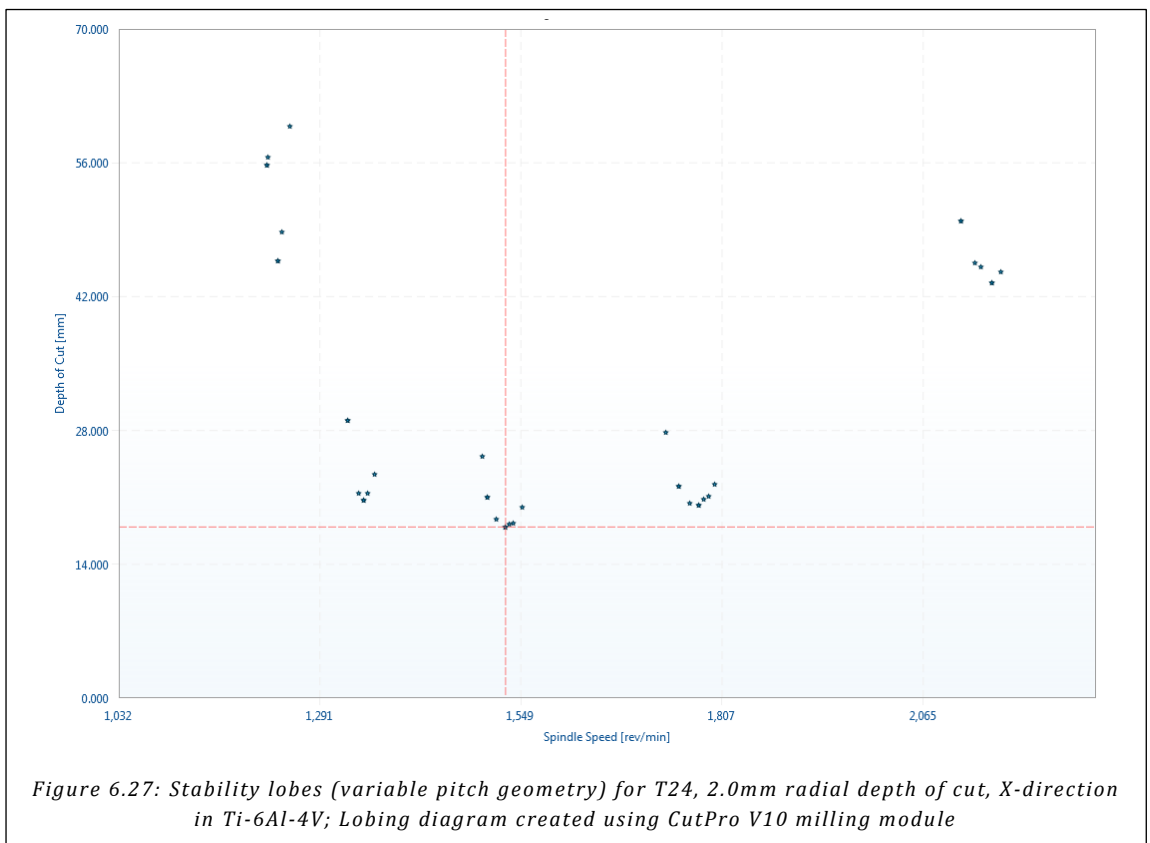


Figure 6.27: Stability lobes (variable pitch geometry) for T24, 2.0mm radial depth of cut, X-direction in Ti-6Al-4V; Lobing diagram created using CutPro V10 milling module

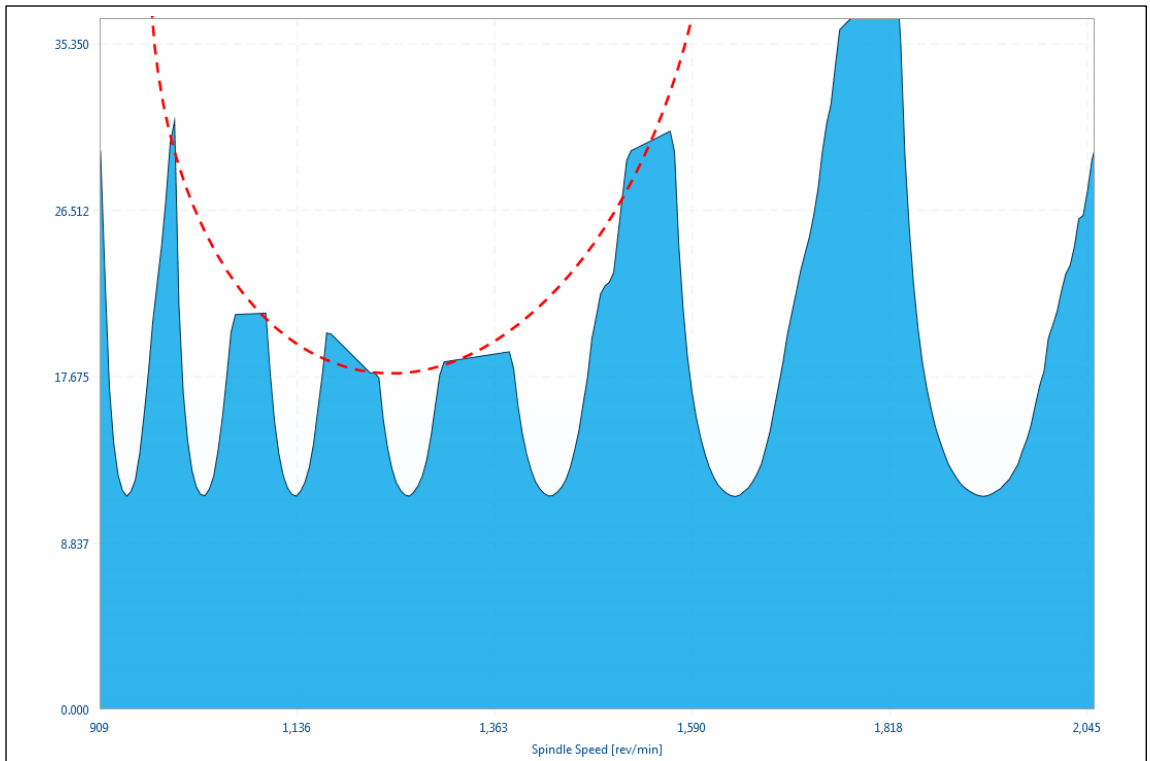


Figure 6.28: Stability lobes (regular pitch geometry) for T24, 2.0mm radial depth of cut, X-direction in Ti-6Al-4V; Lobing diagram created using CutPro V10 milling module

Table 6.2: Cutting tests performed using T24, Ø15.875mm 5-flute cutter with 2.3mm corner radius

Test	Cutting Tool			Machine		Cutting Conditions					Performance	Tool impact
	Diameter	Teeth	Radius	Speed	F	ADOC	RDOC	fz	hmax	Vc	MRR	Engagement angle
	[mm]	[-]	[mm]	[RPM]	[mm/min]	[mm]	[mm]	[mm]	[mm]	[m/min]	[cm <sup>3</sup> /min]	[°]
X1	15.875	5	2.3	1200	991	36.0	1.00	0.165	0.080	59.8	35.7	29.1
X8	15.875	5	2.3	1200	533	36.0	4.50	0.089	0.080	59.8	86.4	64.4
X12	15.875	5	2.3	1550	850	36.0	2.50	0.110	0.080	77.3	76.5	46.8
X15	15.875	5	2.3	1800	983	36.0	2.50	0.109	0.080	89.7	88.5	46.8
Y3	15.875	5	2.3	1800	983	36.0	2.50	0.109	0.080	89.7	88.5	46.8
Y6	15.875	5	2.3	1550	850	36.0	2.50	0.110	0.080	77.3	76.5	46.8
Y9	15.875	5	2.3	1200	663	36.0	2.50	0.110	0.080	59.8	59.7	46.8

For T25, a Ø10mm endmill with 3.0mm corner radius, cutting tests have been performed with a 4-flute Sandvik tool (R216.24 type) and the stable cutting results are tabulated in Table 6.3, the stability lobes with process damping are shown in Figure for 1.3mm radial depth of cut and in Figure for 0.20mm radial depth of cut. In semi-finishing we need to be able to take a 12.0mm deep cut 1.3mm wide at 1941RPM, while for finishing we need to be able to take a 12.0mm deep cut 0.20mm wide at 3883RPM. As can be seen from the table, we can cut at least 4 times wider in semi-finish and 10 times wider in finish. Hence the actual process damping is still stronger than the lobes with process damping indicate. Figure shows a

maximum 4.0mm depth of cut for semi-finish, 1.30mm wide. Figure shows a maximum 10mm depth of cut for finishing, 0.20mm wide.

Later in this guide we also use a  $\varnothing 10\text{mm}$  5-flute Dataflute tool (TiW type), which can be run at the exact same spindle speed and feed rate. The Sandvik tool has a  $50^\circ$  helix angle but the Dataflute has a  $35^\circ$  helix angle. As a result, the maximum uncut chip thickness at a given feed rate is the same whether you use a  $50^\circ$  helix angle & 4 flutes or  $35^\circ$  helix angle and 5 flutes. The Dataflute tool also has variable pitch geometry, which increases stability over the Sandvik tool which has a regular pitch distribution.

Table 6.3: Cutting tests performed using T25,  $\varnothing 10.000\text{mm}$  4-flute cutter with 3.0mm corner radius

Test	Cutting Tool			Machine		Cutting Conditions					Performance	Tool impact
	Diameter	Teeth	Radius	Speed	F	ADOC	RDOC	fz	hmax	Vc	MRR	Engagement angle
	[mm]	[-]	[mm]	[RPM]	[mm/min]	[mm]	[mm]	[mm]	[mm]	[m/min]	[cm <sup>3</sup> /min]	[ $^\circ$ ]
SF1	10.0	4	3.0	1941	596	12.0	1.30	0.077	0.052	61.0	9.3	42.3
SF2	10.0	4	3.0	1941	508	12.0	2.00	0.065	0.052	61.0	12.2	53.2
SF3	10.0	4	3.0	1941	443	12.0	3.00	0.057	0.052	61.0	16.0	66.5
SF4	10.0	4	3.0	1941	411	12.0	4.00	0.053	0.052	61.0	19.7	78.5
SF5	10.0	4	3.0	1941	402	12.0	5.00	0.052	0.052	61.0	24.1	90.0
F1	10.0	4	3.0	3883	939	12.0	0.20	0.060	0.017	121.9	2.3	16.3
F2	10.0	4	3.0	3883	609	12.0	0.50	0.039	0.017	121.9	3.7	25.9
F3	10.0	4	3.0	3883	440	12.0	1.00	0.028	0.017	121.9	5.3	36.9
F4	10.0	4	3.0	3883	367	12.0	1.50	0.024	0.017	121.9	6.6	45.6
F5	10.0	4	3.0	3883	331	12.0	2.00	0.021	0.017	121.9	7.9	53.2

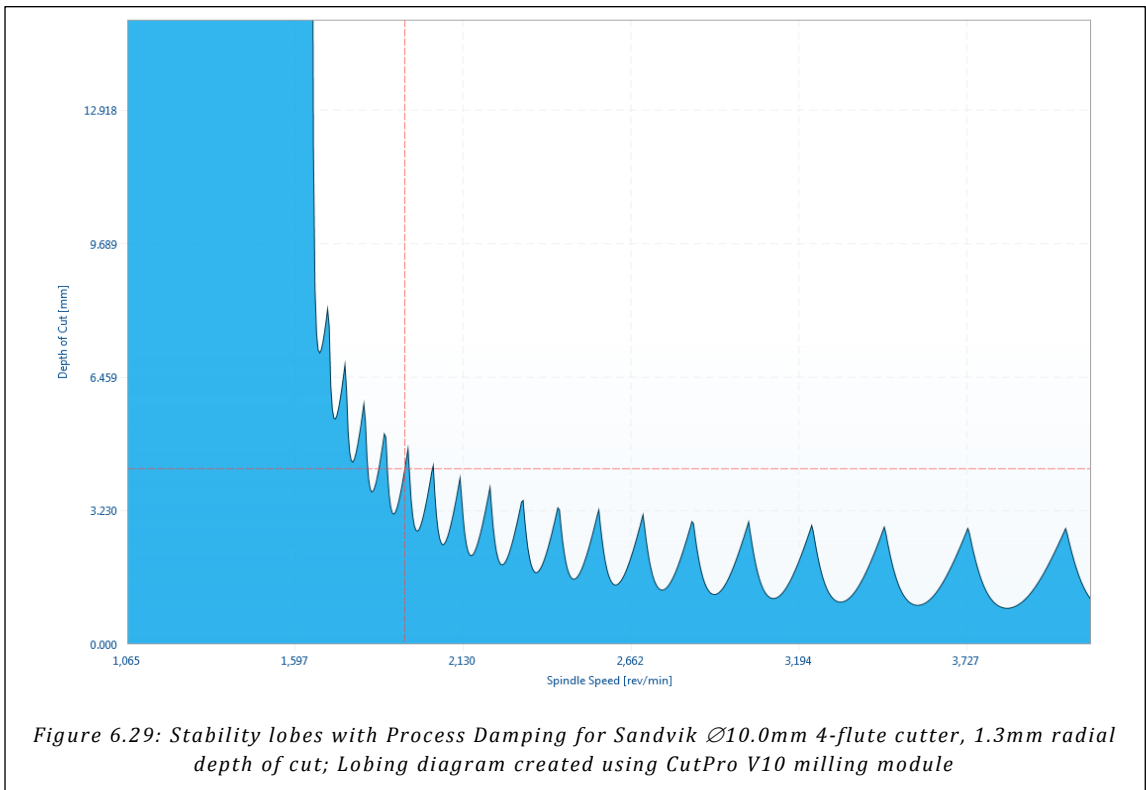


Figure 6.29: Stability lobes with Process Damping for Sandvik  $\varnothing 10.0\text{mm}$  4-flute cutter, 1.3mm radial depth of cut; Lobing diagram created using CutPro V10 milling module

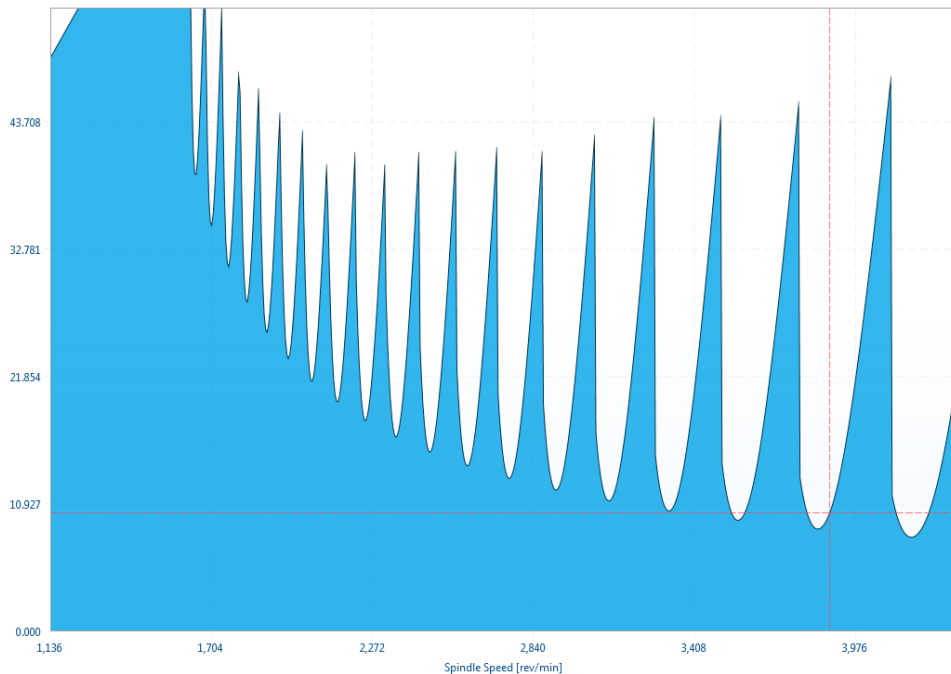


Figure 6.30: Stability lobes with Process Damping for Sandvik Ø10.0mm 4-flute cutter, 0.20mm radial depth of cut; Lobing diagram created using CutPro V10 milling module

### 6.6.5 Thin Wall Machining Experiments

In order to validate the machining steps determined with the 8-to-1 rule in Figure , we have tested the method on Ti-6Al-4V specimens, 75.0x50.0x10.5mm (LxHxW) which were clamped in a vise. The machining steps are illustrated in Figure . The wall is roughed using the Ø5/8” cutter, taking 1.5mm wide and 36.0mm deep passes from either side, roughing the plate to 4.5mm thickness (steps 1-4). Next, the Ø10mm cutter is used to semi-finish level A taking 1.3mm wide and 12.0mm deep passes from either side (step 5&6), followed by finish passes 0.20mm wide and 12.0mm deep (step 7&8). Levels B (steps 9-12) and C (steps 13-16) are completed the same way as level A.

A first plate specimen was machined following these steps, and the work piece was measured using the machine probe (Renishaw OMP60) after steps 2, 4, 6, 8, 10, 12, 14 and 16. The results are shown in Figure (on the left). After roughing the wall is too thick by 0.453-0.691mm, after semi-finish the wall is too thick by 0.304-0.602mm, and after machining is complete, the wall is out of tolerance in 5 out of 9 places. From this we can conclude that either cutter and/or work piece do not behave rigid enough to machine the part within tolerance.

We have analyzed both tool and work piece flexibility for all machining steps. We assumed that the cutting process is static, hence we can use the static stiffness of tool and work piece, and apply the average normal and axial cutting forces to the work piece. The static tool flexibilities for the tools were obtained from the FRFs as  $T24=0.10\mu\text{m}/\text{N}$  and  $T25=0.27\mu\text{m}/\text{N}$ . The roughing, semi-finishing and finishing cuts were simulated in CutPro milling engine (assuming no deflection), and the average normal and axial force on the work piece were obtained. Solid models of the work piece were created in Unigraphics, and as shown in Figure , we analyze the part deflection in the middle of the plate.

The Finite Element package integrated in Unigraphics (Nastran) was used to mesh the work piece and apply the axial and normal cutting forces as distributed loads along the cutting depth, and calculate the resulting work piece deflection. This approach is illustrated for step 5 (semi-finishing cut) in Figure .

The results from our Finite Element analysis on work piece deflection and tool deflection, and their combined effect are tabulated in Table 6.4. Based on the simulation results, we decided to compensate the NC program for the plate with the values shown in the table, each time we chose a round number close to the worst result for each machining step per level. For the finishing cut we always used the same value, to ensure a good blend between the axial steps. Note that compensation at the finishing stage is somewhat dangerous in case the cutter has very little to remove, the part may become under nominal. We do stay within the tolerance band (programmed at -0.050mm, tolerance band  $\pm 0.120\text{mm}$ ).

As can be seen in the right in Figure , the plate machined with NC program compensation is now within tolerance, and we also achieve the target thickness much better at each level of machining (roughing, semi-finish and finish). The compensation values can be optimized further to achieve a more uniform thickness. Reviewing the results in Figure , the finish machined plate #2 is thickest on the left, where the cutter enters and leaves the work piece. Some aircraft components require completely freestanding walls, but often they are supported on one side, as in our demo part, and this situation corresponds to the right side of the plate.

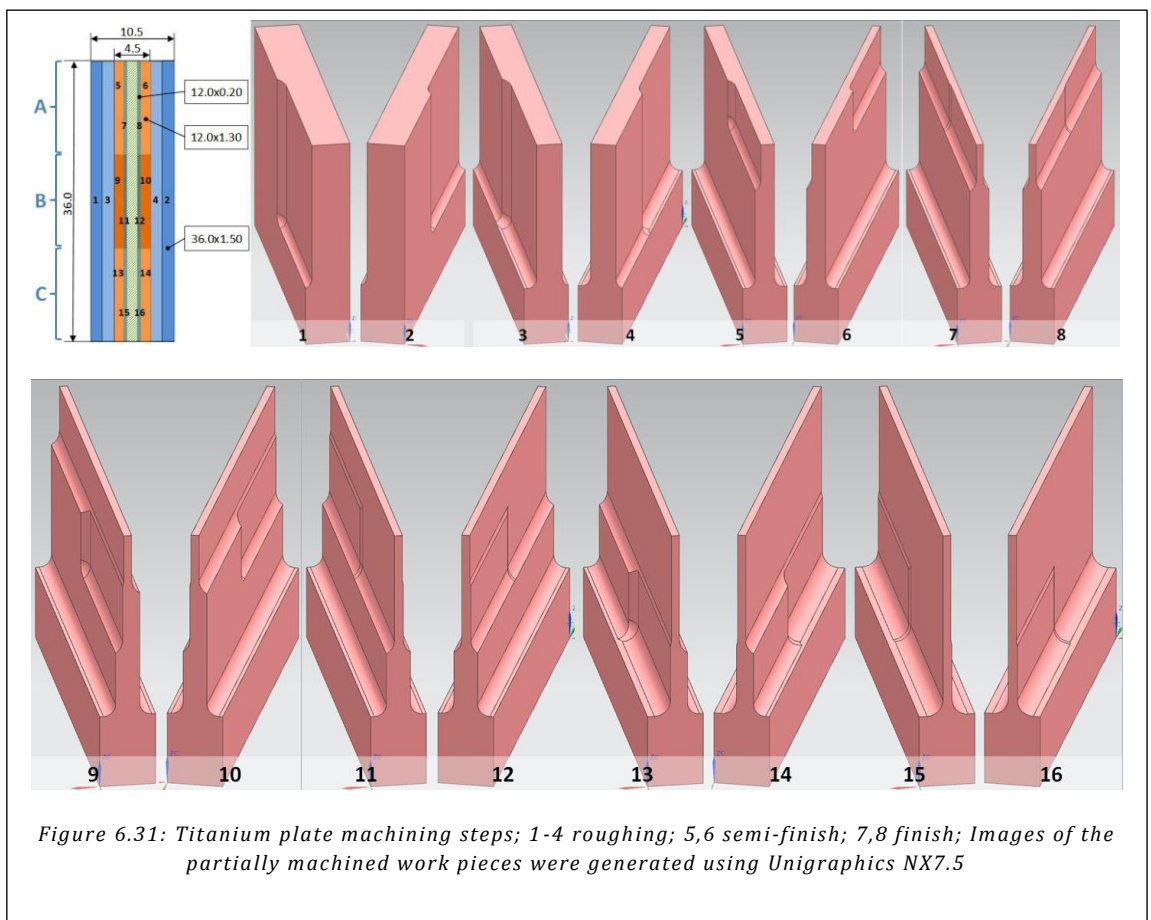


Figure 6.31: Titanium plate machining steps; 1-4 roughing; 5,6 semi-finish; 7,8 finish; Images of the partially machined work pieces were generated using Unigraphics NX7.5

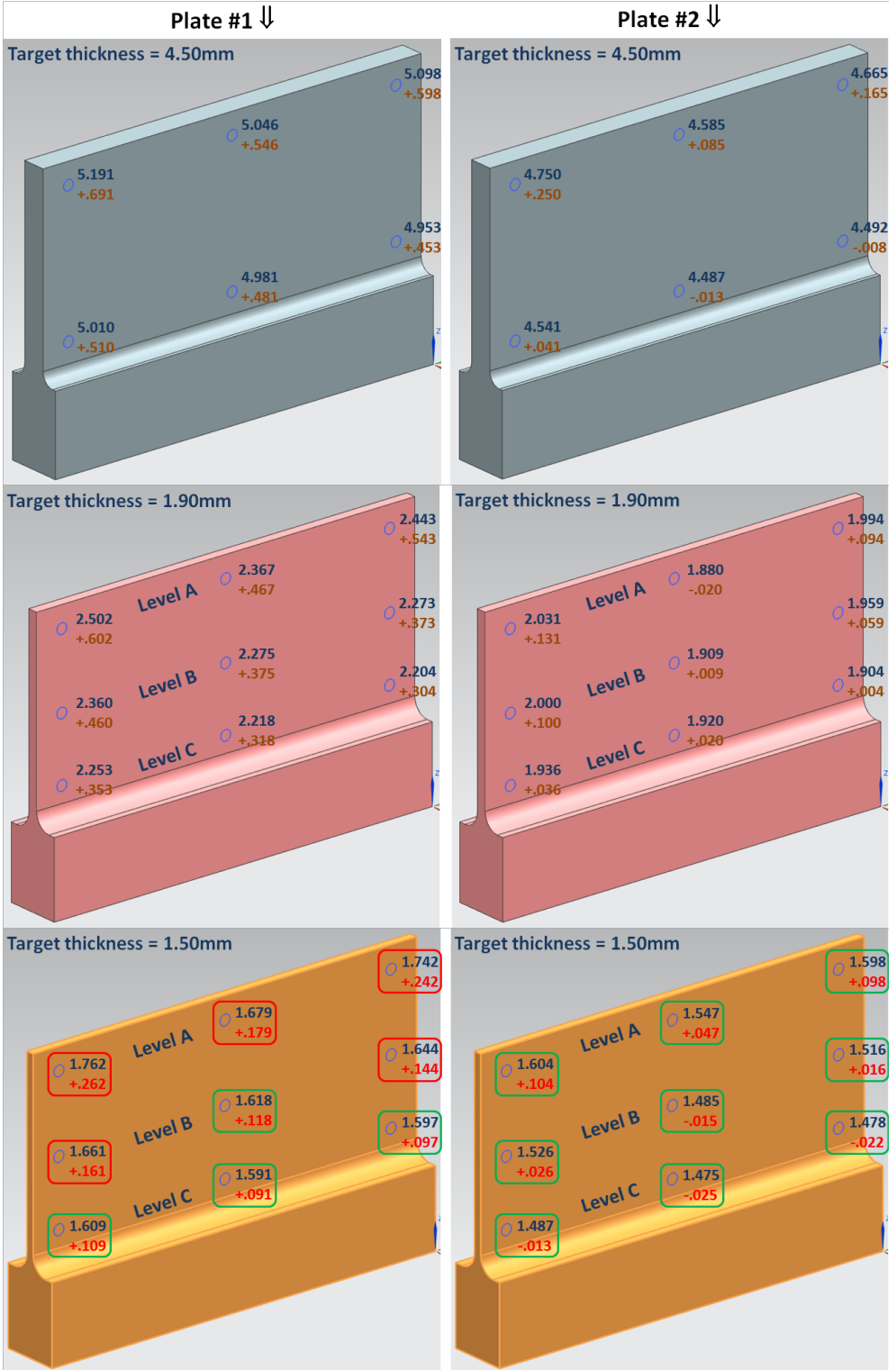


Figure 6.32: Titanium plate #1 & #2 machining measurement results; Top = after roughing (step 4); middle = after semi-finishing (steps 6, 10 & 14); bottom = after finishing (steps 8, 12 & 16); Finished wall thickness tolerance =  $\pm 0.120\text{mm}$

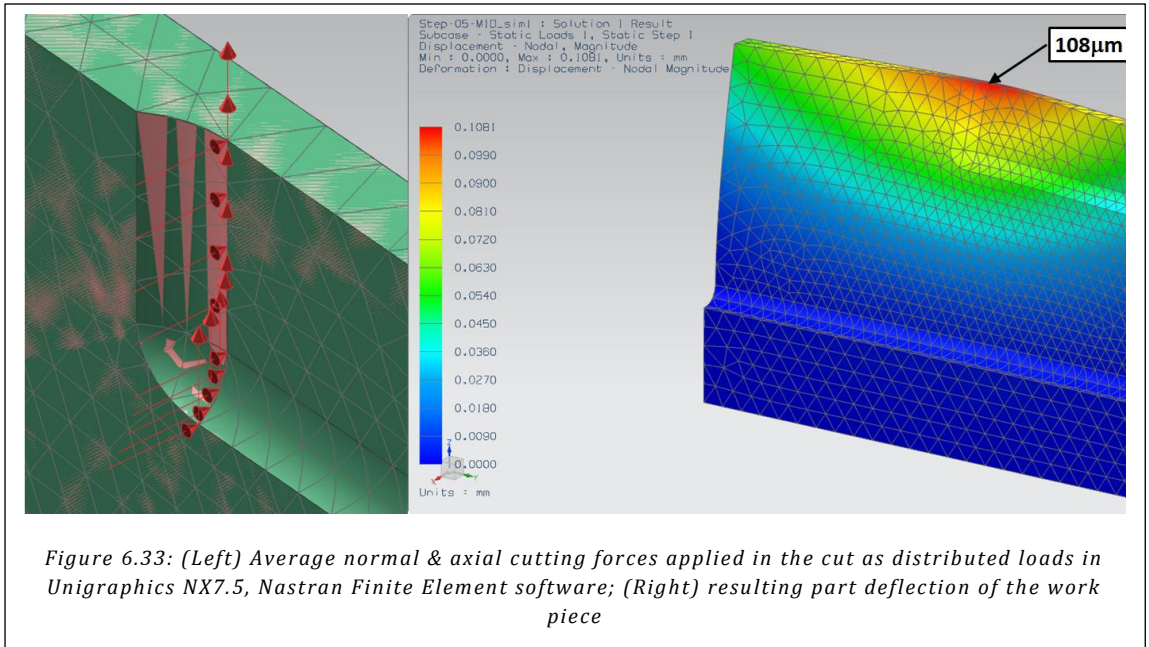


Table 6.4: Part and tool deflections calculated as result of static forces applied to each; Work piece was modeled using Unigraphics NX7.5, Nastran Finite Element software was used to calculate part deformation; The far right column shows the NC program compensation values used to machine plate #2 (thickness results shown on the right in Figure )

Machining Step	Location	Part deflection [µm]	Tool deflection [µm]	Total deflection [µm]	NC program compensation [µm]
Step 1 Roughing	Top	42	130	172	250
Step 2 Roughing	Top	52	130	182	250
Step 3 Roughing	Top	69	130	199	250
Step 4 Roughing	Top	114	130	244	250
Step 5 Semi-finishing	Top	108	117	225	250
Step 6 Semi-finishing	Top	131	117	248	250
Step 7 Finishing	Top	37	28	65	50
Step 8 Finishing	Top	41	28	69	50
Step 9 Semi-finishing	Middle	44	117	161	180
Step 10 Semi-finishing	Middle	60	117	177	180
Step 11 Finishing	Middle	20	28	48	50
Step 12 Finishing	Middle	23	28	51	50
Step 13 Semi-finishing	Bottom	12	117	129	140
Step 14 Semi-finishing	Bottom	25	117	142	140
Step 15 Finishing	Bottom	14	28	42	50
Step 16 Finishing	Bottom	15	28	43	50

### 6.6.6 MACHpro Form Error function

MACHpro [2] can also be used to estimate tool deflection in the machining process. Based on the cutting tool definition – how much the tool sticks out of the holder, the flute length as well as the cutter material, the normal cutting forces on the tool result in form errors. Hence MACHpro can be used to evaluate form errors caused by tool deflection.

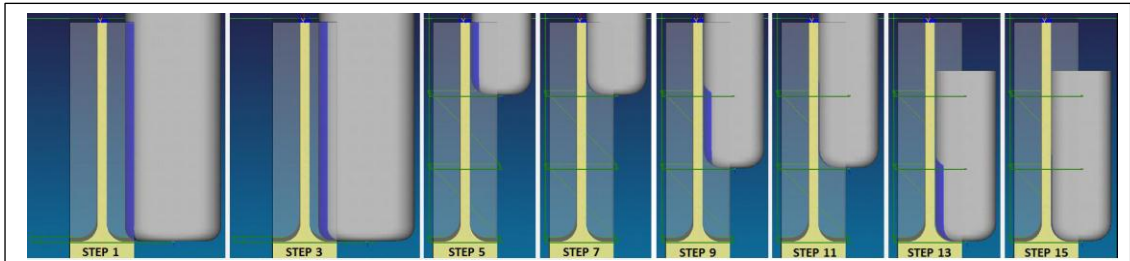


Figure 6.34: Thin Wall Titanium plate machining process visualized in MACHpro Advanced Process simulation and NC Program Optimization System [2]

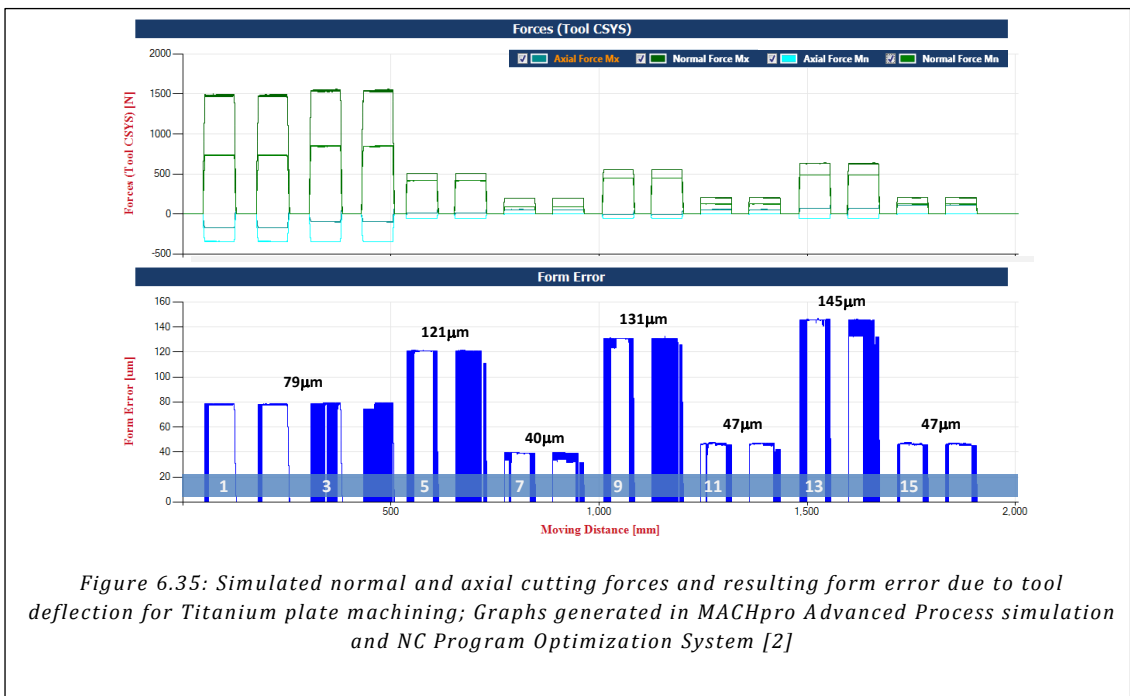


Figure 6.35: Simulated normal and axial cutting forces and resulting form error due to tool deflection for Titanium plate machining; Graphs generated in MACHpro Advanced Process simulation and NC Program Optimization System [2]

The tool deflection predicted in roughing and finishing is smaller than estimated from FRF, 80µm versus 130µm from FRF in roughing, and 40/47/47µm versus 28µm from FRF in finishing. For semi-finishing however, the results are very agreeable, 121/131/145µm versus 117µm from FRF.

### 6.6.7 NC Program Methods

The NC program for the demo part has been created in Unigraphics NX. The tool path settings as well as speed and feed, simulated tool path and Vericut simulation result are shown for S30 (roughing the open pocket - Figure ), S40 (roughing the closed pocket - Figure ) and S70 (plunging the corners where walls meet - Figure ).

All roughing with the  $\varnothing 5/8''$  cutter has been programmed with limited radial engagement, maximum 1.5mm, which is 9.5% and used roughing the periphery of the part (S20). When roughing the periphery, feed is reduced to 18% in the corners. For roughing the open & closed pockets (S30 & S40), a radial stepover of 1.2mm is used. The corner plunging is done with maximum 30% step-over as per supplier recommendations [8].

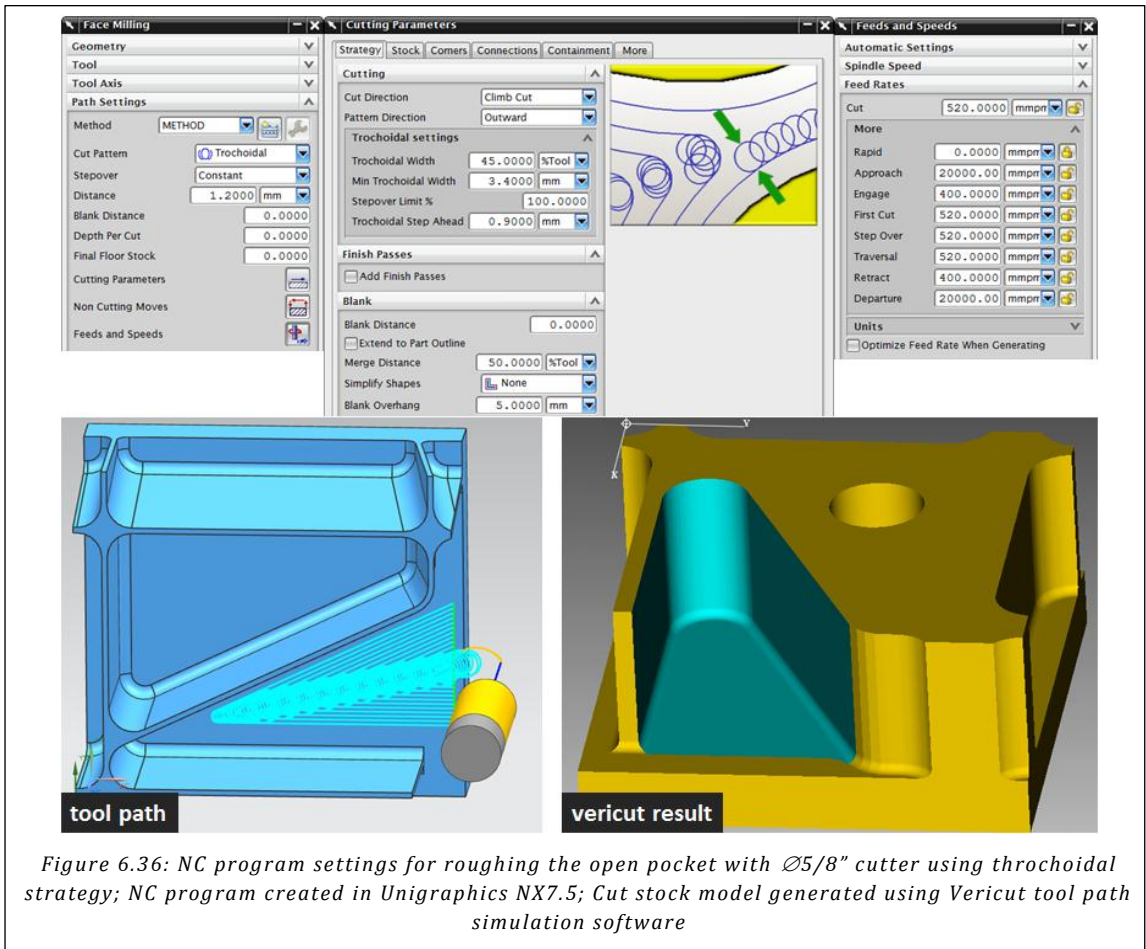


Figure 6.36: NC program settings for roughing the open pocket with  $\varnothing 5/8''$  cutter using trochoidal strategy; NC program created in Unigraphics NX7.5; Cut stock model generated using Vericut tool path simulation software

Table 6.5 provides a summary of programmed feed rates and cutting speeds for the entire NC program, and includes the real machining time as well as Vericut simulation time.

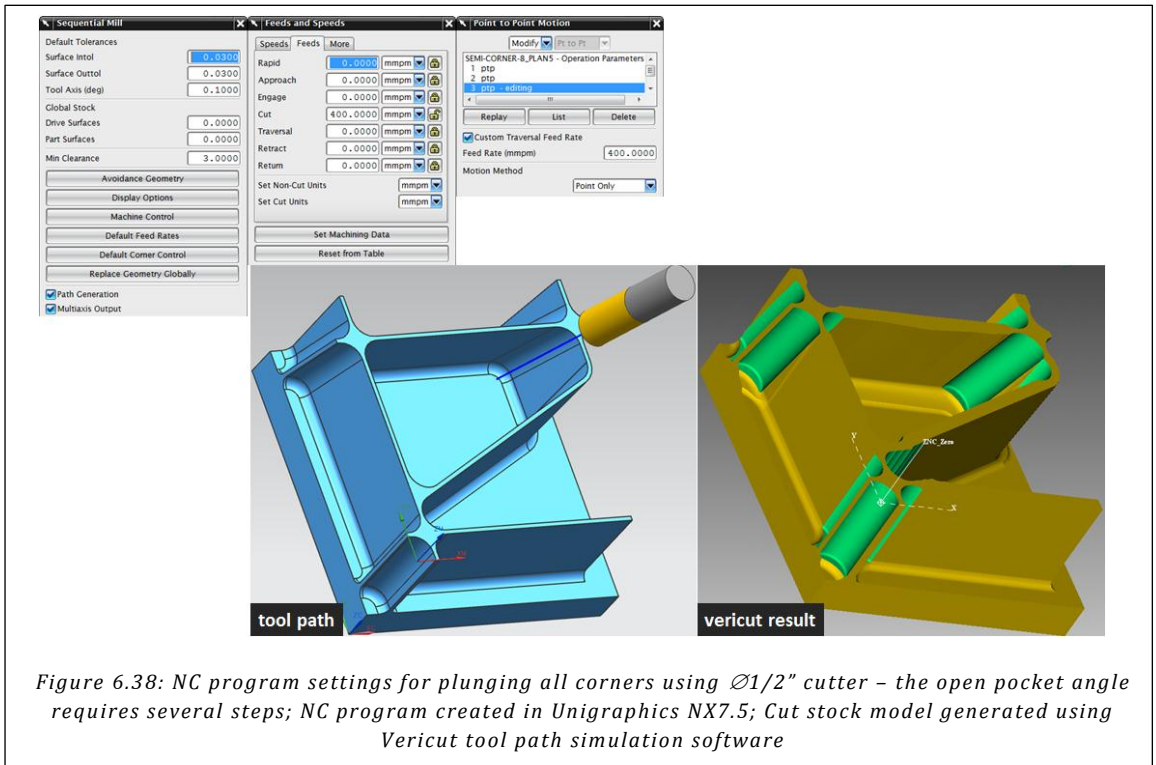
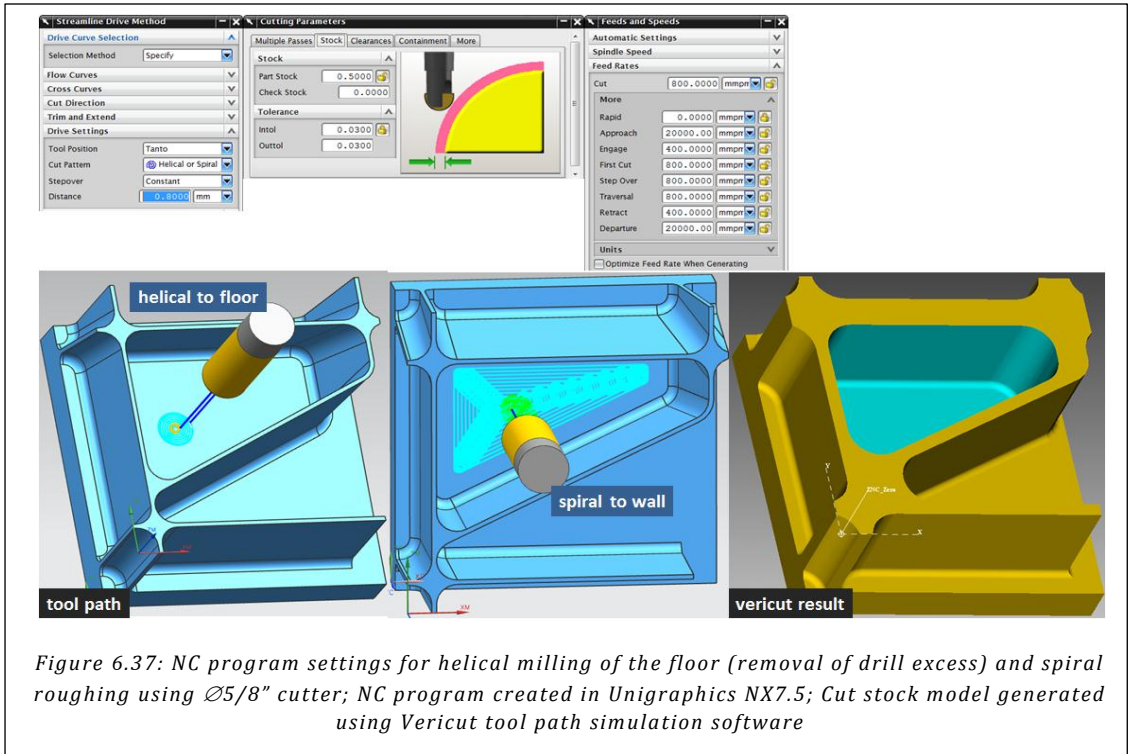


Table 6.5: Cycle Time Summary Titanium Demo Part

Machining Step		Cutting Tool			Machine		Stock		Cutting Conditions					Performance		
		Diameter	Teeth	Radius	Speed	F	Axial	Radial	ADOC	RDOC	fz	hmax	Vc	MRR	Machine	Vericut
		[mm]	[-]	[mm]	[RPM]	[mm/min]	[mm]	[mm]	[mm]	[mm]	[mm]	[mm]	[m/min]	[cm <sup>3</sup> /min]	[mm:ss]	[mm:ss]
Drill hole	S10	21.000	1	N/A	606	97	0.50	N/A	N/A	N/A	0.160	0.160	40	33.6	0:00:42	0:00:47
Rough periphery	S20	15.875	5	2.30	1200	823	0.50	1.50	36.00	1.50	0.137	0.137	60	44.4	0:06:34	0:06:27
Rough open pocket	S30	15.875	5	2.30	1264	520	0.50	1.50	36.00	1.20	0.082	0.082	63	22.5	0:06:43	0:06:46
Rough closed pocket	S40	15.875	5	2.30	1264	520	0.50	1.50	36.00	1.20	0.082	0.082	63	22.5	0:09:33	0:09:35
Finish floor	S50	15.875	5	2.30	2402	800	0.00	1.50	0.50	4.00	0.067	0.067	120	1.6	0:02:44	0:02:36
Rough closed angle areas	S60	15.875	5	2.30	1806	800	0.50	1.50	25.00	1.30	0.089	0.089	90	4.4	0:05:05	0:04:49
Plunge corners	S70	12.700	4	0.80	1521	596	3.00	0.15	12.00	1.30	0.098	0.059	61	9.3	0:03:29	0:03:12
Semi-finish wall	S80A	10.000	5	3.00	1941	596	3.60	0.20	10.80	1.30	0.061	0.041	61	8.4	0:09:24	0:08:40
Finish wall	S80B	10.000	5	3.00	3883	939	3.60	0.00	10.80	0.20	0.048	0.014	122	2.0		
Finish fillet at wall root	S90	10.000	5	3.00	1941	596	0.00	0.00	3.60	1.50	0.061	0.044	61	3.2	0:06:56	0:06:26
Scan closed angle	S100	6.000	4	3.00	5835	1200	0.00	0.00	3.00	0.10	0.051	0.013	110	0.4	0:04:58	0:04:32
														<b>Total</b>	<b>0:56:08</b>	<b>0:53:50</b>

### 6.6.8 Part Machining

Pictures were taken at all stages of machining, shown in Figure through Figure :

- The bulk of the material is removed by drilling & 3-axis roughing with the Ø5/8” end mill in the first four steps (S10-S40)
- In S50 the floor is finished using the Ø5/8” end mill
- In S60, the closed angle areas and the open angled area of the 10° slanted wall are 5-axis roughed with the Ø5/8” end mill; The arrows indicate the machined areas/thinned wall
- In S70, all 14 corners are plunged using a Ø1/2” endmill
- In S80 the Ø10mm endmill is used to semi-finish & finish the wall using the 8-to-1 rule with 12-11-10mm axial depths of cut, which means the last 3mm of the wall are not finished yet
- In S90 the Ø10mm endmill is used to rough the closed angle areas, and then finish the remaining 3mm of the wall height
- In S100 the Ø6mm taper ball endmill is used to scan the closed angle areas

We have taken several caliper measurements on the finished part:

The free standing wall measures 1.58mm thick at the top and 1.46mm at the bottom. On the remainder of the part, the wall thickness at top measures 1.45mm close to the corners but 1.52mm in the middle of walls. There was no equipment available to measure further down the wall.



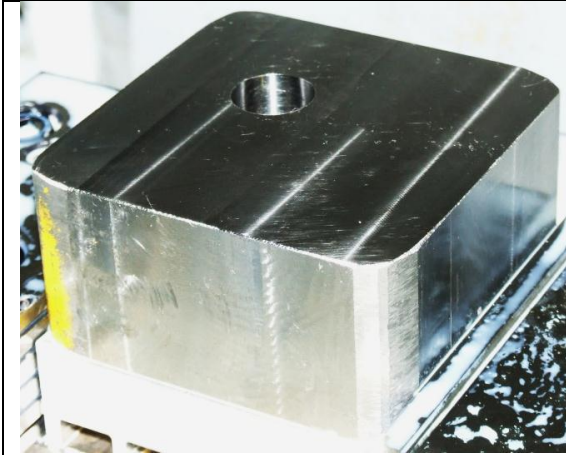


Figure 6.39: S10 - Drill hole

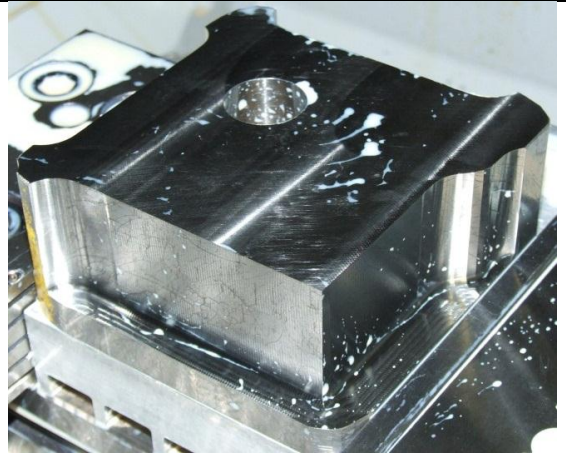


Figure 6.40: S20 - Rough periphery

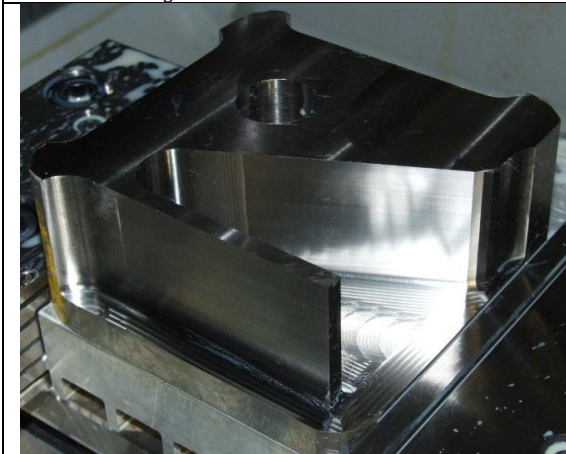


Figure 6.41: S30 - Rough open pocket



Figure 6.42: S40 - Rough closed pocket



Figure 6.43: S50 - Finish floor



Figure 6.44: S60 - Rough closed angle areas

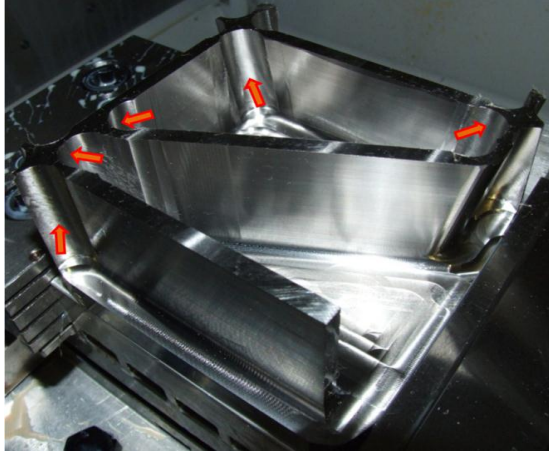


Figure 6.45: S70 - Plunge mill corners



Figure 6.46: S80 - Semi-finish and finish the wall



Figure 6.47: S90 - Finish the fillet at wall root



Figure 6.48: S100 - Scan floor in closed angle areas



## Appendix B – Average Cutting Coefficient Identification in CutPro

After collecting the cutting forces for five or more different feedrates, the data files can be used in CutPro to identify the average cutting force coefficients. CutPro will calculate the average cutting forces in X, Y and Z directions from the measurement data, and from the corresponding feedrates and the depth of cut used it will calculate the average cutting force coefficients.

*Ex07\_CuttingCoef.cws* is an example file which may be used as a reference.

First, we must set the simulation mode to “Cutting coefficient identification” and set our “Machine & Tool” settings. In this example we will use a 3/4” diameter 4fluted rigid endmill.

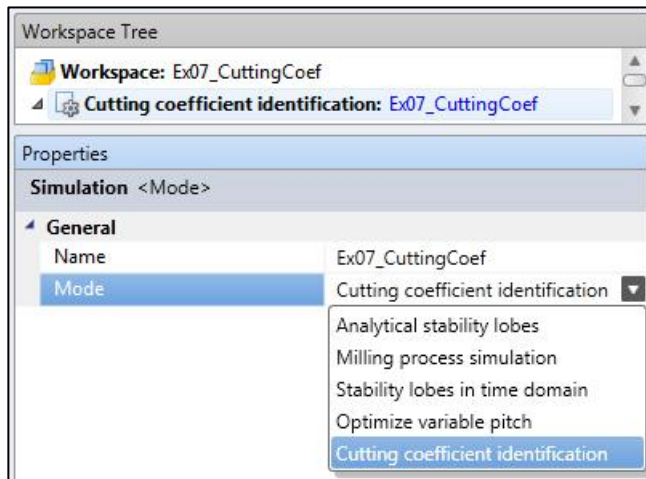


Figure B1: Cutting coefficient identification (Ex07)

Under the “Cutting Conditions” tab we can load our experimental cutting forces as follows:

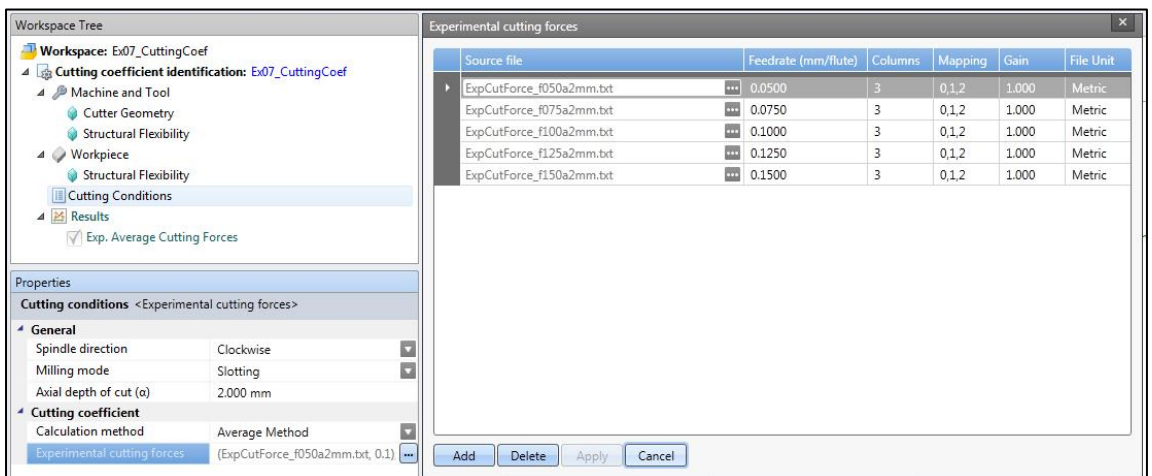


Figure B2: Experimental cutting forces loaded into CutPro Cutting coefficient identification

We can start the simulation and plot the graph shown in figure B3.

By clicking on the points shown, with the desired axis highlighted, coefficient values are displayed for various feedrates and forces.

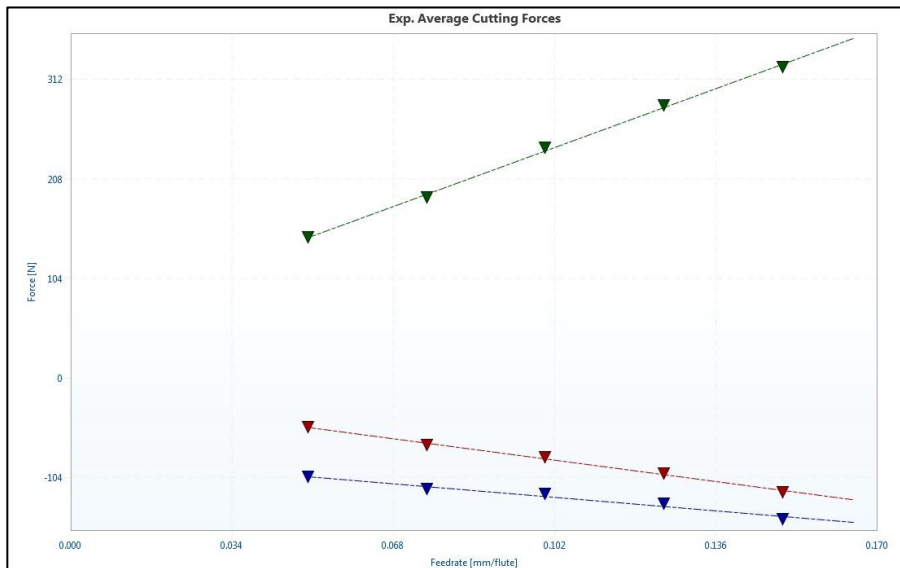


Figure B3: Average Cutting Force Identification in CutPro; Outputs: Graph and coefficients

In order to add this material into CutPro, click on the “Tools” tab on the main toolbar, and select “Workpiece Material” under the “Manager” sub-tab (figure B4). Afterwards, we can fill in the required parameters in a desired unit system, which may be found in figure B5. Click the “New” button, fill in the required parameters, and apply.

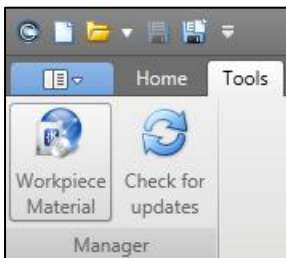


Figure B4: Workpiece material toolbar

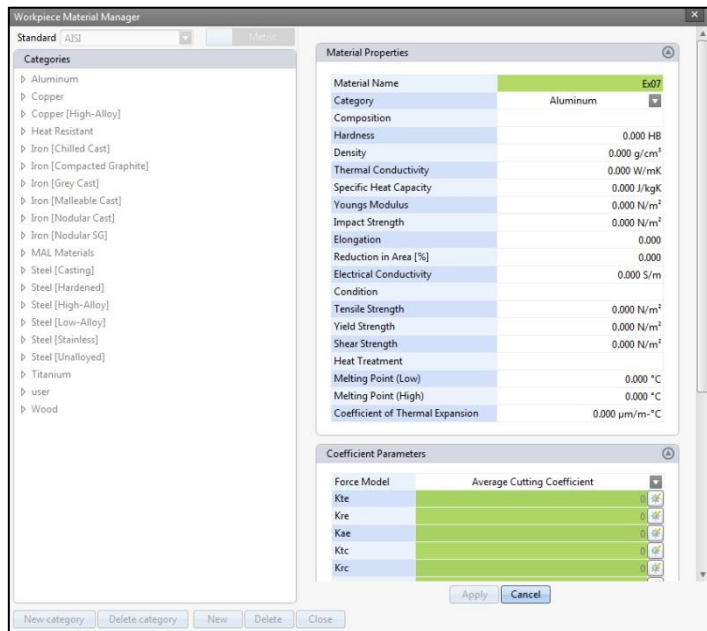


Figure B5: Workpiece material manager

## Appendix C –Time Domain Simulation in CutPro

A simulation in time domain is a simulation in which the machining process is simulated in the highest detail. The machining process is subdivided into small timesteps and CutPro simulates what is happening to the cutting tool and the workpiece. The simulation of the cutting of a chip in a milling process will consist of a big number of steps, during which the cutting tool may vibrate and even jump out of the material. Time domain simulations provide very detailed information on the cutting process, such as cutting forces, tool and workpiece vibrations, surface finish and more, but they also require a significant amount of computation time.

Example 3 of CutPro shows the functionality of the time domain simulations. Running a Single time domain simulation involves simulating only one cutting condition that is one combination of spindle speed, depth of cut, width of cut and chipload. Example 3 is the simulation of a stable cut and example 2 is the simulation of an unstable cut. Figures C1 through C5 show the resulting chip thickness, cutting forces and the tool vibration (respectively for one revolution of the four fluted cutter). From the stable cutting conditions we can see the intended chip thickness is 0.2mm and in the unstable cut it reaches values of 0.5mm.

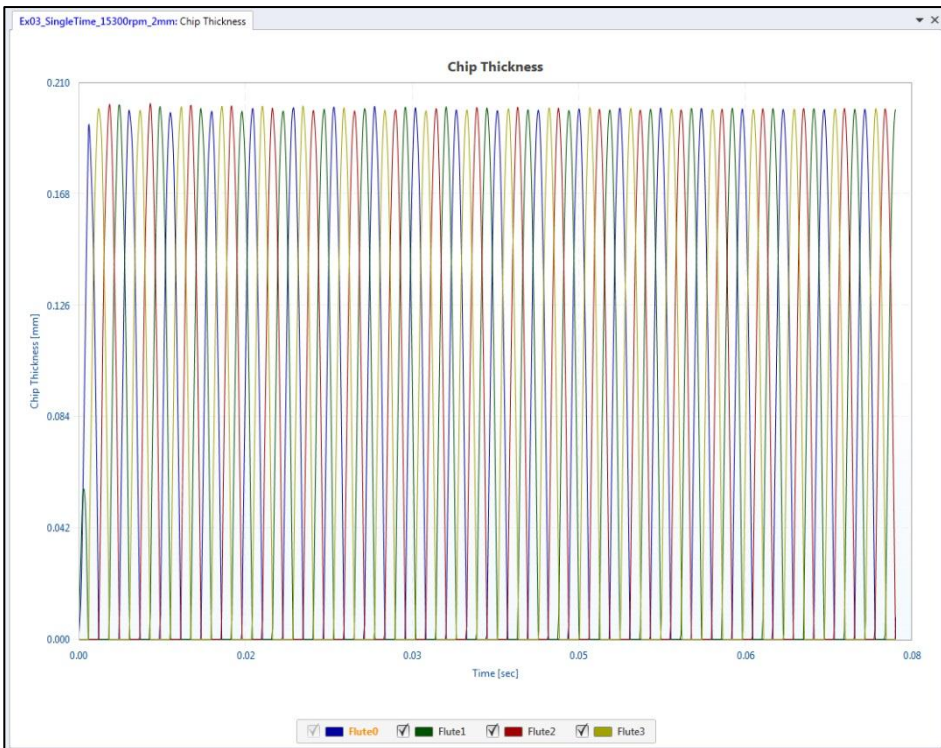


Figure C1: Chip thickness for a stable (15300rpm) cut in full immersion slotting; Note that in the stable cut, the chip thickness does not vary drastically and the maximum chip thickness is stable.

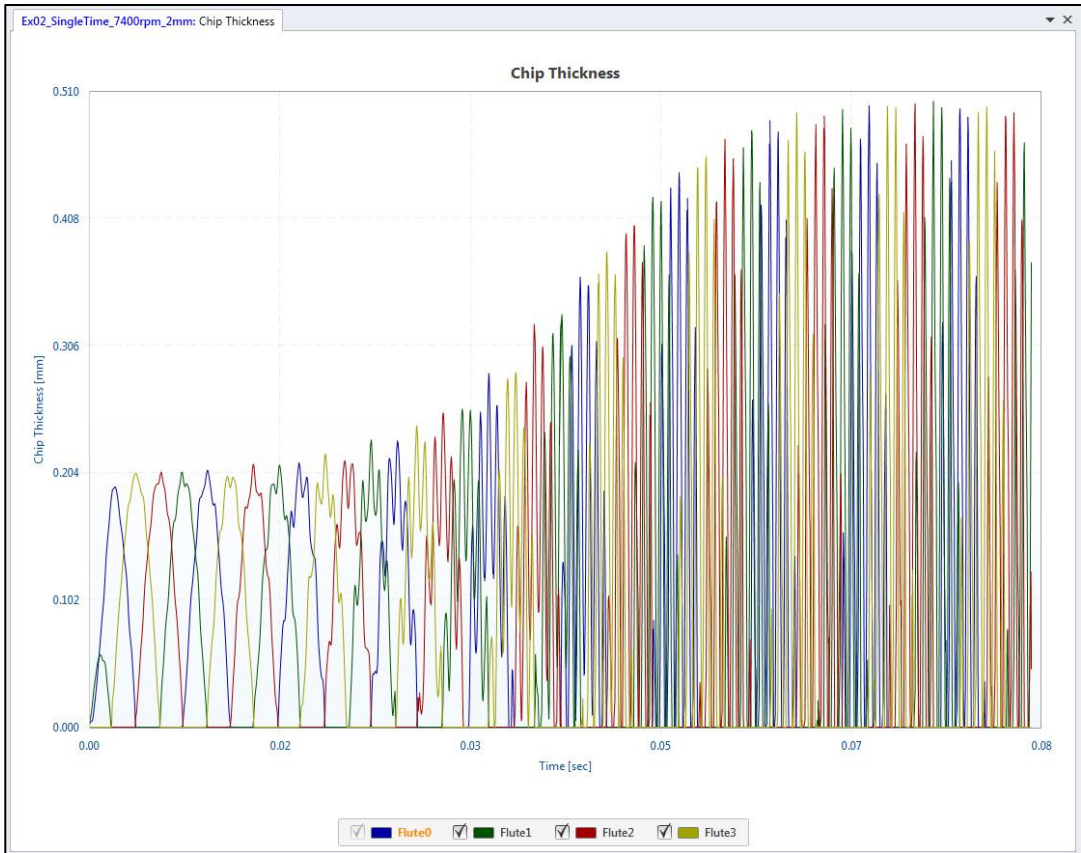


Figure C2: Chip thickness for an unstable (7400rpm) cut in full immersion slotting; Note that in the unstable cut, the chip thickness varies drastically and the maximum chip thickness is unstable.

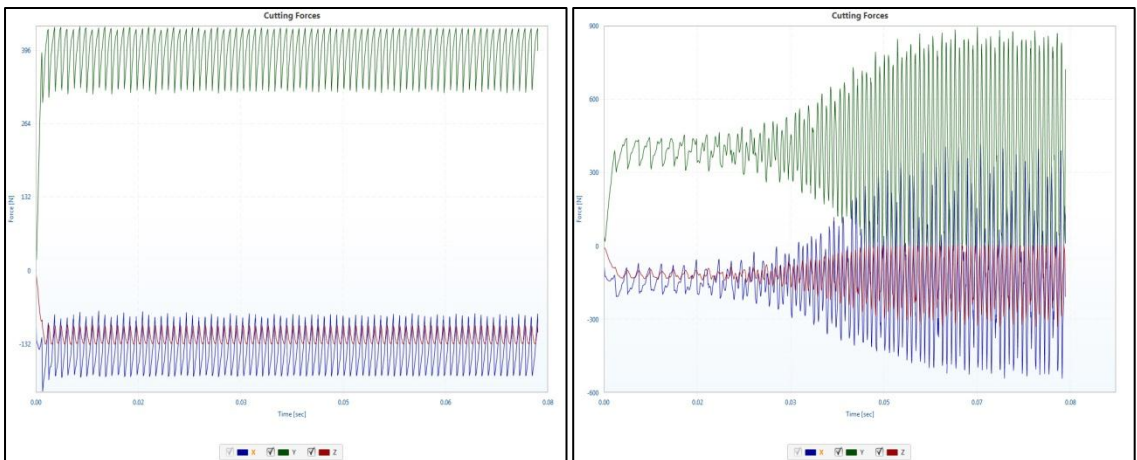


Figure C3: Cutting forces for a stable (15300rpm) and an unstable (7400rpm) cut in full immersion slotting; Note that in the unstable cut, the forces are roughly twice as high as in the stable cut

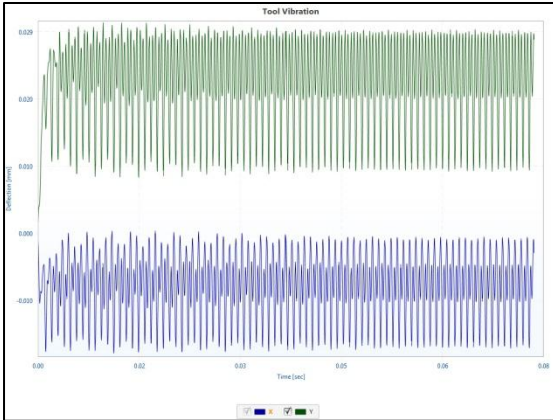


Figure C4: Tool vibrations for a stable (15300rpm) cut in full immersion slotting

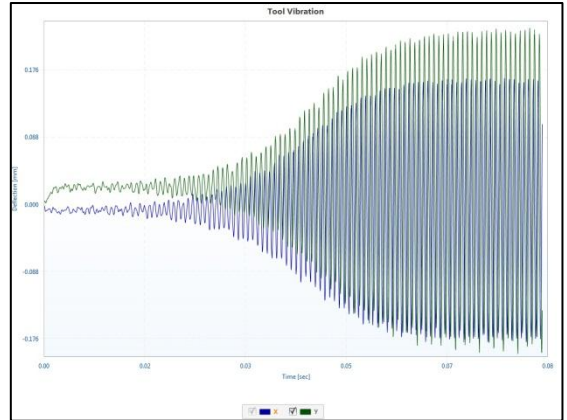


Figure C5: Tool vibrations for an unstable (7400rpm) cut in full immersion slotting

Under each graph there is a FFT button, which will pop up a new window with the Fourier spectrum of the selected graph, so you can evaluate the frequency content. Figures C6 & C7 show the FFT's (Fast Fourier Transform) of the XYZ cutting forces for examples 3 and 2 respectively.

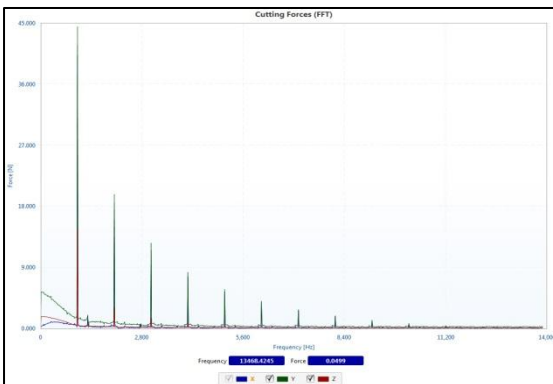


Figure C6: Fourier spectra of the X cutting force for stable (15300rpm) cut in full immersion slotting

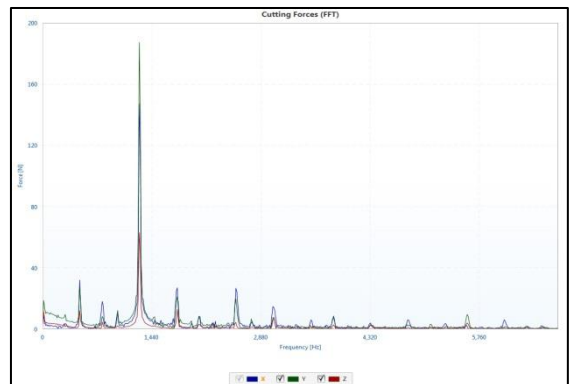


Figure C7: Fourier spectra of the X cutting force for instable (7400rpm) cut in full immersion slotting

The stable spectrum shows a very big peak at 975Hz, which corresponds to the tooth passing frequency and small ones at 2030Hz and 3040Hz, the first two harmonics. The unstable spectrum does show similar peaks locations, however, with different magnitudes. Notice the chatter frequency just before the 1440Hz mark; a maximum force magnitude of roughly 190N was reached (44N in the stable case). Also notice how the frequencies in the instable FFT contain non-harmonic frequencies; causing vibrations to continue.

If you simulate a big number of revolutions (e.g. 50), you can also evaluate the resulting surface finish, as shown in Figure C8.



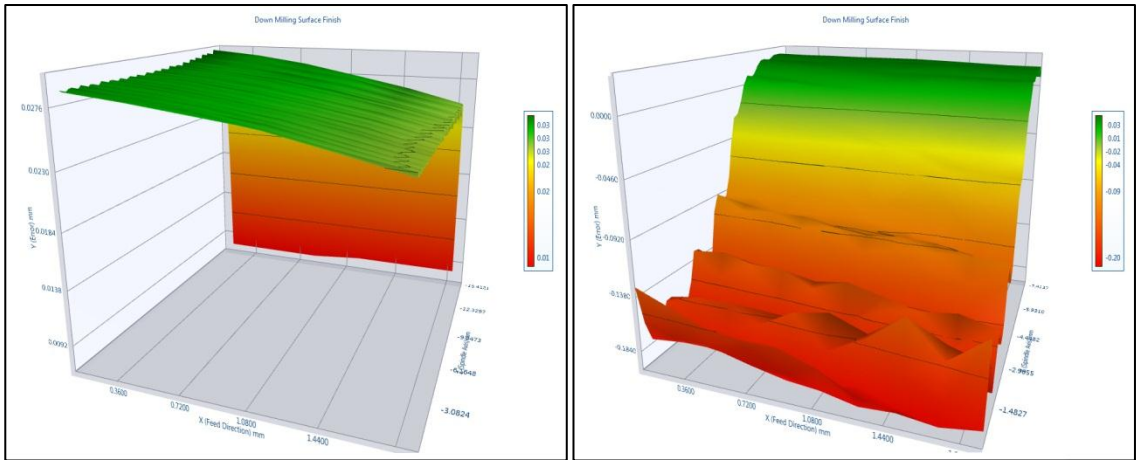


Figure C8: Surface profile for stable (8000rpm) & instable (6000rpm) cut (half immersion downmilling)

## Appendix D – Basics of Modal Analysis

*Single and multi-degree of freedom systems, damped natural vibrations*

This appendix will give a short explanation on modal analysis theory. Figure D1 shows a single degree of freedom (SDOF) system, consisting of a mass, a spring and a damper. The mass is able to vibrate in the vertical direction only. The displacement of the mass from its equilibrium position is denoted by ‘  $x$  ’ and the external force acting on the mass is denoted by ‘  $F$  ’.

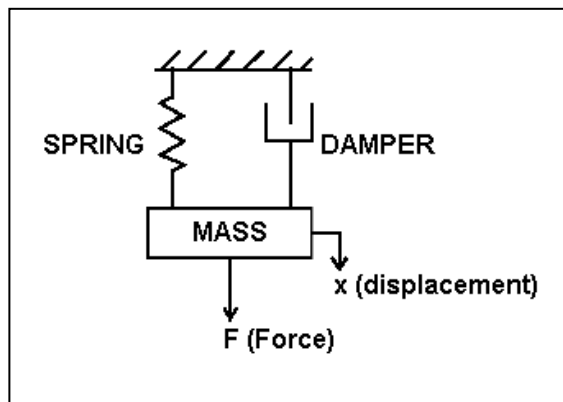


Figure D1: A single degree of freedom vibratory system

The differential equation governing the motion of the mass is:  $m\ddot{x} + c\dot{x} + kx = F(t)$ .

If there is no external force acting on the system and the mass is displaced from its equilibrium position and let go, it will vibrate. This vibration is called a free vibration, as no forces are acting on the system. This vibration will die out (and is therefore also referred to as transient), as the damper is dissipating the energy. The vibration is therefore called a damped vibration. If there was no damper, the vibration would not die out and keep vibrating forever. If there was no damper, the frequency of vibration would be

$\omega_n = \sqrt{\frac{k}{m}}$  in [rad/s], where the subscript ‘n’ indicates this is the natural frequency. In this formula,  $k$  is the spring stiffness in [N/m] and  $m$  is the mass in [kg]. If there is a damper, the frequency of vibration will be  $\omega_d = (\sqrt{1 - \zeta^2}) \sqrt{\frac{k}{m}}$ , where the subscript ‘d’ indicates this is the damped natural frequency.  $\zeta$

is the damping ratio of the system and is defined by  $\zeta = \frac{c}{2\sqrt{km}}$ . In mechanical structures the damping ratio is always less than one. The motion of a damped SDOF system, that is given an displacement  $x_0$  is described by the following equation:  $x(t) = x_0 e^{-\zeta \omega_n t} \cos(\omega_d t)$ , which is shown in Figure D2. The damping causes the vibration with frequency to die out, which can be seen in the solution term  $e^{-\zeta \omega_n t}$ , shown in the graph as the dashed envelope lines. The angular frequency of the sinusoidal vibration is  $\omega_d$  [rad/s] and measuring the damped vibration period  $\tau_d$  [s], allows you to determine the damped natural frequency from:  $\omega_d = \frac{2\pi}{\tau_d}$ . The displacement function is a damped cosine function.

The damping ratio can be determined experimentally by using the formula in the lower right corner of the graph. In this example, the ratio is determined by using the maximum displacement after the first cycle ‘ $x_1$ ’ and four cycles later ‘ $x_4$ ’. The  $\frac{1}{4}$  comes from the four cycles, it is also possible to use less or more cycles.

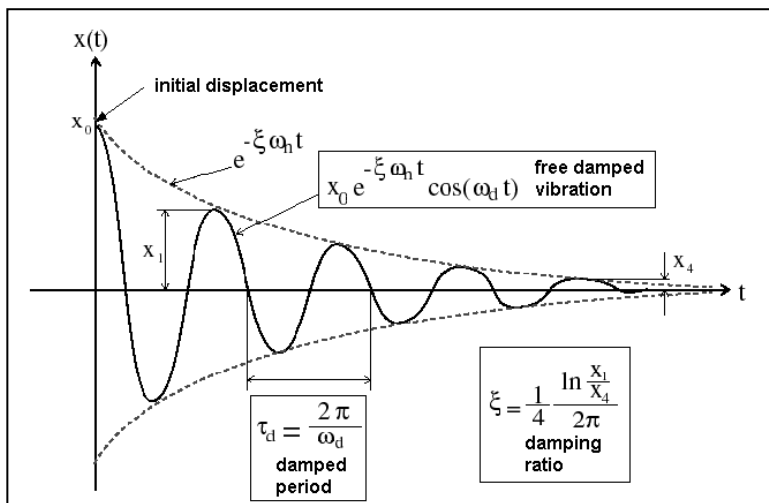


Figure D1: A damped free vibration of a single degree of freedom system

Hammer testing involves giving a blow to a mechanical structure with an instrumented force hammer, which will cause the structure to exhibit natural vibrations. Because the hammer is instrumented, we know the force with which we are exciting the structure. The free vibration is measured using either a displacement sensor, which measures the displacement  $x[m]$ , a velocity sensor, which measures the velocity  $\dot{x}[m/s]$ , or an accelerometer, which measures the acceleration  $\ddot{x}[m/s^2]$ . From the measurement of the hammer (force) and the accelerometer (acceleration) the modal mass, stiffness and damping of the structure can be determined. The determination of mass, stiffness and damping values is called modal analysis.

In practical applications, such as a machine tool structure, we are not dealing with a single mass-spring-damper system, but a with complex structures that have more than one degree of freedom, and are therefore called multi degree of freedom systems (MDOF). Thus, in practical systems we have several masses, springs and dampers. In a hammer test, we excite one point of the structure and we measure the response at the same location. This is called a ‘direct transfer function’. The hammer blow will excite all of the masses and we measure the combined response at the excitation point. Therefore, we will measure the combined displacement at the excitation point of several damped natural frequencies with different amplitudes. Figure D3 shows an example of how three different vibrations combine to a MDOF response such as measured during a hammer test. Thus, during a hammer test, we will usually see not one damped vibration, but a combination of a few different ones.

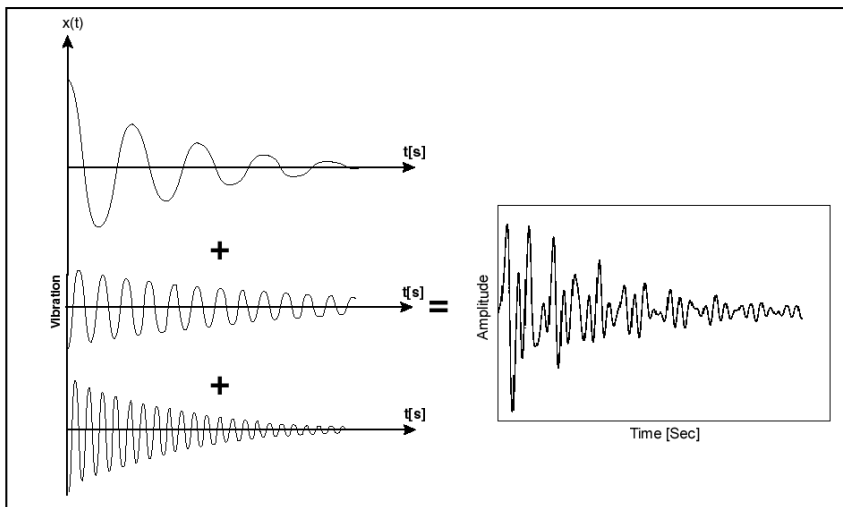


Figure D3: Three different vibrations (SDOF) combine to a MDOF response

### Frequency response function

A hammer blow excites a structure over a certain frequency range, depending on the contact time between the structure and the hammer, which is explained and illustrated in chapter 3.3. We will now take a closer look at the signals we come across during a hammer test. Figure D4 shows the time responses and the Fourier spectra of the hammer and the accelerometer signals.

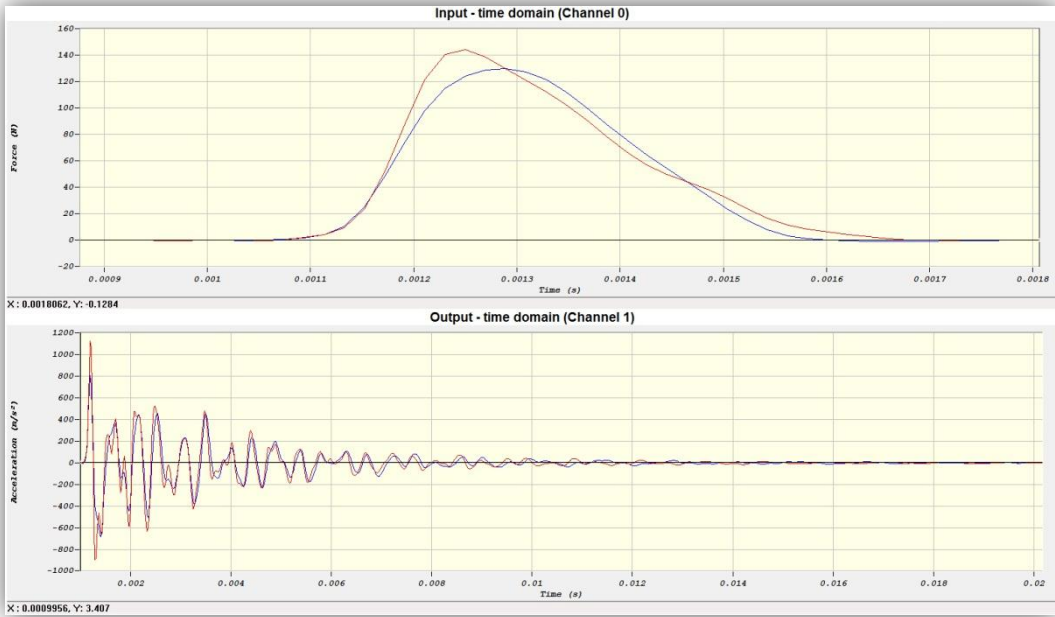


Figure D4: Signals of force and acceleration during a hammer test

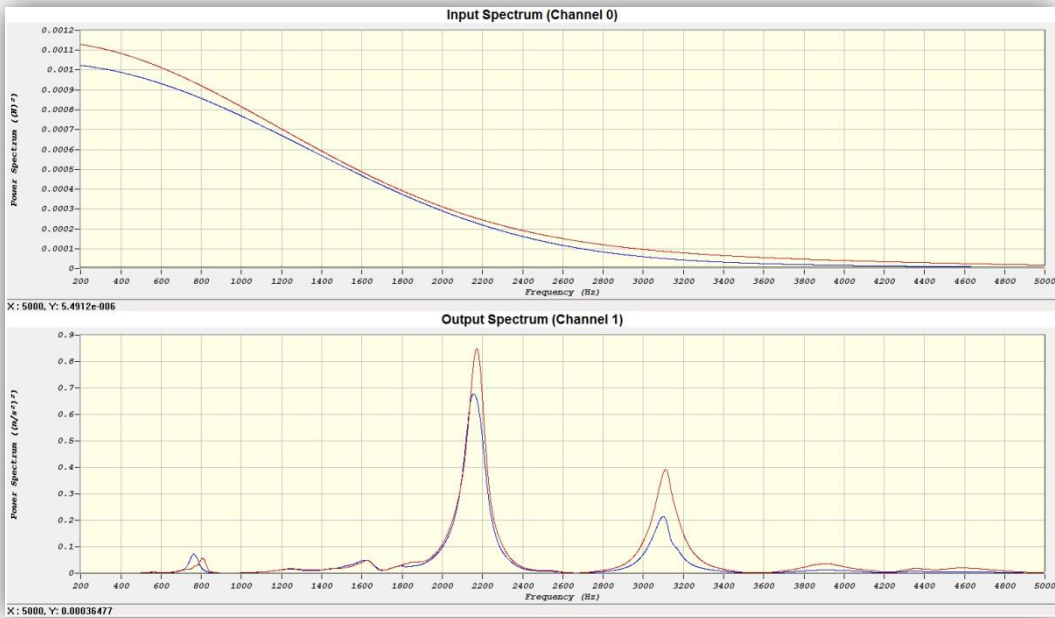


Figure D5: Signals regarding Fourier spectra during hammer test

If we look at the force signal, we can see that the duration of the impact is about 0.0005s. The shape of the signal is a smooth bump (impact). The Fourier spectrum of the force signal shows the (force) magnitude of the excitation as a function of the excitation frequency. The higher the frequency is, the smaller the exciting force becomes. The acceleration signal, the vibration of the tooltip, is a combination of damped sine waves as explained above. The signal has almost died out after 0.02s. The Fourier spectrum of the acceleration signal is flat, except for a few peaks at 780, 2150, 3100 and 3900 Hz. These peaks correspond to the dominant natural frequencies of the system, also called dominant modes. We call these peaks the dominant modes, because they are very strong compared to the rest of the spectrum (especially 2150 Hz). Every continuous system (such as a spindle structure) has an infinite number of modes. Usually only a few of that infinite number are very flexible, and exhibit a clear response to the excitation of an instrumented hammer. The other modes also respond to the hammer blow, but because they are much stiffer, you won't be able to distinguish them in the measurement. These most flexible modes of the structure dominate the behavior of the system.

From the two spectra, we can determine the frequency response function (FRF) of the machine tool structure. This function gives dynamic stiffness of the structure as a function of the frequency. This information is very useful to assess the performance of the machine tool. The FRF looks a little different from the acceleration signal. The peaks are at the same frequencies however.

The two most commonly used representations of the FRF are magnitude/phase and real/imaginary parts, as shown in Figure D6 & Figure D7.

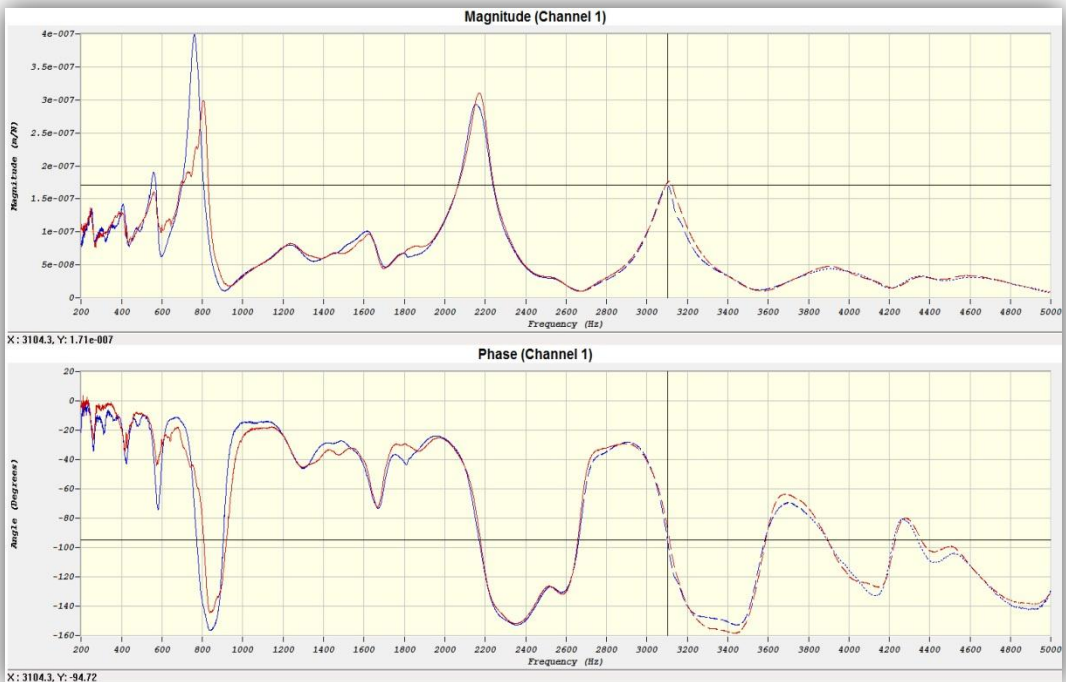


Figure D6: Representations of the Frequency Response Function: Magnitude/Phase parts

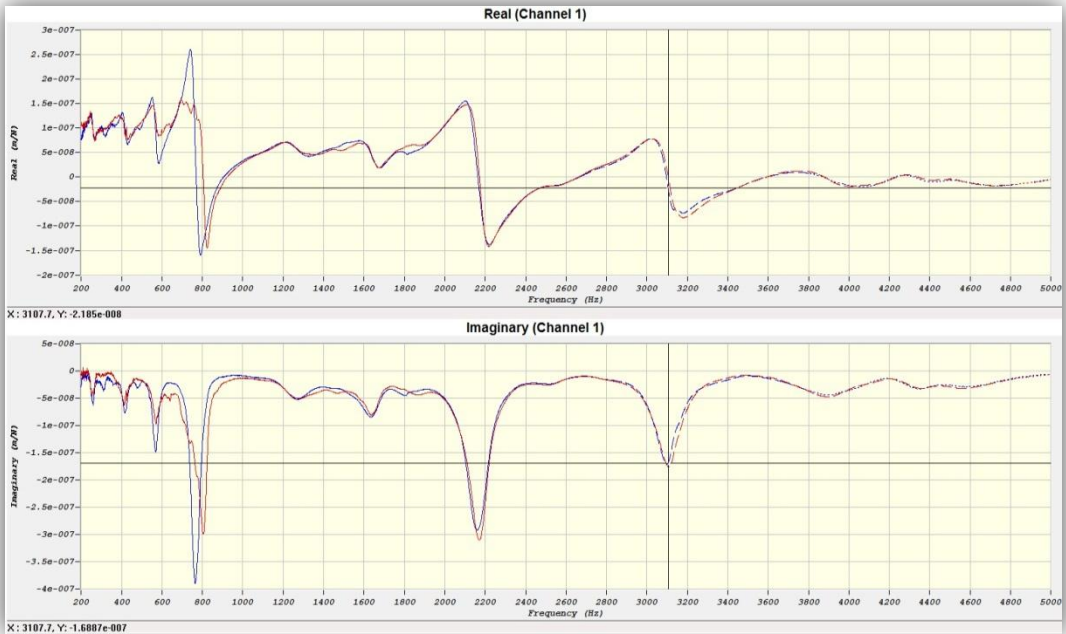


Figure D7: Representations of the Frequency Response Function: Real/Imaginary parts

In the magnitude/phase and the real/imaginary parts of the FRF you will see peaks at the same frequencies as you can see in the acceleration signal. The relative magnitudes are different however, as the acceleration is integrated twice to get to displacement. The magnitude and imaginary parts look very similar. The imaginary shows the location of the modes very clearly. In the magnitude of the FRF you should be able to see the static stiffness at the point where the frequency is 0Hz. This FRF is measured with an accelerometer which means the signal needs to be integrated twice. In this integration, the signal is divided by the second power of the frequency ( $\text{frequency}^2$ ), which means that if the frequency approaches zero, you are dividing by a very small number. The result is that the magnitude goes to infinity and it is not clear what the static stiffness is. If you use a displacement sensor to measure the FRF, there is no integration necessary, and the magnitude will show the static stiffness at nearly zero frequency, as shown in Figure D8:

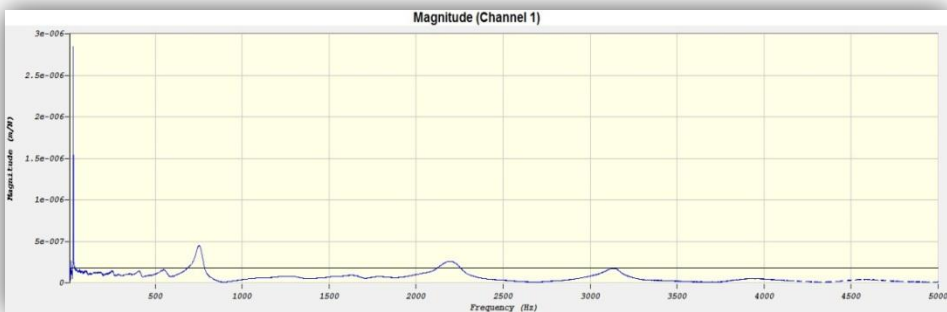


Figure D8: Magnitude when measuring with a displacement laser

## Determination of the mass, stiffness and damping from a Frequency Response Function

From the Real part of the FRF, we can determine stiffness and the damping as follows (see Figure D7):

1. Find the point where the real part intersects with the frequency axis, this is the natural frequency,  $\omega_n$  (3100 Hz)
2. Find the highest point of the real part, just to the left of the intersection, this is  $\omega_1$  (3030)
3. Find the lowest point of the real part, just to the right of the intersection, this is  $\omega_2$  (3135)

4. The damping ratio is found from  $\zeta = \frac{\omega_2 - \omega_1}{2\omega_n} = \frac{3135 - 3030}{2 \times 3100} = 0.0169$

5. Find the lowest point in the imaginary part of the FRF,  $\text{Im}_{\min}$  (-1.69E-7 m/N)

6. The stiffness can then be found from :

$$k = \frac{-1}{2\zeta \text{Im}_{\min}} = \frac{-1}{2 \times 0.0169 \times -1.69E-7} = 1.75E8 \text{ N/m}$$

7. The mass can be determined from:  $m = \frac{k}{(2\pi \times \omega_n)^2} = \frac{1.75E8}{(2\pi \times 3100)^2} = 0.461 \text{ kg}$

## Appendix E – List of main Equipment used in Document

Impact Hammer(s):

- *Endevco 2302-10*

Data Acquisition Device:

- *National Instruments NI 9234 Data Acquisition Card*

Sensor(s):

- *Endevco 25B (Accelerometer)*
- *Polytec CLV-2534 (Laser Vibrometer)*

Machine:

- *Mori Seiki NMV 5000DCG*

Material:

- *AL 7050-T7451*
- *Ti6Al4V*

Software(s):

- *CutPro v10.0.480.1 Beta*
- *CutPro v9.3*

Accessories:

- *BNC Cables*
- *Wax Adhesive*
- *Exchangeable hammer tips*



## References

- [1] CUTPRO®, 2001, Advanced Milling Process Simulation System, <http://www.malinc.com>
- [2] MACHPRO® Advanced Process simulation and NC Program Optimization System, <http://www.malinc.com/>
- [3] High Speed Machining of Aluminum – Boeing Technology, Phantom Works: [http://www.mfg-labs.com/FileDownload/Papers\\_Presentations/High\\_Speed\\_Aluminum\\_Machining\\_Presentation.pdf](http://www.mfg-labs.com/FileDownload/Papers_Presentations/High_Speed_Aluminum_Machining_Presentation.pdf)
- [4] Altintas, Y., 2012, Manufacturing Automation: Metal Cutting Mechanics, Machine Tool Vibrations, and CNC Design. Cambridge University Press
- [5] High Performance Ti Machining – Boeing Technology, Phantom Works: <http://www.theinnovationmachine.com/The%20Learning%20Library/Boeing%20Titanium%20Machining%20Presentation.pdf>
- [6] Merdol, S.D., Altintas, Y., 2008, Virtual Simulation and Optimization of Milling Operations: Part I – Process Simulation, Trans. ASME, J. Manufac. Sc. and Eng., vol. 130, pp. 051004.
- [7] Merdol, S.D., Altintas, Y., 2008, Virtual Simulation and Optimization of Milling Operations: Part II – Optimization, Feed Rate Scheduling, Trans. ASME, J. Manufac. Sc. and Eng., vol. 130, pp. 051005.
- [8] Sandvik Coromant – Application Guide Titanium Machining (C-2920:22 ENG/01), 2004.12

